# FINAL REPORT

## Combining Mass Balance Modeling with Passive Sampling at Contaminated Sediment Sites to Evaluate Continuing Inputs and Food Web Responses to Remedial Actions

## SERDP Project ER-2429

DECEMBER 2021


Philip Gschwend
E. Eric Adams
**Massachusetts Institute of Technology**

Mandy Michalsen
**U.S. Army Engineer Research Developmental Center**

Katherine von Stackelberg
**NEK Associates LLC, Harvard Center for Risk Analysis & Harvard School of Public Health**




SERDP
DOD ▪ EPA ▪ DOE

# REPORT DOCUMENTATION PAGE

*Form Approved*
*OMB No. 0704-0188*



| 1. REPORT DATE (DD-MM-YYYY) | 2. REPORT TYPE | 3. DATES COVERED (From - To) |
|---|---|---|
| 17/12/2021 | SERDP Final Report | 9/29/2014 - 3/28/2020 |

**4. TITLE AND SUBTITLE**
Combining Mass Balance Modeling with Passive Sampling at Contaminated Sediment Sites to Evaluate Continuing Inputs and Food Web Responses to Remedial Actions

**5a. CONTRACT NUMBER**
W912HQ-14-C-0034

**5b. GRANT NUMBER**

**5c. PROGRAM ELEMENT NUMBER**

**6. AUTHOR(S)**
Philip M Gschwend, E. Eric Adams, Mandy Michalsen, and Katherine von Stackelberg

**5d. PROJECT NUMBER**
ER-2429

**5e. TASK NUMBER**

**5f. WORK UNIT NUMBER**

**7. PERFORMING ORGANIZATION NAME(S) AND ADDRESS(ES)**
Massachusetts Institute of Technology, 77 Massachusetts Ave., Cambridge MA 02139

**8. PERFORMING ORGANIZATION REPORT NUMBER**
ER-2429

**9. SPONSORING / MONITORING AGENCY NAME(S) AND ADDRESS(ES)**
SERDP/ESTCP Program Office
Dr. Andrea Leeson
901 North Stuart Street,
Suite 303
Arlington VA 22203

**10. SPONSOR/MONITOR'S ACRONYM(S)**
SERDP

**11. SPONSOR/MONITOR'S REPORT NUMBER(S)**
ER-2429

**12. DISTRIBUTION / AVAILABILITY STATEMENT**
DISTRIBUTION STATEMENT A. Approved for public release: distribution unlimited.

**13. SUPPLEMENTARY NOTES**

**14. ABSTRACT**
This project has sought to address the very common situation in which contaminated sediments in an aquatic ecosystem do not "respond" well to efforts to clean them up as measured by improved health of the organisms living in that environment. This, of course, translates to increased risks for humans and other predators (e.g., birds) that capture food from those sites.

**15. SUBJECT TERMS**
passive sampling, sediments, polychlorinated biphenyls, PCBs, inverse modeling, food web models, FWMs

| 16. SECURITY CLASSIFICATION OF: | | | 17. LIMITATION OF ABSTRACT | 18. NUMBER OF PAGES | 19a. NAME OF RESPONSIBLE PERSON |
|---|---|---|---|---|---|
| a. REPORT | b. ABSTRACT | c. THIS PAGE | | | Philip Gschwend |
| UNCLASS | UNCLASS | UNCLASS | UNCLASS | 94 | 19b. TELEPHONE NUMBER (Include area code) 617-253-1638 |

# FINAL REPORT

Project: ER-2429

## TABLE OF CONTENTS

# TABLE OF CONTENTS (Continued)

**Page**

# TABLE OF CONTENTS (Continued)

# LIST OF FIGURES

**Page**

# LIST OF FIGURES

**Page**



**SECTION 3**

# LIST OF TABLES

# LIST OF TABLES

**Page**



**SECTION 3**

# ACRONYMS AND ABBREVIATIONS

| | |
|---|---|
| ACoE | U.S. Army Corps of Engineers |
| ADCP | acoustic doppler current profiler |
| AIC | akaike information criterion |
| CTD | conductivity-temperature-depth profiler |
| CV | coefficient of variation |
| DoD | U.S. Department of Defense |
| EFDC | environmental fluid dynamics code |
| EPA | U.S. Environmental Protection Agency |
| FWMs | food web models |
| GCMS | gas chromatography-mass spectrometry |
| HOCs | hydrophobic organic compounds |
| LDW | Lower Duwamish Waterway |
| MBM | mass balance model |
| MC | Monte Carlo |
| MIT | Massachusetts Institute of Technology |
| MSS | Marine Sampling Systems, Inc. |
| PAHs | polycyclic aromatic hydrocarbons |
| PCBs | polychlorinated biphenyls |
| PE | polyethylene |
| PRC | performance reference compound |
| PSU | practical salinity unit |
| RI/FS | remedial investigation/feasibility study |
| RM | river mile |
| RMS | root mean square |
| SERDP | Strategic Environmental Research and Development Program |
| WBL | water boundary layer |

# ACKNOWLEDGEMENTS

This research was funded by Strategic Environmental Research and Development Program (SERDP) under U.S. Army Corps of Engineers (ACoE) contract W912HQ-14-C-0034. Any opinion, findings, or conclusions or recommendations expressed in this material are those of the authors and do not necessarily reflect the views of the U.S. Department of Defense (DoD).

Much of the research in this project was performed by an excellent group of students, postdocs, and research associates including: Jennifer Apell, Dan Prendergast, Megan Burke, Tanguy Raguenez, Catherine Sobchuk, Toby Harvey, Ishita Shrivastava, Peter Israelsson, and John MacFarlane.

We also thank Sean Sheldrake and the U.S. Environmental Protection Agency (EPA) Region 10 dive team, Bill Jaworski and Dale Dickinson of Marine Sampling Systems, Inc. (MSS), Tim Thompson, Mandy Michalsen (AcoE) and Kristen Kerns (AcoE) for their assistance in the field sampling. Cheronne Oreiro and Sue Dunnihoo also generously provided us with space to process newly recovered samples at ARI. Bruce Nairn and Earl Hayter for helped with the EFDC, and Rose Wang for helpful discussion on bed-water fluxes.

# Combining Mass Balance Modeling with Passive Sampling at Contaminated Sediment Sites to Evaluate Continuing Inputs and Food Web Responses to Remedial Actions

(Submitted in response to ERSON-14-03 Improved Understanding of the Impact of Ongoing, Low Level Contaminant Influx to Aquatic Sediment Site Restoration)

Philip M. Gschwend, E. Eric Adams, Mandy M. Michalsen, and Katherine von Stackelberg

date: April 2021

## ABSTRACT

This project has sought to address the very common situation in which contaminated sediments in an aquatic ecosystem do not "respond" well to efforts to clean them up as measured by improved health of the organisms living in that environment. This, of course, translates to increased risks for humans and other predators (e.g., birds) that capture food from those sites.

To improve our abilities to address such sites, we proposed a coordinated use of both measurement and modeling "tools" that can be applied to achieve better results. These tools include:

(a) Using passive samplers to characterize the presence of contaminants like polycyclic aromatic hydrocarbons (PAHs), polychlorinated biphenyls (PCBs), and nonionic pesticides in all of the media including sediments. Such data allows comparison of "passive sampler concentrations" in adjacent media such that directions of fluxes can be discerned. Further, translation to corresponding concentrations in other media like water allow quantitative estimation of fluxes as well as a metric suited to calculating bioaccumulation.

(b) Using mass balance modeling synthesis of the passive sampling results so as to develop whole-ecosystem distributions of the chemicals evaluated by the passive samplers. Such whole-ecosystem expectations can then be compared with direct measures of the chemicals in well mixed fluid (e.g., surface waters) and any significant mismatch implies ignorance of the chemical's sources or sinks (as was found in this project for the surface water in the Lower Duwamish Waterway (LDW). In the case of "missing" inputs, there should be a major effort to ascertain whether sediment beds are actually controlling exposures in overlying waters or some other discharge is responsible. Obviously, rectifying the dominant contaminant source is the most effective means for diminishing risks in those systems.

(c) As found in this project, locating and quantifying important PCB sources in the LDW proved to be difficult for a variety of reasons (e.g., inability to access suspected source locations.) This led us to utilize inverse modeling so that our limited contaminant measures could be most effectively used to locate and quantify likely contaminant inputs. This approach appears to be an extremely effective means for guiding site investigations.

(d) Since environmental sampling is always limited in spatial and temporal coverage, coupling measures with modeling facilitates interpolation of contaminant presence at unsampled locations and times. This synthesis of the measurements has the huge advantage of greatly improving our knowledge of exposures to organisms in the environment of interest. And, of course, such "exposure fields" are suited for food web modeling.

(e) So the final "tool" used in this project was a food web model (FWM), FishRand. This modeling tool allowed us to employ the measurement results, together with their synthesis via use of the mass balance modeling tool, the Environmental Fluid Dynamics Code (EFDC), to more fully drive the estimates of contaminant uptake by the various trophic levels present in the LDW. Establishing this bioaccumulation potential, not only permitted clearer connections to deliberations concerning risks due to contamination at the site, but also provided a tool to assess the degree of site improvement/risk reduction associated with particular remedial options.

**Keywords** passive sampling, sediments, polychlorinated biphenyls, PCBs, inverse modeling, food web models, FWMs

# EXECUTIVE SUMMARY

## INTRODUCTION

Despite efforts to remediate sediments contaminated with toxic organic compounds like polycyclic aromatic hydrocarbons (PAHs), polychlorinated biphenyls (PCBs), pesticides, project managers often remain uncertain about the value of their remedial choices and the likelihood of long term reduction in exposures to the contaminants. This is, at least in part, due to the presence of continuing unchecked inputs of the same contaminants from nearby sources such as combined sewer overflows, groundwater discharges, and temporally infrequent phenomena such as localized sediment resuspension events. The research described herein sought to clarify such situations. To this end, we assumed that successful cleanups result in reduced risks to aquatic life and other organisms (birds and humans) due to significantly decreasing the presence of contaminant exposures experienced by those organisms.

Fortunately, food web models (FWMs) (Arnot and Gobas, 2004; Gobas and Arnot, 2010; von Stackelberg et al. 2017), are available to connect the concentrations of contaminants in a site's surface water, sediments, and pore waters to the body burdens of all the organisms making up the food web. As a result, risks to ecosystems and humans can be estimated as a function of the system's distribution of contaminants, as long as such distributions are understood as functions of space and time.

However, knowledge of the spatially variable and temporally changing concentrations of contaminants of concern at a contaminated site's surface waters and pore waters, needed for such FWMs, is generally limited. Contaminant measures in pore waters are almost never made, and sediment concentration data do not readily reveal freely dissolved porewater concentrations of relatively insoluble compounds like individual PCB congeners. Moreover, chemical mass balance models (MBMs) that reveal a given site's changing surface water and pore water concentrations of these organic contaminants are rarely, if ever, developed at corresponding levels of detail.

Two examples are revealing. First, Gobas and Arnot (2010) developed a complex FWM for PCBs in San Francisco Bay. To drive their model, they used PCB cycling calculations done by Davis (2004). This latter effort treated all of San Francisco Bay as a single, well-mixed body of water, and it assumed single values of rate coefficients to apply everywhere in the system (e.g., degradation rate of PCBs at 0.000034 $d^{-1}$). While Davis' mass balance modeling effort was a valuable starting point to identify data needs and a few important conclusions (notably, only 10 kg PCB inputs leaking into the entire bay each year was enough to delay food web "depuration" of PCBs in this ecosystem), the resultant model was clearly too simple to exploit for site-specific understanding of PCB concentration changes and how they would change in response to local sediment cleanup efforts.

In a second example, as part of the Lower Duwamish Waterway (LDW) Remedial Investigation (Windward 2010), the Gobas FWM was employed again. But this time, the PCBs in the system were modeled by Nairn (2009) using a site-calibrated version of the Environmental Fluid Dynamics Code (EFDC). In this case, the modeler considered exchanges of water with upstream (river flow) and downstream (tides). He also assumed diffusive fluxes from the bed to the overlying bottom water, where the Duwamish sediments were characterized using surface area weighted averages of measured PCB concentrations in the bed over four regions.

Unfortunately, the model treated all the PCBs as a single entity (∑PCBs) with singular properties (for example, an aerially constant $K_d$ value of 140,000 L/kg used to calculate porewater concentrations everywhere). In this case, the mass balance model (MBM) results may have showed the right trends (e.g., salty bottom water entering with the tides from Elliott Bay were expected to have lower PCB concentrations than the overlying freshwater flowing out of the LDW at the same stations, although in this project we found evidence of PCB sources located near the bottom entering the estuary from the direction of Elliott Bay!) Finally, the previous model was calibrated by adjusting a mass transfer coefficient for fluxes of PCBs from the bed sediments to allow matching the few measured water column ∑PCB concentrations (King County, 2006). Unfortunately, this approach does not truly identify the most important times and places from which the PCB contamination emanates. Hence, efforts to impact the system are inhibited since where to start is not clear!

In using this approach, the average water column and porewater concentrations of ∑PCB concentrations were estimated and used in the Gobas FWM (LDW Remedial Investigation, Appendix D, 2010). The resultant FWM also unfortunately run with the ∑PCBs treated as a singular compound with singular properties (despite the fact the PCB congener log $K_{ow}$ values range over about 3 orders of magnitude), was also calibrated to fit observed tissue concentrations. Unfortunately, this type of modeling does not currently allow us to answer a question like, "how will PCB pore water and surface water concentrations, and hence aquatic organism tissue concentrations, change if we do …?"

Hence, it was the overarching purpose of this research to develop chemical MBMs suited to addressing questions about what will happen if certain chemical sources are removed, while others are left untouched. We also pursued this integrative modeling effort in conjunction with the use of passive samplers to make measures of contaminant chemical gradients between pore waters and overly bottom water (and also surface water vs air), thereby permitting estimated fluxes in the relevant environmental compartments. In addition, we explored the use of inverse mass balance modeling to ascertain the locations and strengths of contaminant sources needed to fit distributions of those chemicals in the tested ecosystem. Finally, we utilized the mass balance modeling to estimate how changing inferred sources would diminish the presence of contaminants at the site, and then used this modeling estimate as an input to the site's FWM to ascertain the impact of such source removals.

## OBJECTIVES

Given the need for tools to guide site assessments and to make informed remedial designs for contaminated sediment sites, we pursued the following coordinated modeling and passive sampling measurement objectives seeking:

1. To develop a contaminated-sediment-site MBM that calculates the expected water column concentrations assuming a particular set of sources (e.g., diffusion from sediment in particular regions) and at least one quantifiable sink (e.g., flushing of the contaminants of concern from the aquatic site of interest). Hydrodynamic information was used to estimate bottom boundary layer thicknesses, and a polyethylene (PE) passive sampling-based method was used to characterize bed-to-water contaminant concentration gradients.

2. To develop PE passive sampler-based methods suited to quantifying the freely dissolved concentrations of low-solubility contaminants like PCBs in the overlying water column, thereby allowing assessment of the accuracy of the water column concentration estimates using our MBM, the EFDC.
3. To extend our understandings of the study site's set of PCB sources by using an Inverse Modeling approach that utilizes the known hydrodynamics (mixing, flushing) of the LDW and measures of the PCB distributions in the water column to locate and quantify the sources needed to explain the distribution of PCBs in that estuary.
4. To integrate the use of a FWM with the PCB concentration fields produced using passive sampling measures and synthesized using the EFDC to demonstrate the impacts of PCB bioaccumulation from surface water, pore water, and sediment solids.
5. To exercise the mass balance and FWMs together to assess the impacts of "what if" scenarios resulting from continuing low-level contaminant inputs after targeted sediment hot spots are remediated.

## TECHNICAL APPROACHES

### Passive Sampling and Mass Balance Modeling Approaches

To begin, we sought to quantify the diffusive fluxes of individual PCB congeners from the sediment beds into the overlying waters of the LDW. We did this by deploying PE passive samplers, pre-loaded with a set of 13C-labelled PCB congeners as performance reference compounds (PRCs), across the sediment-water interface at about 20 sites in the LDW. Upon sampler recovery, we measured the PCBs and PRCs, used that data and our PRC correction program (Tcaciuc et al.) to calculate the equilibrium PCB concentrations in the PE. And with these estimates of PCB equilibrium concentrations in the PE, we could use the PE-water partition coefficients, $K_{PEw}$, of each congener to solve for its concentration in the porewater for PE in the bed or in the water column for PE suspended above the bed.

This effort was augmented by special use of an acoustic Doppler current profiler (ADCP) which we deployed on a tripod to sample water velocities as a function of height above the sediment bed. These data were processed to reveal the diffusive boundary layer thickness above the bed at each passive sampling site. Together with the PCB concentration gradients, this boundary layer information allowed us to make upper-limit estimates of each PCB's diffusive flux out (or in to) the sediment bed.

Combining all these results enable us to estimate the spatially varying diffusive fluxes from bed to water column. Integrating these fluxes over the entire LDW bottom yielded a total source strength for PCBs entering the water column from the bed.

Finally, using this spatially varying source strength for the 20 congeners we specifically measured as inputs to the EFDC which had been tuned to match tidal amplitudes, we could solve for the resulting distributions of each PCB in the LDW water column. It is important to note that passive sampling of the riverine influx of PCBs to the LDW was also performed to account for that PCB input source too. Combining these, we could not explain the presence of most of the PCB load in the LDW water column.

In a subsequent effort, we sought to ascertain whether bioirrigation might account for the necessary additional PCB fluxes (Apell et al. 2018). This one done by measuring Rn222/Ra226 profiles at the same locations where passive samplers were deployed to quantify PCBs in the porewater. Using radon-radium disequilibria, we found the bioirrigation rates. Coupling this information to the PCB concentrations in the irrigated porewater still did not get close to explaining the "missing" PCB source.

And in still another effort, we considered the possibility that the atmosphere might be the "missing source" (Apell and Gschwend, 2017). PE samplers were used to measure if PCBs truly dissolved in surface waters AND occurring as vapors in the lower atmosphere. These gradients proved to be from the water to the atmosphere, so clearly the air was not the "missing source."

**Inverse Modeling**

In light of this "missing source" problem, we decided to employ inverse modeling to locate the missing PCB sources. The strategy was that the locations of key sources would be key to helping us identify sources, often underwater, such as outfalls or seeps.

To perform this "inverse modeling," we ran the EFDC with singular sources to generate a concentration profile that was unique to each putative source location. Then combining these concentration profiles using a least root mean square (RMS) error fitting approach such that the total PCB distributions in the water column could be explained by only a few sources, we located a series of likely places in the estuary where PCBs were probably being introduced. The weightings of these inputs clearly indicated the relative importance for each of the PCB congeners that were fit.

**Food Web Modeling**

Finally, we employed our PCB concentration data for sediments, porewater, and surface water to drive a new version of the food web FWM, FishRand. This model was parameterized for the organisms living in the LDW. Operation of the model yielded biota concentrations that were consistent with past measures of PCBs in those organisms.

Having established this linkage with the passive sampler measures and the EFDC modeling, we showed that the FWM could be exercised to change PCB concentration conditions that might result from various remediation efforts. This effort clearly revealed the degree of biota response to particular changes in PCB exposures due to investments in clean up.

**REFERENCES**

Apell, J.N.; Shull, D.H.; Hoyt, A.M.; Gschwend, P.M. Investigating the Effect of Bioirrigation on In Situ Porewater Concentrations and Fluxes of Polychlorinated Biphenyls Using Passive Samplers. Environ, Sci. Technol. 52(8), 4565-4573, 2018. DOI: 10.1021/acs.est.7b05809

Apell, J.N. and P.M. Gschwend. The atmosphere as a source/sink of polychlorinated biphenyls to/from the Lower Duwamish Waterway Superfund site. Environ. Pollution 227: 263-270, 2017.

# SECTION 1 ESTIMATING THE DIFFUSIVE SEDIMENT-WATER FLUXES OF POLYCHLORINATED BIPHENYLS USING PASSIVE SAMPLING AND THEIR CONTRIBUTIONS TO ESTUARINE MASS BALANCES

## 1.1 BACKGROUND

Hydrophobic organic compounds (HOCs)—at levels deemed to be hazardous—contaminate a significant portion of the sediment underlying US surface waters.[1] Such deposits of legacy pollutants may act as a continuing source to overlying water for decades or longer. Knowledge of these contaminants' potential for continuously dosing the aquatic ecosystem is needed to estimate food web exposures and to design the most effective remediation approaches to protect the health of humans and the environment.

The sediments of the Lower Duwamish Waterway (LDW) Superfund site are extensively contaminated with polychlorinated biphenyls (PCBs) (Figure 1).[2] Continuing releases from such sediment deposits are commonly assumed to be important sources of HOC contamination to the overlying aquatic ecosystem.[3, 4,5,6] Known sedimentary hotspots in the LDW are being remediated; but like many sites, there is concern that other continuing PCB inputs into the waterbody may prevent substantial improvement of this complex urban estuary.

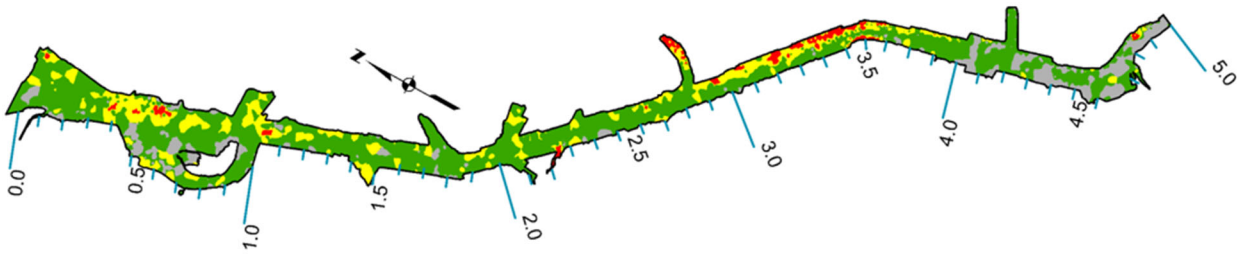


**Figure 1. Map of the LDW Study Area, with North Generally to the Left.[2]**

*Numbered ticks indicate the distance [miles] from the downstream edge of the study area. Colors represent sediment concentration of total PCBs determined by the U.S. Environmental Protection Agency (EPA) remedial investigation/feasibility study (RI/FS) in 2006, prior to remediation.[2] Gray indicates the detection limit (ca. 30 µg ΣPCBs/kg), and yellow/red indicates the legal benchmarks for investigation (yellow, >240 µg ΣPCBs/kg) and action (red, >1,300 µg ΣPCBs/kg).*

Historically, estimating the fluxes of PCBs between sediment beds and the overlying water column in the field was difficult to accomplish, largely due to inadequate techniques for measuring truly dissolved HOCs in both pore water and overlying water.[5,6,7] Thus, modelers would estimate the diffusive gradients assuming the porewater concentrations were given by the sediment concentrations, normalized by sorption coefficient, $K_d = f_{oc}K_{oc}$,[4,8,9] and the overlying water column concentrations could be accurately determined using filtered water samples. We now knows that (a) accurate estimation of HOC sorption to sediments often requires more complex $K_d$ formulations (e.g. considering black carbons)[10,11,12,13] and (b) filtered water samples always contain colloids, often at levels sufficient to cause measurements of dissolved levels to be inaccurate.[9,14]

The sediment-water mass transfer parameters of Fickian models of sediment-water fluxes that were 'tuned' to match concentrations measured in the water column[4,15] had to compensate for inaccuracies in the diffusion gradients and so may have suffered from the assumption that HOC fluxes from the sediment bed were the primary source to the water column.

This study tested the hypothesis that the primary sources of PCBs to the water column of the LDW were molecular diffusive fluxes from the contaminated sediment bed. Direct, *in-situ* estimation of the concentration gradients ($\Delta C$) across the sediment-water interface were obtained by using low-density PE passive samplers. Such passive samplers have been used at many sites contaminated with HOCs,[5,6,7,16 and 17 and refs therein] due to their ability to infer the freely dissolved concentrations in both the sediment porewater and the near-bed water column, thereby revealing bed-to-water concentration gradients. We also sought to estimate an upper limit of the bed-to-water fluxes assuming they were only set by the diffusive water boundary layer (WBL) thickness above the bed $\delta_w$, and the compounds' molecular diffusivities in water $D_w$:

$$F = (D_w/\delta_w)(C_{pw}-C_w) = k_f(C_{pw}-C_w) = k_f \Delta C \qquad (1)$$

where $C_w$ and $C_{pw}$ are concentrations directly above the bed and in the uppermost porewater, respectively, and $k_f$ is the mass transfer coefficient. We estimated the WBL thickness ($\delta_w$) using measurements from an ADCP. By combining these two measurements, we estimated the directions and magnitudes of the specific PCB congeners' diffusive fluxes at many sampling stations distributed through the LDW (Figure 2). We then used these flux estimates as inputs to the Environmental Fluid Dynamics Code (EFDC)[18,19] to calculate the steady state PCB concentrations in the water column solely due to the estimated bed-to-water diffusive fluxes. These results were then compared to dissolved PCB concentrations measured in the LDW water column using additional passive samplers, thereby enabling us to evaluate the hypothesis that PCB diffusion from the sediments was the dominant source of these HOCs to the water of the LDW.

## 1.2 MATERIAL AND METHODS

### 1.2.1 Passive Sampler Preparation and Analysis

Details regarding the preparation, recovery, and analysis of the passive samplers can be found in previous publications, notably by Fernandez et al.[7] and Apell and Gschwend.[21] Briefly, 25 µm thick PE was cut into 8 cm wide strips, solvent cleaned, and loaded with performance reference compounds (PRCs) ($^{13}$C-labeled PCB congeners 28, 54, 47, 97, 111, 153, 178), prior to deployment. Two days before deployment, the PE sheets were mounted into aluminum frames, exposing the PE in an 8 cm × 50 cm window, then these sediment bed samplers were tightly wrapped in aluminum foil and stored in a cooler for shipping and transport. For water column samplers, PE sheets were cut into approximately 1 g strips (8 cm wide × 32 cm long × 51 µm thick), cleaned with solvents, loaded with PRCs, sealed inside aluminum mesh, tightly wrapped in aluminum foil, and stored with the framed samplers. At the time of sampler assembly, subsamples were taken from the PE sheets to quantify initial PRC concentrations before sampler deployments.

Samplers in aluminum frames were deployed in the LDW at 19 stations (Figure 2) by inserting them into the sediment bed such that about one third of the PE window was above the bed.

Deployments occurred during July 21-23, 2014 by EPA Region 10 divers and August 18-19, 2014 by Marine Sampling Systems, Inc. (MSS) via hydraulic insertion operating from a lowered platform. Insertions were confirmed either visually (divers) or through a video camera (MSS). At five stations, a water column sampler and buoy were attached to the top of the frame by a 1 m line. All samplers were recovered October 6-8, 2014. Deployment and recovery specifics can be found in Appendix A. Within 12 h of recovery, all samplers were taken to Analytical Resources, Inc. Laboratory (Tukwila, WA) for processing. The bed-water interface was clearly visible from discoloration on the PE and sampler frame. Samplers were wiped clean with Kimwipes® and cut into 5 cm segments starting at the sediment-water interface. PE segments were stored for shipping in 40 mL amber vials with a few drops of deionized water added to maintain 100% relative humidity in the vials. Four field blanks, consisting of PE strips identical to deployed strips, were exposed on the vessel as if being handled in samplers during both deployment and retrieval activities.

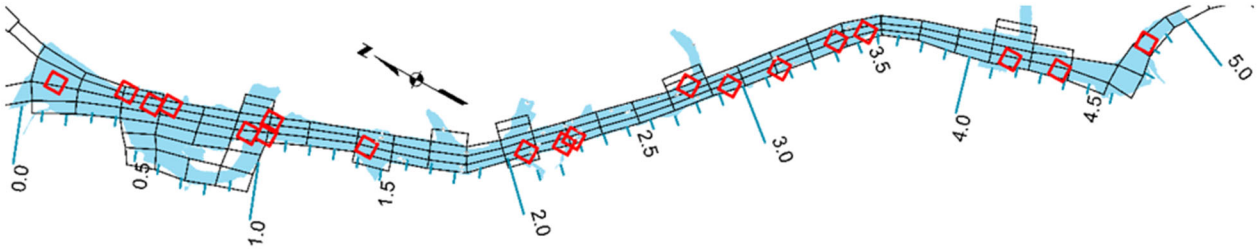


**Figure 2. Map of the LDW with Red Squares Indicating Passive Sampler Stations, and Black Lines Showing the EFDC Grid Used in this Study.**

Upon return to the Massachusetts Institute of Technology (MIT), each PE sample in its 40 mL vial was spiked with surrogate recovery standards ($^{13}$C-labelled PCB congeners 19, 52, 105, 167, and 194), extracted three times with dichloromethane, and those extracts were combined. Combined extracts were concentrated to about 50 µL, dosed with injection standards, and analyzed via capillary gas chromatography-mass spectrometry (GCMS) using a 60 m long x 0.25 mm ID Agilent DB-5MS column in a JEOL GCmate (JEOL Ltd., Tokyo, Japan) operating in the selected ion monitoring mode. PCB congener concentrations were corrected for each sample using surrogate recoveries of identical or nearest chlorination levels. Surrogate recoveries were all between 70-120%, except for the trichlorobiphenyl surrogate which averaged 67±9% (ranged from 46 to 90%). Repeated measurements of surrogates gave a method precision of better than or equal to ±14%.

### 1.2.2 Passive Sampler Calculations

PRC losses showed the varying extent of PE equilibration (Appendix B for sediments, Appendix C for bottom water, and Appendix D for water 1 meter above the sediment bed) for the range of target PCB congeners.[20,21] To adjust the measured target PCB values to equilibrated PE concentrations, PRC losses were fit using mass transfer models for samples in the sediment[20,22] or water,[5,23] according to the medium in which the PE had been deployed. After adjusting to equilibrium levels, the concentrations in the freely dissolved phase were calculated using PE-water partition coefficients, $K_{PEW}$. Values used in this study, were corrected for temperature and salinity.

Notably, we judged the statistical significance of a PCB's concentration gradient using the fugacity ratio of PE segments taken just above the interface, $f_W$, to that just below it, $f_S$. This ratio is equivalent to the ratio of the corresponding equilibrium PE concentrations (ng/g). Testing whether concentration gradients were significantly different from zero (before converting to freely dissolved concentrations) avoided a calculation step using literature $K_{PEW}$ values that have relatively large uncertainties,[17,24] thereby improving confidence in sediment locations that are identified as PCB sources to the overlying waters.

### 1.2.3 Acoustic Doppler Current Profiler Measurements

The diffusive boundary layer along the bottom of the LDW was characterized using an ADCP. A three-beam ADCP (Aquadopp HR-Profiler, Nortek USA, Boston, MA) was operated in pulse-coherent mode at 2 MHz with a 1.5 cm bin size. The ADCP was mounted in a frame facing downward, and held 1.25 m above the bed for 15-30 min at each station. Tilt sensors included in the ADCP confirmed the vertical orientation of the measured profile. The distance between sensor and sediment bed was determined using the amplitude of the acoustic signal, with a strong echo occurring at the interface. The velocity profiles generated by the ADCP ranged from 0.015 to 1.15 m above the sediment bed. Profiles were recorded every 30 s, representing the average of 30 measurements (1 Hz sampling). Data processing removed velocity ambiguities, and discarded data with auto-covariance less than 0.7. Within the LDW, seven stations were measured that met data quality standards, providing snapshots of a range of locations and times in the tidal cycle (Table S15).

Due to bottom shear stress, the near-bed velocities, $u$(x), follow a logarithmic profile

$$u(x) = \frac{u*}{k}\ln(x/z_o) \qquad (2)$$

where $u*$ is the shear velocity, $\kappa = 0.4$ is von Karman's constant, x is elevation above the bottom, and $z_o$ is a characteristic roughness height where the extrapolated velocity goes to zero.[25] The shear velocity, in turn, can be used to estimate the thickness of the laminar boundary layer, $\delta_W$:

$$\delta_W = 10\,\nu\,Sc^{-1/3}/u^* \qquad (3)$$

where $\nu$ is the kinematic viscosity of the water, and $Sc = \nu/D_W$.[26] Subsequently, Schmidt numbers ($Sc$) were used to deduce the thickness of the laminar boundary layer, $\delta_W$, for the PCBs.

### 1.2.4 EFDC Model Development

Freshwater enters the 5-mi long LDW from the south and is eventually transported to the saline Elliott Bay located to the north. The LDW is a vertically stratified estuary with 3 m semi-diurnal tides and an average depth of 8 m. The saline water of the bay causes a salt wedge to push upriver with every flood tide, reversing the direction of the current when river discharge is low and inhibiting vertical mixing. These characteristics invalidate simple hydrodynamic models of the estuary and so require advanced techniques to determine the transport of contaminants in the estuary's water column. Previous transport modeling for the LDW estuary has been accomplished using the EFDC, tuned to this site's geometry, tidal amplitudes, and varying river discharge.[19]

Hence, we used the EFDC, a finite difference numerical model, to simulate the three-dimensional estuarine water flows and the transport of PCBs in the LDW. The EFDC was originally set up and validated for the site by King County, WA in 1999.[27] The model was updated in 2006 by King County and used in the RI/FS phase of Superfund remediation.[2] Site bathymetry was based on surveys conducted in 2003.[2] A curvilinear-orthogonal horizontal grid was used to represent the LDW study area (Figure 2), as well as Elliott Bay and an upriver section 7 mi in length. The LDW was represented by 35 cells longitudinally, and at least three cells laterally, giving an average cell size of 240 m long by 60 m wide for 115 total cells. Vertically, the water column was represented by 20 evenly spaced layers, allowing layer thickness to vary with total depth (stretched sigma). Courant number constraints, quantified during model development, necessitated a time step of 2 s. The model simulation began 1 month before the passive sampler deployment date, which was confirmed to be a sufficient warm-up period to "forget" initial conditions. For this work, we updated the boundary conditions for the summer of 2014. This included tidal forcing at the west end of Elliott Bay,[28] Green River discharge measured approximately 18 km and 2 km south of the river mile 5 of the LDW site,[29] and flow from storm water outfalls calibrated to rainfall data through a runoff model.[19]

The only calibration step involved matching water levels and their tidal timing to observations at a gauge located at Seattle Pier, Elliott Bay. Model validation was done using field measurements taken during sampler deployment and recovery. These included: conductivity, temperature, and depth measurements (conductivity-temperature-depth profiler (CTD)-Diver, Van Essen, Delft, Netherlands), as well as ADCP profiles of the entire water column (WorkHorse Sentinel, Teledyne Marine, Boston, MA). Depths were accurate to within 0.5 m (Table S15), and velocities to within 0.4 cm/s (Table S16). Salinity values matched within 0.3 practical salinity unit (PSU) for most areas, but measured vertical profiles tended to have a sharper halocline than the EFDC model estimates. This issue arose from insufficient resolution of the vertical grid through the estuary's halocline. However, in this paper all our water column samples were located within 1 m of the sediment bed, well within the salt wedge for all but the most upriver samples.

The impacts of PCB fluxes from the sediment bed were modelled in the water column by assuming the PCBs behaved as conservative, dissolved-phase tracers introduced in the model to the bottom layer of the water column grid. We note that the typical particulate organic carbon concentration in the LDW is about 0.3 mg/L[30]; this implies PCB congeners with $K_{oc}$ values less than $10^{6.6}$ (i.e., most heptachlorobiphenyls and less chlorinated congeners based on $K_{oc}$ values of Hansen et al.[31]) are mostly dissolved. Input locations were based on PE sampler stations, and Thiessen polygons were used to interpolate between stations. Thiessen polygons are appropriate for sparse data where a semivariogram cannot be developed and are well suited for EFDC's curvilinear grid. The magnitudes of simulated PCB inputs were set to match the sampler-estimated fluxes, including their confidence intervals deduced using Monte Carlo (MC) methods (see below).

### 1.2.5 Error Analysis

Propagation of uncertainty was calculated using MC methods, where each input was randomly varied based on a normal distribution with a standard deviation equal to its literature uncertainty or observed variance. These iterations ($N$=$10^4$) created an empirical distribution, which was used to judge the significance of results based on percentiles corresponding to typical confidence intervals. MC error distributions have been successfully applied to passive sampling elsewhere.[24,32]

## 1.3 RESULTS AND DISCUSSION

### 1.3.1 Sediment Porewater-Bottom Water Concentration Differences

Freely dissolved concentrations of individual PCBs were readily measured in both LDW porewater and the water column at picogram per liter levels (Figure 3 and Appendix E for porewater, Appendix F for bottom water, and Appendix G for water 1 m above the sediment bed) using the PE passive samplers as we have reported previously for a small number of stations.[24, 33] Aggregating, we found "total measured" PCBs (= $\Sigma_{18}$ NOAA congeners[34] plus two dioxin-like congeners 77 and 126 and henceforth referred to here as $\Sigma_{20}$PCB) in the porewater of the uppermost sediment across 19 stations ranged from 350-1800 pg/L, with an arithmetic mean of 850 pg/L. Across all stations, bottom water concentrations tended to be lower, with a range of 380-900 pg/L and average value of 640 pg/L. Porewater concentrations were also much more variable (coefficient of variation (CV) of 48%) than the bottom water concentrations (26% CV), including larger differences between stations (Figure 3). The lower degree of variation in the water was likely due to better homogenization in the water column than in the sediment bed. Three 'hotspots' were detected at sediment stations near river miles 0.5, 2.2, and 3.6 (Figure 3), corresponding to known hotspots previously reported[2] (Figure 1).

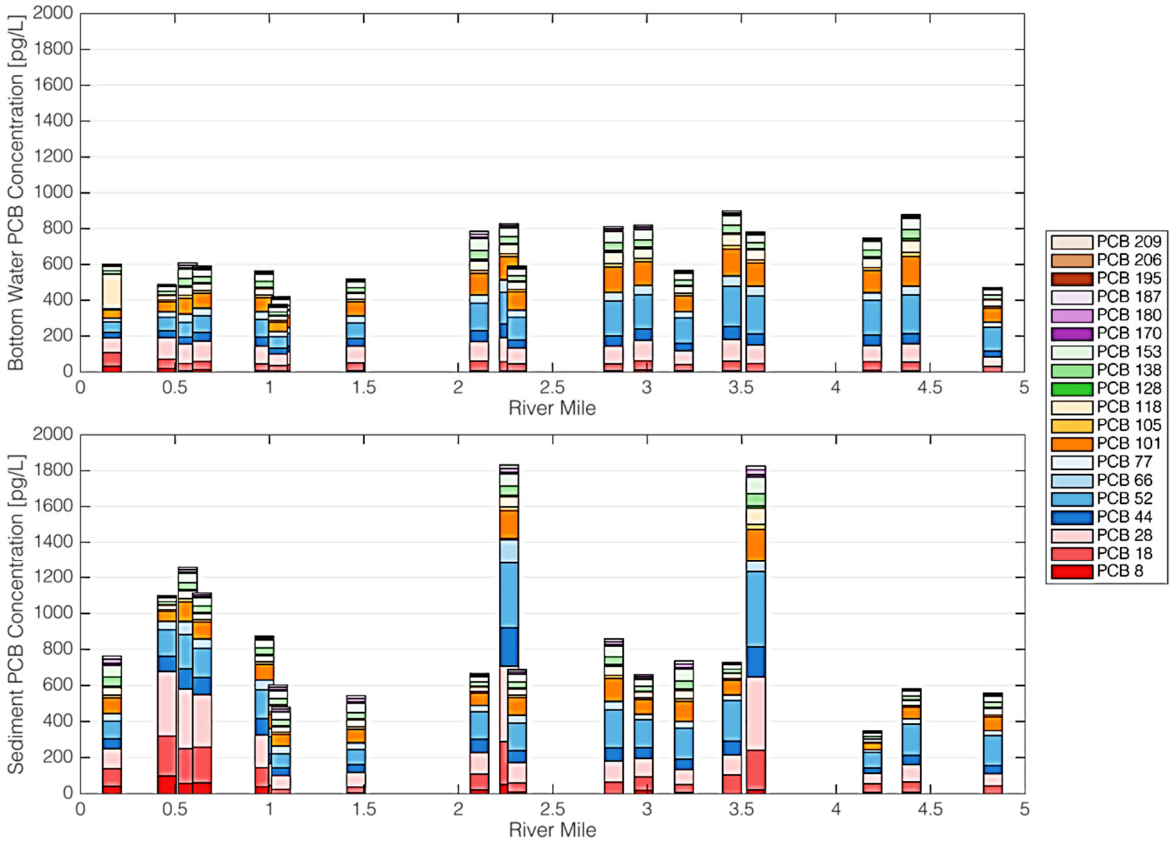


**Figure 3. Freely Dissolved PCB Concentrations in Bottom Water (Upper Panel, 0-5 cm Above Interface) and Sediment porewater (Lower Panel, 0-5 cm Below Interface) as a Function of Position Indicated by River Mile.**

*Colors correspond to individual PCB congeners, ordered by congener number, and color-grouped by degree of chlorination (e.g., reds all trichloro, blues all tetrachloro, etc.) Congener 126 was not detected.*

Individual PCB congeners showed unique behaviors. Lighter congeners (congener #s 8 to 77 with 2 to 4 chlorines) make up a majority of the mass of freely dissolved PCBs, and tended to have net fluxes out of the sediment. Congeners with a higher degree of chlorination (congener #101 and higher with 5 to 7 chlorines) tended to have either a net flux into the sediment or showed no statistically significant bed-to-water gradient. Our minimum (statistically significant) ΔC was about 15 pg/L. Most of the stations with negative fluxes (i.e., negative ΔC values implying transport into the bed) were located upstream of river mile (RM) 2.8, although positive flux locations could be found throughout the LDW, especially for smaller congeners.

### 1.3.2 Estimation of Mass Transfer Rates

Having estimated the freely dissolved concentration gradients using passive samplers, the remaining parameter in diffusive flux calculations is the diffusive boundary layer thickness, $\delta_W$ (Eq. 3). The ADCP velocity profiles gave fitted shear velocities, $u^*$, between 0.33-1.15 cm/s, with coefficients of variation of 16-38%. These observed shear velocities were similar to results reported by others for shallow, tidal environments[35,36,37]. The observed shear velocities implied the diffusive boundary layer, $\delta_W$, was typically between 100 and 300 μm.

In order to compute the diffusive WBL thicknesses ($\delta_W$) over the entire waterway, the EFDC was used to find $u$(EFDC) for the seven times/places where we got ADCP results. Then using a logarithmic interpolation of the bottom cell's top and bottom interfacial velocities, $u^*$(EFDC) was found in a manner consistent with how the source code calculates bottom shear stress[38]. Finally, these seven specific EFDC-inferred $u^*$ results were correlated with shear velocities derived from the ADCP measurements (Figure 4a). This correlation was then used to compute the EFDC-estimated $u^*$ for use in Equation (3) at all the passive sampling sites.

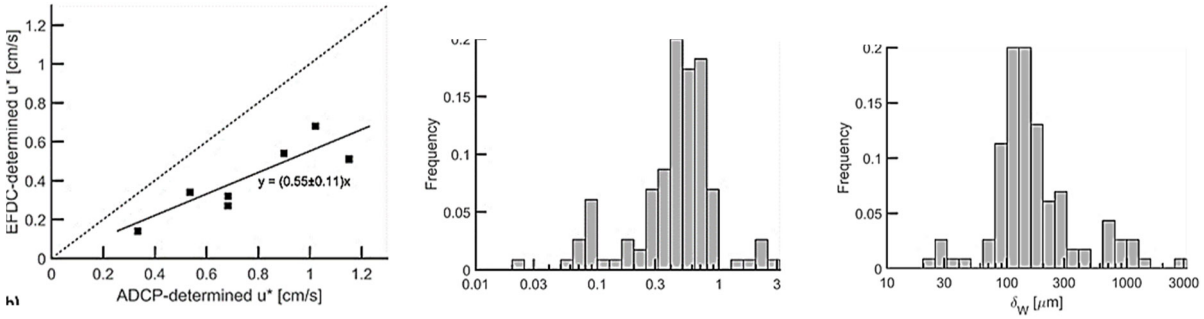


**Figure 4. (a) Comparison of ADCP-determined Shear Velocities u* [cm/s] and EFDC-Inferred Shear Velocities at the Same locations and times. The Solid Line Is the Linear Least Squares Best Fit with a Zero Intercept (r2=0.77). (b) Frequency Distribution of Time-averaged EFDC Predictions, Using the Fit from (a), Plotted on a Log Scale. (c) Frequency Distribution of $\delta_W$ [μm], converted from values in (b) Using Equation 3 and a Congener-average Aqueous Diffusivity, $D_w$.**

The usefulness of EFDC-predicted shear velocities was demonstrated by examining their spatial distribution across the entire LDW site. The majority of $u^*$ values fall between 0.3-1 cm/s, with a median of 0.5 cm/s and a longer tail toward lower values (Figure 4b). The corresponding $\delta_W$ values (Equation 3) fall between 60-500 μm with a median value of 140 μm (Figure 4c).

Unsurprisingly, maps of $\delta_W$ across the LDW showed that the largest values occur in stagnant areas: the slips that jut laterally from the main channel, the tidal flats to the west of the RM 0.5 island, and upstream corners where the channel was artificially widened. The lowest values, and thus the largest mass transfer coefficients ($=D_W/\delta_W$), occurred in the narrow upstream portion of the study site, and at RM 1.3 and RM 2.5, where active storm water outfalls introduce water to a relatively narrow point of the LDW. During deployment, a rainfall event caused these outfall discharges to be comparable to the river discharge, increasing local velocities. Overall, the spatial variation of $\delta_W$ was comparable to the between-station variation in ΔC. Thus, both factors significantly affect between-station PCB flux estimates, and reinforce the necessity of using a model to capture the spatial distribution of bed-to-water inputs.

### 1.3.3 PCB Flux Distribution

PCB fluxes were calculated for each congener at each of the 19 stations. Of the 380 possibilities (19 stations times 20 congeners), 297 paired samples had concentrations above detection limits both above and below the bed-water interface. Four congeners, 126, 195, 206, and 209, accounted for 76 of the 83 undetected cases. Of the 297 ΔC values calculated, 67% indicated a net flux into the water column, although only 11% were significantly different from zero at the 2σ significance level, and 37% at the 1σ level. The largest concentration gradients, ΔC, occurred at river miles 0.5, 2.3, and 3.6, and these translated to the largest fluxes (Figure 5). The uncertainties associated with the ΔC results were logarithmic, with a larger uncertainty in the positive flux direction (caused by uncertainties in the sediment porewater concentration). Thus, the largest flux (PCB 28 at RM 3.6) has a median value of 100 ng/m$^2$/d, but a ±1σ confidence interval of 23-260 ng/m$^2$/d. In general, most of the upward fluxes were composed of lighter PCBs, especially congeners 18, 28, 44 and 52. Conversely, the largest fluxes into the bed were on the order of -30 ng/m$^2$/d for pentachlorinated congeners (e.g., #101) and some tetra- and hexa- chlorinated congeners. Larger congeners showed near equilibration across the study area, with absolute fluxes of less than 6 ng/m$^2$/d.

The congener-specific fluxes were dominated by the same three hotspots identified by ΔC measurements. These hotspots had much larger fluxes (18-100 ng/m$^2$/d for individual congeners) than the other stations. Outside of the hotspots, nearly all of the congeners showed a net positive flux into the water column for RM 0 to 2.5, with the reverse occurring upstream. This suggests a portion of the mobilized PCBs are being reintroduced to the upstream sediment bed after downstream mobilization, likely assisted by the reverse current imposed by the advancing salt wedge during flood tides. We noted that the EFDC model, running with the river discharge condition at the time of the sampling, showed that the salt wedge extends to about RM 2 at low tide, but then goes past RM 4.5 at the high tide. Hence, calculating the extent of this upstream PCB transport contribution requires a mass balance that incorporates such complex hydrodynamic transport.

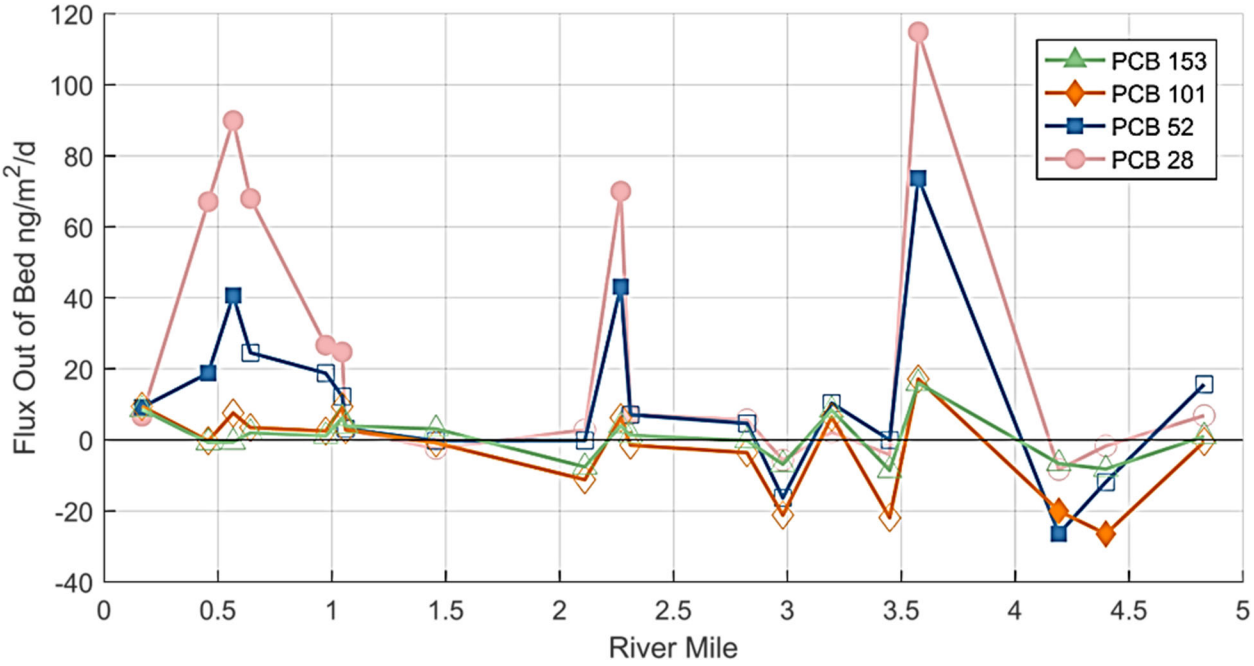


**Figure 5. Estimated Diffusive Fluxes of Selected Congeners as a Function of RM in the LDW.**

*Filled symbols indicate the fugacity ratio was more than two standard deviations from unity. All confidence intervals can be found in Table S17. Lines are included for visual aid only.*

### 1.3.4 Diffusive Mass Input Rate

Fluxes for each PCB congener from the 19 stations were summed, after weighting with Thiessen polygon areas, across the entire study area to calculate the overall diffusive mass input into the LDW. The time-averaged values of $u^*$ from EFDC-ADCP modeling and $\Delta C$ from passive sampler measurements were used to calculate time-averaged fluxes. We expected a time-invariant value to represent the fluxes accurately over the deployment time because there was only a single significant rain event to change upstream discharge (average value of 19.0 $m^3/s$ with rain event, 18.3 $m^3/s$ without). In addition, contaminant fluxes based on tidal-average shear velocities differed only slightly from integrating tidally varying fluxes over a tidal cycle.[39]

Sediment-source diffusive inputs of specific PCBs, once integrated across the study area, ranged from 0.6 mg/d (PCB 77) to 52 mg/d (PCB 28), with a $\Sigma_{20}$PCB value of 240 [200,320] mg/d. The MC-derived flux uncertainties were carried into the site-wide integrations, allowing for propagation of passive sampler and ADCP data uncertainties. Notably, the Thiessen polygon weighting technique caused the spatially integrated PCB source strengths to have a normal distribution, likely due to its similarity to arithmetic averaging. However, the spatial distribution is heterogeneous. For example, the polygon corresponding to RM 0.5 contributed 11% of the total diffusive mass input of $\Sigma_{20}$PCBs, despite only covering 2.2% of the total area, making it a prime target for remediation. At the same time, 43% of the diffusive mass input occurred in areas not identified as hotspots, making complete remediation difficult if diffusive inputs from the sediment bed are an important ongoing input.

### 1.3.5 The Diffusive Source from the Sediment Bed Hypothesis

The hypothesis that PCB diffusion from the sediment is the most important source to the LDW water column was first tested using a direct comparison of simulated and observed water column PCB concentrations. EFDC-inferred water column concentrations were calculated assuming diffusive inputs from the sediment bed, as determined by interfacial passive samplers and ADCP/EFDC WBL estimates, were the only PCB source fluxes. The resultant EFDC-simulated PCB congener concentrations were all near 1 pg/L. However, PE-determined water column concentrations of PCB congeners were much larger (10-100 pg/L), even at the 95% confidence limits (Figure 6). Thus, the concentration gap indicates that diffusive flux from the sediment bed is not sufficient to account for the concentrations seen in the water column. Lower limit estimates of the size(s) of the missing source(s) can be estimated by taking the difference between the LDW-wide estimates of diffusion from the sediments minus the overall flushing of PCBs assuming only river flow flushing (i.e., neglecting tidal dispersion of PCBs into Elliott Bay) (Table 1). These calculations, with associated error bounds, strongly suggest other important sources or bed-to-water transfer mechanisms are present at this site and/or time.

**Table 1. Mass Balances of Selected Congeners.**

*Total diffusive inputs were obtained using an LDW sediment surface area of 1.8x106 m2. Flushing rates assumed an average discharge of 1.7x10$^6$ m$^3$/day. Brackets indicate the 1σ confidence limits, [lower upper] from error propagation. The negative net mass balances indicate missing source(s).*

| | **PCB 28** | **PCB 52** | **PCB 101** | **PCB 153** | **$\Sigma_{20}$ PCBs** |
|---|---|---|---|---|---|
| Area-weighted Diffusive Fluxes [ng/m$^2$/d] | 29 [19 49] | 20 [8.5 41] | 5 [-2 18] | 6 [2 15] | 130 [110 180] |
| Diffusive Mass Inputs [mg/d] | 52 [32 90] | 35 [15 75] | 8 [-4 33] | 11 [3 27] | 240 [200 320] |
| Average Water Concentrations [ng/m$^3$] | 99 [59 170] | 130 [82 220] | 84 [54 130] | 37 [22 60] | 660 [510 860] |
| Flushing Rates [mg/d] | 160 [97 280] | 220 [130 370] | 140 [89 220] | 60 [37 99] | 1100 [520 1400] |
| Net Mass Balances [mg/d] (In-Out) | -110 [-190 -74] | -180 [-290 -140] | -130 [-180 -100] | -49 [-76 -33] | -840 [-1000 -720] |

The varying gap between modeled and measured water column concentrations of individual PCB congeners speaks to the nature of the missing source. While the averaging metric, $\Sigma_{20}$PCB, would need to have a 14-fold increase in fluxes for EFDC modeling to match the water column concentrations, the missing source strength needs to be elevated by only about a factor or 10 for PCB trichloro- and heptachloro-congeners, but by a much larger factor of about 60 for the pentachloro- congeners. As the diffusive source strength goes down moving through the series #28: #52: #101: #153 (Table 1), uniformly amplifying the diffusion source of all congeners will not explain the water column congener presence found. Hence, the missing source/mechanism(s) must mostly enhance the pentachlorinated congener fluxes, while affecting both lighter and heavier congeners to less extent. We note that active mechanisms, such as bioirrigation, are best suited to transferring lighter congeners,[40] while mechanisms such as colloid-assisted diffusion from the bed or desorption from resuspended sediment particles would favor the heavier congeners.[9] Hence, further work is needed to identify these missing source(s)/mechanism(s).

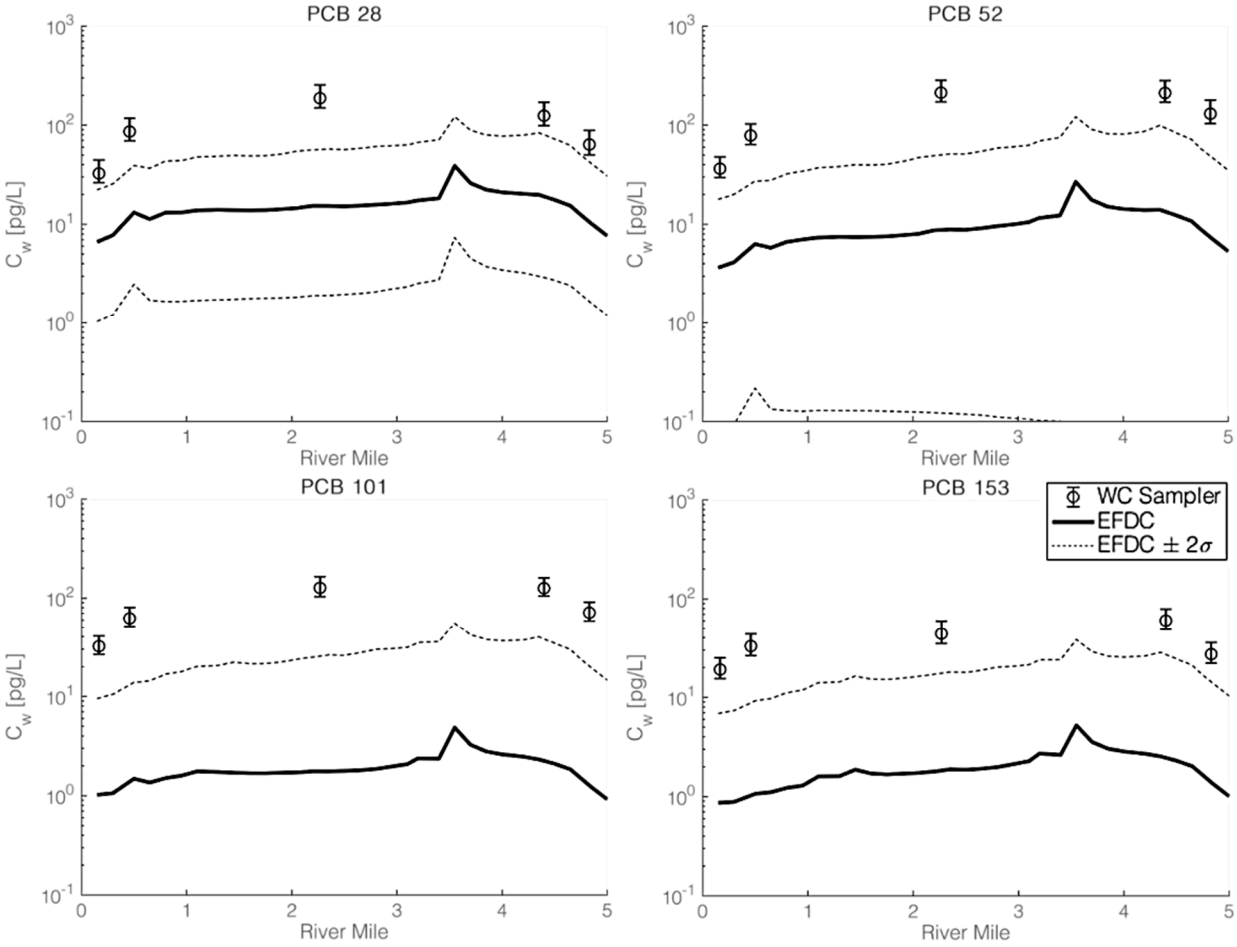


**Figure 6. Freely Dissolved Concentrations of Four PCB Congeners Over Longitudinal River Distance.**

*Black circles are passive sampler-estimated concentrations measured 1 m above the sediment bed with ±1σ uncertainty. The black lines are time-averaged EFDC concentration predictions at 1 m above the bed in the water column. Dashed lines are the upper and lower uncertainty bounds on unscaled EFDC predictions.*

## 1.4 LIMITATIONS AND FUTURE STUDIES

Most of the steps taken in this work to quantify the PCBs' diffusive fluxes from the sediment bed erred on the side of over-estimating their magnitudes. For example, given the ADCP-based boundary layer thickness and assuming that only molecular diffusion across a WBL limited overall PCB fluxes from the bed for the LDW, this site's bed-water diffusive mass transfer coefficient, kf, should have been about 20-60 cm/d for the weighted average PCB. This is larger than what has been found necessary to fit PCB data at other sites such as the Hudson River [4,15].

Despite using assumptions that maximized the flux estimates, our results imply the PCB inputs necessary to generate observed concentrations in the water column have to be substantially larger than our diffusive flux estimates. It is theoretically possible that the 19 stations distributed across a 4.7-mile-long site missed hotspots. However, the 'missing hotspot' would have to be about 20

times larger than the hotspot at RM 0.5 in either gradient magnitude (total $\Sigma_{20}$PCB input of 990 mg/d) or bottom area (covering more than three times the 1.8 $km^2$ study area), which are both unlikely. In addition, considering the spatial distributions of the RI/FS sediment concentration data (Figure 1), the sampler locations should have had higher sediment concentrations than the site as a whole, leading to a positive bias for overall diffusive flux estimates.

We note that inputs from upstream were insufficient to explain the water column concentrations that was found. Also, bioturbation of the sediment does not appear sufficient to cause the needed PCB inputs.[40] Either other bed-to-water transfer mechanisms (e.g., colloid-mediated diffusive transfers or repeated sediment resuspensions of PCB-contaminated sediment with associated PCB desorption)[9] or other inputs (e.g., outfalls with PCB-contaminated effluents) must be important contributors. This implies dredging of quiescent, contaminated sediments may not be an effective approach for lowering the chemical activities of pollutants in the waters overlying such a site.

We suggest further, spatially distributed; water column measurements can be used to obtain a more accurate understanding of the PCB's sources at such a complex site. In particular, passive sampling taken both below and above the salt wedge would be especially valuable, as they may reveal PCB sources such as storm water runoff and groundwater seeps. For other dynamic, aqueous environments, a combination of passive sampler measurements with hydrodynamic modelling will likely produce the detailed spatial concentration map necessary for source determination and contaminant exposure.

## 1.5 LITERATURE CITED


1. *The Incidence and Severity of Sediment Contamination in Surface Waters of the United States National Sediment Quality Survey: Second Edition;* EPA-823-R-04-007; EPA; Washington, D.C., 2004.

2. AECOM. Site Setting, RI Summary, and Current Conditions. *Final Feasibility Study, Lower Duwamish Waterway;* U.S. Environmental Protection Agency: Seattle, WA, 2012; 67.

3. Velleux, M.; Endicott, D. Development of a mass-balance model for estimating PCB export from the lower Fox River to Green Bay. *J. Great Lakes Res.* **1994,** 20, 416-434.

4. Connolly, J.P.; Zahakos, H.A.; Benaman, J.; Ziegler, C.K.; Rhea, J.R.; Russell, K. A model of PCB fate in the Upper Hudson River. *Environ. Sci. Technol.* **2000**, 34, 4076-4087.

5. Booij, K.; Hoedemaker, J.R.; Bakker, J.F. Dissolved PCBs, PAHs, and HCB in pore waters and overlying waters of contaminated harbor sediments. *Environ. Sci. Technol.* **2003,** 37, 4213-4220.

6. Cornelissen, G.; Wiberg, K.; Broman, D.; Arp, H.P.H.; Persson, Y.; Sundqvist, K.; Jonsson, P. Freely dissolved concentrations and sediment-water activity ratios of PCDD/Fs and PCBs in the open Baltic Sea. *Environ. Sci. Technol.* **2008,** 42, 8733-8739.

7. Fernandez, L.A.; MacFarlane, J.K.; Tcaciuc, A.P.; Gschwend, P.M. Measurement of freely dissolved PAH concentrations in sediment beds using passive sampling with low density polyethylene strips. *Environ. Sci. & Technol*. **2009**, 43, 1430-1436.

8. Di Toro, D.M., Zarba, C.S., Hansen, D.J., Berry, W.J., Swartz, R.C., Cowan, C.E., Pavlou, S.P., Allen, H.E., Thomas, N.A., and Paquin, P.R. Technical basis for establishing sediment quality criteria for nonionic organic chemicals using equilibrium partitioning. *Environ. Toxicol. Chem*. **1991**, 10, 1541-1583.

9. Achman, D.R., Brownawell, B.J., and Zhang, L. Exchange of polychlorinated biphenyls between sediment and water in the Hudson River Estuary. Estuaries **1996**, 19(4), 950-965.

10. Gustafsson, Ö., Haghseta, F., Chan, C., MacFarlane, J.K., and Gschwend, P.M. Quantification of the dilute sedimentary soot phase: Implications for PAH speciation and bioavailability. *Environ. Sci. Technol*., **1997**, 31, 203-209.

11. Accardi-Dey, A. and P.M. Gschwend. Assessing the combined roles of natural organic matter and black carbon as sorbents in sediments. *Environ. Sci. Technol*., **2002**, 36, 21-29.

12. Lohmann, R., MacFarlane, J.K., and Gschwend, P.M. Importance of black carbon to sorption of native PAHs, PCBs, and PCDDs in Boston and New York harbor sediments. *Environ. Sci. Technol.* **2005,** 39, 141-148.

13. Koelmans, A.A., Michiel T.O. Jonker, M.T.O. Effects of black carbon on bioturbation-induced benthic fluxes of polychlorinated biphenyls. *Chemosphere* **2011**, 84, 1150–1157.

14. Totten, L.A, Brunciak, P.A., Gigliotti, C.L., Dachs, J., Nelson, E.D., Eisenreich, S.J. Dynamic air−water exchange of polychlorinated biphenyls in the New York−New Jersey Harbor Estuary. *Environ. Sci. Technol.*, **2001**, 35(19), 3834–3840.

15. Thibodeaux, L.J.; Bierman, V.J., 2003. The bioturbation-driven chemical release process. *Environ. Sci. Technol.* **2003,** 37(13), 252A.

16. EPA/SERDP/ESTCP. **2017**. Laboratory, Field, and Analytical Procedures for Using Passive Sampling in the Evaluation of Contaminated Sediments: User's Manual. EPA/600/R-16/357. Office of Research and Development, Washington, DC 20460.

17. Ghosh, U., Kane Driscoll, S., Burgess, R.M., Jonker, M.T.O., Reible, D., Gobas, F., Choi, Y., Apitz, S.E., Maruya, K.A., Gala, W.R., Mortimer, M., and Beegan, C. Passive sampling methods for contaminated sediments: Practical guidance for selection, calibration, and implementation. *Integr. Environ. Assess. Manag*. **2014**, 10(2), 210-223.

18. Hamrick, J.M.; Wu, T.S. Computational design and optimization of the EFDC/HEM3D surface water hydrodynamic and eutrophication models. In *Next generation Environmental Models and Computational Methods*; Society for Industrial and Applied Mathematics; Philadelphia, **1997**; p 143.

19. Nairn, B. EFDC *Calibration Process for predicting PCB water concentrations in Lower Duwamish Waterway.* King County Department of Natural Resources: Seattle, WA, **2009**.

20. Fernandez, L.A.; Harvey, C.F.; Gschwend P.M. Using performance reference compounds in polyethylene passive samplers to deduce sediment porewater concentrations for numerous target chemicals. *Environ. Sci. Technol.* **2009,** 43(23), 8888-8894.

21. Apell, J.N.; Gschwend, P.M. Validating the use of performance reference compounds in passive samplers to assess porewater concentrations in sediment beds. *Environ, Sci. Technol.* **2014,** 48, 10301-10307.

22. Tcaciuc, A.P.; Apell, J.N.; Gschwend, P.M. 2014. Passive Sampler PRC Calculation Software and User's Guide. https://www.serdp-estcp.org/content/download/31378/299829/file/ER-200915 Passive Sampler PRC Calculation Software User's Guide.pdf.

23. Tcaciuc, A.P.; Apell, J.N.; Gschwend, P.M. Modeling the transport of organic chemicals between polyethylene passive samplers and water in finite and infinite bath conditions. *Environ. Toxicol. Chem.* **2015,** 34(12), 2739-2749.

24. Apell, J.N.; Gschwend, P.M. The atmosphere as a source/sink of polychlorinated biphenyls to/from the Lower Duwamish Waterway Superfund site. *Environ. Pollut.* **2017,** 227, 263-270.

25. Tennekes, H.; Lumley, J.L., A first course in turbulence, 300 pp. The MIT Press, Cambridge, MA. 1972.

26. Shaw, D.A., Hanratty, T.J. Turbulent mass transfer rates to a wall for large Schmidt numbers. *AICHE J.* **1977**. 23, 28-37.

27. King County Combined Sewer Overflow Water Quality Assessment for the Duwamish River and Elliott Bay. *Appendix B1: Hydrodynamic and Fate and Transport Numerical Model for the Duwamish River and Elliott Bay;* King County Department of Natural Resources: Seattle, WA, 1999.

28. NOAA Tides & Currents. https://tidesandcurrents.noaa.gov/stationhome.html?id=9447029 (accessed June, 2017).

29. USGS Current Conditions for the Nation. https://waterdata.usgs.gov/usa/nwis/uv?12113415 (accessed June, 2017).

30. Windward Environmental. Lower Duwamish Waterway Remedial Investigation. June 2010.

31. Hansen B.G., Paya-Perez A.B., Rahman M., Larsen B.R. QSARs for $K_{ow}$ and $K_{OC}$ of PCB congeners: A critical examination of data, assumptions, and statistical methods. *Chemosphere* **1999**, 39: 2209-2228.

32. Liu, Y.; Wang, S.; McDonough, C.A.; Khairy, M.; Muir, D.; Lohmann, R. Estimation of uncertainty in air-water exchange flux and gross volatilization loss of PCBs: A case study passed on passive sampling in the lower Great Lakes. *Environ. Sci. Technol.* **2016,** 50(20), 10894-10902.

33. Apell, J.N.; Gschwend, P.M. *In situ* passive sampling of sediments in the Lower Duwamish Waterway Superfund site: Replicability, comparison with *ex situ* measurements, and use of data. *Environ. Pollution* **2016,** 218, 95-101.

34. Fikslin, T.J., Santoro, E.D. PCB congener distribution in estuarine water, sediment and fish samples: Implications for monitoring programs. *Environ. Monitor. Assess.* **2003, 87, 197-212.**

35. Cheng, R.T.; Ling, C.-H.; Gartner, J.W. Estimates of bottom roughness length and bottom shear stress in South San Francisco Bay, California. *J. Geophys. Res*. **1999**, 104, 7715-7728.

36. Kim, S.-C.; Friedrichs, C.T.; Maa, J.P.-Y.; Wright, L.D. Estimating bottom stress in tidal boundary layer from acoustic Doppler velocimeter data. *J. Hydraulic Eng*. **2000,** 126, 399-406.

37. Inoue, T.; Glud, R.N.; Stahl, H.; Hume, A. Comparison of three different methods for assessing in situ friction velocity: A case study from Loch Etive, Scotland. *Limnol. Oceanogr. Methods.* **2011**, 9, 275-287.

38. Tetra Tech, Inc. The Environmental Fluid Dynamics Code Theory and Computation. Volume 2: Sediment and Contaminant Transport and Fate. see Section 4, Eq. 4.16 and following. Fairfax, Va. 96 pp. June 2007.

39. Wang, Y. Sediment Flux Modeling of Nutrients and Organic Pollutants. Ph.D. Thesis, Tufts University, February 2017.

40. Apell, J.N.; Shull, D.H.; Hoyt, A.M.; Gschwend, P.M. Investigating the effect of bioirrigation on *in situ* porewater concentrations and fluxes of polychlorinated biphenyls using passive samplers. *Environ. Sci. Technol.* **2018** 52, 4565-4573.

# SECTION 2 INVERSE MODELING TO FIT PCB CONCENTRATION DISTRIBUTIONS FOUND BY PASSIVE SAMPLING IN THE SITE'S WATER COLUMN

## 2.1 BACKGROUND

In waterbodies where pollution sources have distinguishable signatures depending on their location, an inverse model can in principle be used to infer source locations and strengths from measured dissolved phase concentrations. This approach does not require an initial hypothesis of source locations or types and can begin to provide insights with a relatively small number of measurements.

Dissolved phase PCB concentrations measured during the three passive sampling campaigns show widespread contamination in the LDW, which was used as a test bed for the inverse modeling approach. There are various ways in which these PCBs could have been introduced to the water column. Possible sources of dissolved PCB contamination to the water column include, but are not limited to, (a) the sediment bed within the domain, which may act as a source to the water column via diffusion or advection processes (e.g., sediment mixing, bio-irrigation, hyporheic flow or groundwater flow) or by desorption from sediments resuspended by natural currents or human activity (e.g., tug boats); (b) the upstream freshwater input or the tidal exchange with Elliott Bay at the downstream boundary; (c) lateral sources such as combined-sewer overflows, stormwater outfalls, and direct runoff; and (d) atmospheric inputs (air-water exchange or atmospheric deposition). In order to guide further site characterization and remediation efforts, it is desirable to assess the type and location of sources of pollution.

### 2.1.1 The Inverse Model

An inverse problem generally involves using measurements to infer the parameters that generated them, contextualized by a physical model (Tarantola, 2005). Inverse problems have been used in many fields, including heat transfer (Ozisik, 2018), electromagnetism (McCormick, 1992), geophysics (Wiggins, 1972), and groundwater transport (Yeh, 1986). Research in atmospheric transport has also used this approach to locate pollution sources by coupling reaction-transport models to inverse model solutions (Foy et al., 2012; Henze et al., 2009; Stohl et al., 2009); with prior estimates of ground source emissions, these models can be used to estimate source strengths from a large grid of potential sources.

For the present application of assessing water column PCB contamination in the LDW, we are interested in using measurements of dissolved phase PCB concentrations to help identify the likely location of the sources that resulted in the measured concentrations. By the principle of super-position, the concentration measured at a given location will reflect the sum of concentrations at that location contributed by a multitude of sources. In this framework, the contribution from a particular source location to a particular measurement location may be expressed as the contribution of a source with unit strength multiplied by a weighting factor to estimate the actual strength of that source. Therefore, the measured concentration ($C_l$) at any sampling location $l$ can be represented by a sum of contributions from a multitude of different unit sources ($s$) weighted by their relative strengths ($w_s$), i.e.,

$$C_l = w_{s=1} b_{l,s=1} + w_2 b_{l,2} + w_3 b_{l,3} + \cdots = \sum_{s=1}^{S} w_s b_{l,s} \qquad (1)$$

Here, $b_{l,s}$ is the concentration at the sampling location $l$ from a unit source of contamination at location, $s$. The inverse model uses concentration measurements to infer source strengths. The inverse model allows the user to:

- Assess the potential location of sources of contamination and source strengths that are consistent with field measurements.
- Predict contaminant concentrations throughout the domain of interest which are generated by the sources identified by the method.
- Assess potential benefits of removing the sources identified by the method.

## 2.2 METHODS

Eq. (1) shows how the concentration measured by a sampler depends on the response from various sources and their strengths. For a total $L$ sampler locations and $S$ potential sources, this relationship can be represented as a linear system of equations. In matrix form, the system is represented as:

$$\begin{bmatrix} C_1 \\ C_2 \\ \vdots \\ C_L \end{bmatrix} = \begin{bmatrix} b_{11} & b_{12} & \cdots & b_{1S} \\ b_{21} & b_{22} & \cdots & b_{2S} \\ \vdots & \vdots & \ddots & \vdots \\ b_{L1} & b_{L2} & \cdots & b_{LS} \end{bmatrix} \begin{bmatrix} w_1 \\ w_2 \\ \vdots \\ w_L \end{bmatrix} \qquad (2a)$$

or equivalently

$$\boldsymbol{C_L = b_{L,S} w_S} \qquad (2b)$$

The matrix $\boldsymbol{b_{L,S}}$ represents the "fingerprints" of each potential source at the sampler locations, which depend on the transport characteristics of the waterbody and the contaminant of interest.

The inverse model simultaneously solves the system of equations for source strength ($w_S$) of each potential source, given the sampler measurements ($C_L$), and the fingerprint matrix ($\boldsymbol{b_{L,S}}$). For this application of the inverse model to assess source locations, we have constrained the fitted source strengths to be non-negative, i.e., the model does not allow for a contaminant sink in fitting the solution. We note that the passive sampling measures across the bed-water interface (Section 1 of this report) sometimes identified locations, especially at up-river stations, where gradients would imply some PCB congeners would be diffusing from the water column into the bed. The inverse model was also tested without this constraint but these results are not reported as they were characterized by unrealistically large sources and offsetting sinks in the domain.

The fingerprint matrix is quantified using numerical simulations of tracers in the water column. For each potential source location, a unique tracer is introduced to the system at the location of the source, and its influence on the domain is simulated for the period of interest. In the present application, this was done using the hydrodynamic model, EFDC, developed by the EPA, to simulate passive tracers, i.e., substances assumed to undergo no transformations. All tracer inputs were set to the same magnitude (1 mg/s) and, as passive tracers, they do not interact with water column organic matter, the sediment bed, or the atmosphere1. The value of each source "fingerprint" ($b_{l,s}$) is calculated by averaging the model-predicted tracer concentrations of the unit sources over the deployment period.

Because the LDW is a tidal system with significant changes in water surface elevation over the measurement period, it was necessary to account for the time-varying vertical position of a fixed passive sampler within the model grid (EFDC). For example, if a sampler is located 2 ft below the water surface and the instantaneous water depth at that location is 10 ft, then the sampler will be located in the 17$^{th}$ vertical layer in the EFDC implementation applied herein (EFDC was here set up to have 20 vertical layers of equal thickness2 at each horizontal location and the first layer is at the bottom of the water column). As the water depth at a given horizontal location changes with time (due to the tides), the vertical layer in which this sampler resides also changes with time. Figure 1 shows the tracer concentrations resulting from one source and the vertical position (in terms of layer index) of 4 samplers deployed at one horizontal location, but at 4 different depths (2 and 5 ft below the surface and 2 and 5 ft above the sediment bed).

1 Simulating dissolved contaminant concentration using passive tracers means that hydrodynamic advection and dispersion are the only transport processes accounted for, which ignores several processes that may influence concentration dynamics and the mass balance in a contaminant-specific fashion. This was judged to be an acceptable simplification because the focus of the present effort was on exploring an inverse modeling approach that may be used in combination with passive samplers to assess source dynamics. The inverse modeling technique described herein is generally compatible with any predictive transport model, and future efforts could evaluate how inclusion of chemical-specific transformation and transport processes influence the inverse model's source assessment. The EFDC model used herein is equipped to represent sediment transport and chemical fate and transport processes, but these were not parametrized or calibrated in the LDW configuration adopted and it was beyond the scope of the present investigation to incorporate them.

2 EFDC uses a sigma-coordinate system, meaning that the vertical layers are always of equal thickness and they expand and contract in response to changes in the water surface elevation.

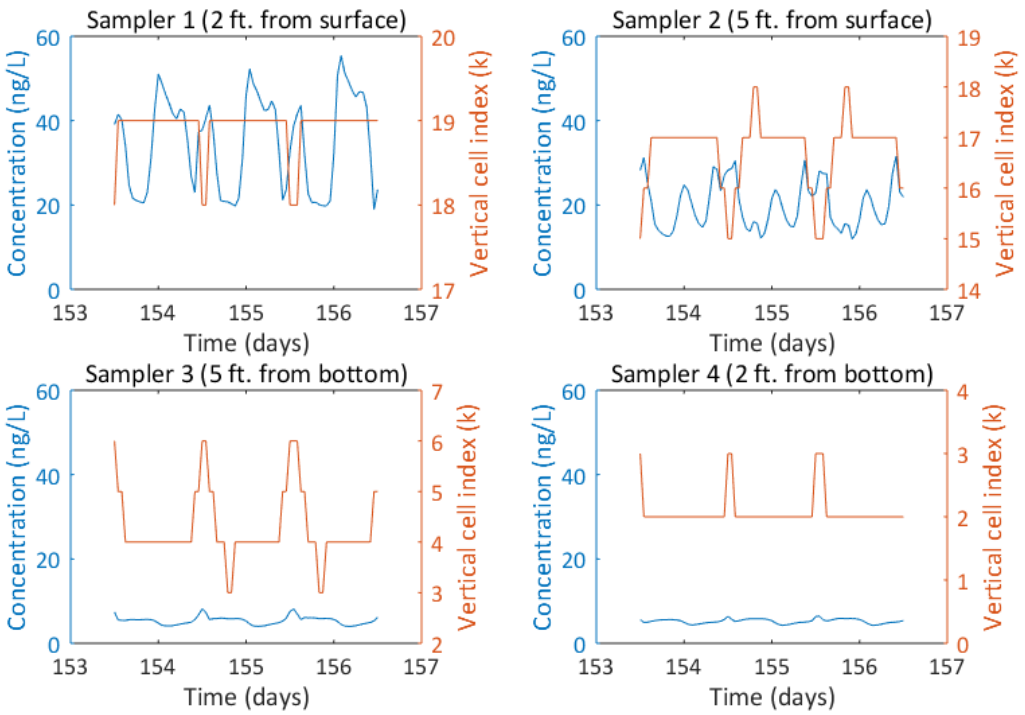


**Figure 1. Tracer Concentrations (Shown in Blue) Seen By Four Samplers and the Time-Variable Vertical Location of the Samplers (Shown in Orange as Model Layers) at a Given Horizontal Location.**

*The samplers are deployed to measure a vertical profile of concentrations.*

The time-variable uptake of the passive samplers can in principle also be accounted for in averaging concentrations over the sampling period. The concentrations measured by a sampler reflect exponentially declining exposures from previous times, and consequently an exponential filter can be applied to calculate $b_{l,s}$. The characteristic time period for the exponential filter would be different for different congeners. Our analysis showed that the use of an exponential filter results in a small difference as compared to a straight arithmetic average. Thus, we have used a straight arithmetic average to generate fingerprints illustrated below.

### 2.2.1 Choice of Sources

An important factor in the inverse model implementation is the choice of potential sources modeled. Because no prior information is assumed about source location, sources need to be chosen to provide adequate spatial coverage within the area of interest. The EFDC model used herein has 115 horizontal cells within the LDW, each with 20 vertical layers, resulting in 2300 potential source locations. However, since each chosen source requires a unique tracer simulation, representing all potentiation source locations within the LDW would mean 2,300 tracer simulations. To reduce the number of simulations, potential tracer sources were chosen to be at the surface (20$^{th}$ vertical layer) and on the sediment bed (1$^{st}$ vertical layer), but not in the middle of the water column. For most cases illustrated below, sources were introduced along the center channel, roughly every 0.3 miles (every other longitudinal cell). Sources on the banks and at every longitudinal cell along the center channel are also considered in a subset of the evaluations.

### 2.2.2 Fitting Schemes and Interpretation of Results

Another choice in the inverse model implementation is the choice of fitting schemes. If the number of potential sources is more than the number of measurements, then the system of equations [Eq. (2)] is over-determined. The most common way of solving an over-determined system is to use the least square approximation. Here, we try three different variants:

- Minimizing sum of squared error in absolute concentrations $\left[\sum\left(c_{fit} - c_{meas}\right)^2\right]$
- Minimizing sum of squared error in natural log of concentrations $\left[\sum\left[\ln c_{fit} - \ln c_{meas}\right]^2\right]$
- Minimizing sum of squared error in normalized concentrations $\left[\sum\left\{\left(c_{fit} - c_{meas}\right)/c_{meas}\right\}^2\right]$

These three fitting schemes allow the user to consider different forms of uncertainty and result in somewhat different source distributions and strengths identified by the inverse model. The first scheme assigns greater importance to larger measured concentrations, whereas the second and third schemes reduce the influence of these concentrations to more heavily weight smaller measured concentrations. Unless specified otherwise, results were calculated by minimizing the squared error in absolute concentrations (the first approach) because its heavier weighting of the larger measured concentrations is consistent with these being of greater importance from a risk perspective.

When the number of potential sources considered exceeds the number of measurements (which is expected to be true typically), it is theoretically possible that the fit of the inverse model will continue to improve as the number of selected sources is increased. If the modeler believes that this is not realistic (e.g., if sources are known to be localized instead of distributed), then one can introduce a penalty applied to model complexity. The Akaike Information Criterion (*AIC*) (Akaike, 1974) provides one approach of doing this. For a linear system with relatively small number of measurements ($n/p < 40$), the *AIC* can be expressed as (Burnham and Anderson, 2004):

$$AIC = n \ln\left(\frac{RSS}{n}\right) + 2p + \frac{2p(p+1)}{n-p-1} \tag{3}$$

where $RSS$ is the residual sum of squares of the fit, $n$ is the number of measurements and $p$ is the number of sources. The first term in Eq. (3) represents the usual log-likelihood function of a linear system, the second term is the penalty applied to the model complexity, and the third term is a correction factor for small number of measurements (Sugiura, 1978). $AIC$ is defined such that the objective is to find the minimum value among candidate models.

To use $AIC$, one starts with all possible choices of a single source and calculates the fit and the *AIC* values for these choices. Next, the user considers all possible choices of two sources and calculates the best fit and *AIC* values. If the minimum $AIC$ value with 2 sources is less than the minimum value with one source, then the optimum number of sources is 2 or more. In that case, the user considers all possible choices of 3 sources, and so on. For a certain number of sources, the improvement in the fit will be marginal and insufficient to offset the *AIC* penalty for adding another source. When that happens, the $AIC$ score will be higher than in the previous iteration, and the optimum number of sources is the number of sources considered in the previous iteration.

In principle, using $AIC$ provides a reasonable way of controlling the number of sources. However, when evaluating the PCB concentrations measured in the LDW, the number of sources identified by the inverse model was generally small (typically, 4-6 sources were chosen in test cases with 34 potential sources). Thus, the $AIC$ criterion was not used to limit the number of sources further in the applications described below.

### 2.2.3 Illustrative Example

To illustrate the behavior of the inverse model approach, it was also applied here to a simpler setup for which the concentration field was specified analytically: a vertically well-mixed rectangular channel with tidal flow and no through flow. In such a setting, the tidal excursion made to be proportional to the distance downstream from the head ($x$), and the longitudinal dispersion coefficient is $E_L = \alpha x^2$. The concentration distribution from a continuous plane source (located at $x = x_d$) was calculated analytically as:

$$c(x) - c_L = \frac{q''}{\alpha\kappa}\left[\frac{x^{-1/2-\kappa/2}}{{x_d}^{1/2-\kappa/2}} - \frac{x^{-1/2+\kappa/2}}{L^{\kappa}{x_d}^{1/2-\kappa/2}}\right] \text{ for } x > x_d \qquad (4)$$

$$c(x) - c_L = \frac{q''}{\alpha\kappa}\left[\frac{x^{-1/2+\kappa/2}}{{x_d}^{1/2+\kappa/2}} - \frac{x^{-1/2+\kappa/2}}{L^{\kappa}{x_d}^{1/2-\kappa/2}}\right] \text{ for } x < x_d$$

where $\kappa = \sqrt{1 + 4\,k/\alpha}$, $k$ is the first order decay rate for the contaminant (e.g., by water-to-air exchanges averaged over the entire water depth_, $q''$ is the mass injection rate per unit area for the source, $L$ is the length of the channel, and $c_L$ is the concentration at $x = L$. Figure 2 shows the response from unit sources at various locations.

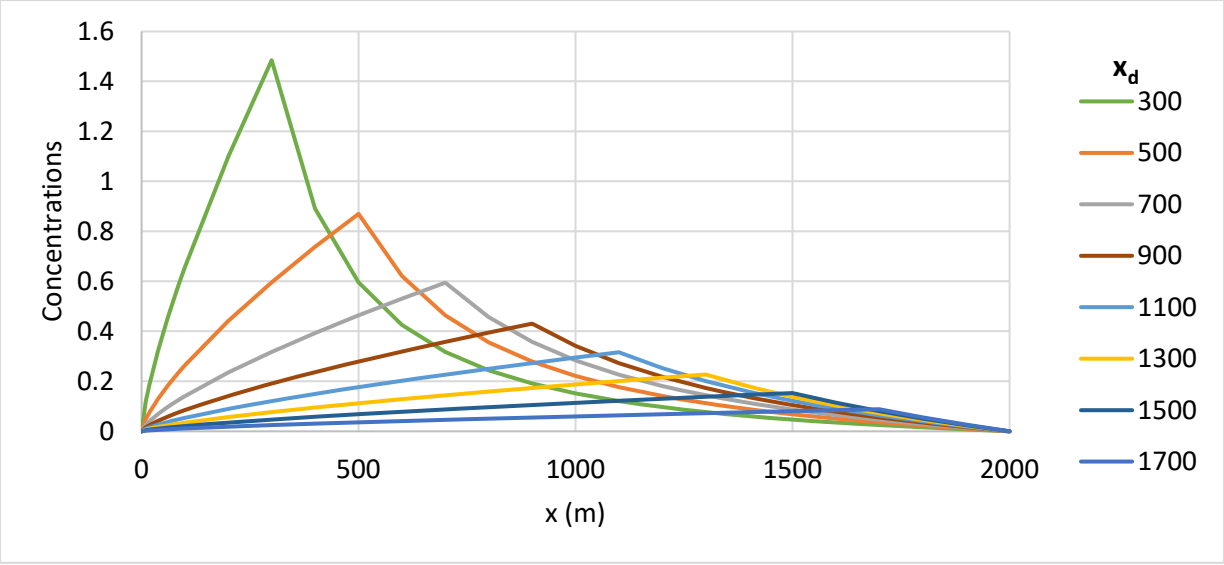


**Figure 2. Concentrations from Unit Sources at Various Locations in a Rectangular Channel with Tidal Flow, no through Flow, and Decay at 0.1 Day$^{-1}$.**

*(Channel dimensions: 2000 m long, 5 m deep, 200 m wide; $k$ = 0.1 day$^{-1}$, $\alpha = 9 \times 10^{-7}$ $s^{-1}$ and $c_L = 0$).*

The setup of a vertically well-mixed rectangular channel with no through flow and first order decay of contaminants is not intended to be a simplified version of the LDW (which has a freshwater input and is vertically stratified). Rather, this setup is used to test the inverse model's ability to identify sources in a one-dimensional case where concentration distributions for various source configurations can be calculated analytically [using Eq. (4)].

For this example, "measurements" at six locations ($x$ = 300, 600, 900, 1200, 1500 and 1800 m) were generated [using Eq. (4)] by considering two sources – located at 600 m and 1200 m with strengths equal to 8 and 20, respectively. The source strengths were calculated by minimizing the squared error in absolute concentrations, using the approach described previously.

### 2.2.4 Results with Potential Sources that Include the Original Sources

Potential sources were chosen to be located every 100 m between $x$ = 100 and 1900 m. Note that this choice of potential sources includes the original sources at 600 m and 1200 m. When the inverse model is used to calculate the source strengths, the following sources are identified: at 600 m with strength of 8.00, at 1200 m with strength of 19.99, at 1800 m with strength of 0.03. Thus, the inverse model is able to accurately identify the correct sources in this case.

### 2.2.5 Results with Potential Sources that Do Not Include the Original Sources

Next, 33 potential sources were chosen to be located between 100 and 1900 m (located every 56.25 m). In this case, the original sources at 600 and 1200 m are not included as possible options. When the inverse model is used for this case, the following sources were identified: at 550 m with strength of 0.15, at 606.25 m with strength of 7.98, at 1168.75 m with strength of 5.24, and at 1225 m with strength of 15.24 (corresponding to a total loading of 28.61). Because the actual sources are not part of the set of potential sources, the model picks sources near the actual ones. In doing so, it reproduces the correct solution as closely as is possible with the sources with which it was provided.

### 2.2.6 Results When Measurements Include Uncertainty

The measurements used for the case above were modified to include uncertainty. 1000 realizations each were considered with the concentrations modified randomly to include 10% and 30% uncertainty. 33 potential sources between 100 and 1900 m (located every 56.25 m) were considered. The average source strengths (from 1000 realizations) are shown in Table 1. Only sources with average strength greater than 1 are listed, i.e., trace sources are here ignored.

**Table 1. Source Strengths Calculated Using the Inverse Model Assuming True Inputs of Known Source Strengths from Only Two Sources (at 600 m with Strength of 8 and at 1200 m with Strength of 20) that Were then Used as Inputs the EFDC to Generate PCB Concentrations at All Positions in the LDW (Referred to as "Measurements" Below).**

*Then, 33 equally spaced potential sources between 100 and 1900 m located every 0.25 m were considered by the inverse model. Model results include cases where "EFDC-inferred measurements" are modified to include uncertainty, typical of real world sample analyses. Only sources with average strength greater than 1 are listed for cases when results from multiple realizations are averaged.*

| Source locations (m) | Fitted source strengths (using measurements with no uncertainty) | Fitted average source strength (using measurements with 10% uncertainty) | Fitted Average source strength (using measurements with 30% uncertainty) |
|---|---|---|---|
| 550 | | 1.2 | 1.2 |
| **606.25** | **8.0** | **5.2** | **4.1** |
| 662.5 | | 1.1 | |
| 831.25 | | | 1.5 |
| 887.5 | | | 1.1 |
| 943.75 | | | 1.3 |
| **1168.75** | **5.2** | **7.5** | **5.1** |
| **1225** | **15.2** | **9.6** | **7.0** |
| 1337.5 | | | 1.0 |
| 1450 | | 1.0 | 1.5 |
| 1506.25 | | | 1.7 |
| 1900 | | | 1.2 |
| **Total loadings** | 28.6 | 25.6 | 26.7 |

It can be seen from Table 1 that the largest sources picked by the inverse model correspond to the locations of the actual sources, even when "reasonable" measurement uncertainty is added. However, with increasing uncertainty, the model picks more small sources, i.e., it tends toward a more distributed solution. It follows that, in general, an inverse model's ability to correctly identify sources is limited by the precisions of the measurements.

### 2.2.7 Effect of Contaminant Decay

For the above examples, the PCBs were assumed to have a first order decay rate of 0.1 $day^{-1}$. We note that Apell and Gschwend (2017) estimated the water-to-air exchanges of PCB congeners, normalized by the average LDW depth, were about 0.04 $d^{-1}$. With a higher decay rate (1 $day^{-1}$), the source signatures are more distinct (Figure 3) and consequently the model performs better even when the measurements include uncertainty. This is demonstrated in Table 2, where the actual source locations are more correctly identified than in the lower decay case.

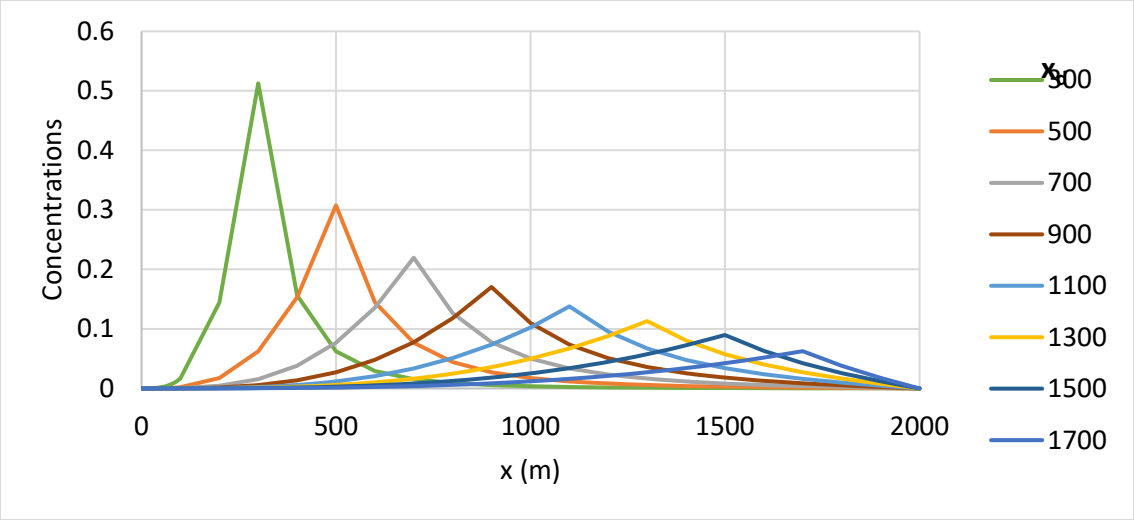


**Figure 3. Concentrations from Unit Sources at Various Locations in a Rectangular Channel with Tidal Flow, no through Flow, and Decay at 1 Day$^{-1}$.**

*(Channel dimensions: 2000 m long, 5 m deep, 200 m wide; $k$ = 1 day$^{-1}$, $\alpha = 9 \times 10^{-7}$ $s^{-1}$, and $c_L = 0$).*

**Table 2. Similar to Table 1, but with Higher Decay Rate of 1 Day$^{-1}$.**

*Source strengths calculated using the inverse model with measurements from 2 sources (at 600 m with strength of 8 and at 1200 m with strength of 20). As above, 33 equally spaced potential sources between 100 and 1900 m are considered. Results include cases when measurements are modified to include measurement uncertainty. Only sources with average strength greater than 1 are listed for cases with measurement uncertainty (where results from multiple realizations are averaged).*

| Source Location (m) | Source strength (using measurements with no uncertainty) | Average strength (using measurements with 10% uncertainty) | Average strength (using measurements with 30% uncertainty) |
|---|---|---|---|
| 550 | 0.5 | | 1.6 |
| 606.25 | 7.9 | 7.5 | 6.6 |
| 1112.5 | | | 1.2 |
| 1168.75 | 6.4 | 7.2 | 7.5 |
| 1225 | 14.8 | 13.2 | 10.5 |
| 1450 | | | 1.2 |
| **Total Load** | **29.6** | **27.9** | **28.6** |

## 2.3 RESULTS AND DISCUSSION

### 2.3.1 Example Using the LDW Setup

Next, an illustrative example with the EFDC setup for the LDW is considered with the 26 sampler locations from the 2016 measurement campaign (Appendix H). "Measurements" for these 26 locations were generated using the EFDC-predicted concentration field produced by 5 bottom sources (at RM 1.0, 1.4, 1.7, 2.0 and 2.3) with strengths equal to 20 mg/d each (i.e., the fingerprints calculated for the 2016 sampler locations from these 5 sources were used to generate "measured" values). Potential sources chosen were located at the surface and the bottom of 17 longitudinal locations along

the center channel (located roughly every 0.3 miles). Using the "measurements" specified with 4 decimal places (for a mean concentration of 46), the inverse model was able to identify the 5 original sources and did not identify any additional source. When the measurements were rounded off to the nearest integer, the inverse model still identified the five original sources (with strengths equal to 21.0, 17.2, 21.0, 18.8 and 20.9), but also identified four additional sources (two surface sources and two bottom sources) with smaller strengths (Table 3). Thus, the inverse model's source assessment is somewhat susceptible to spurious results if insufficient numerical precision is used.

The "measurements" were also modified to include uncertainty (10%, 30%, 50% and 100%) with 1000 realizations each and the inverse model was used to calculate source strengths (using 4 decimal precision). The average source strengths are listed in Table 3.

**Table 3. Source Strengths Calculated Using the Inverse Model with "measurements" Generated from 5 Sources (at RM 1.0, 1.4, 1.7, 2.0 and 2.3 with Strength of 20 mg/d each).**

*34 potential sources are considered – at the surface and bottom of 17 longitudinal locations. Results include cases when measurements are modified to include uncertainty. Only sources with average strength greater than 1 are listed for cases with measurement uncertainty (where results from multiple realizations are averaged).*

| Source location (RM) | Source strength using EFDC-inferred measurements without uncertainty | | Average source strength using measurements with uncertainty | | | |
|---|---|---|---|---|---|---|
| | Concentrations specified with 4 decimal places | Concentrations rounded off to nearest integer | With 10% uncer-tainty | With 30% uncer-tainty | With 50% uncer-tainty | With 100% uncer-tainty |
| 0.1 Bot | | 0.1 | 1.6 | 2.9 | 3.9 | 4.4 |
| 0.4 Bot | | 0.4 | | | | |
| 0.8 Bot | | | 1.4 | 2.5 | 2.5 | 1.8 |
| **1.0 Bot** | **20.0** | **21.0** | **21.3** | **17.6** | **15.9** | **14.3** |
| **1.4 Bot** | **20.0** | **17.2** | **8.3** | **6.1** | **3.6** | **1.7** |
| **1.7 Bot** | **20.0** | **21.0** | **26.2** | **29.7** | **31.3** | **30.4** |
| **2.0 Bot** | **20.0** | **18.8** | **17.8** | **13.5** | **12.8** | **11.2** |
| **2.3 Bot** | **20.0** | **20.9** | **17.3** | **18.0** | **16.4** | **16.3** |
| 2.9 Bot | | | | | 1.4 | 2.2 |
| 3.2 Bot | | | 1.8 | 4.1 | 7.4 | 12.9 |
| 3.8 Bot | | | 1.1 | 2.5 | 4.2 | 6.3 |
| 4.1 Bot | | | | | 1.6 | 2.4 |
| 0.1 Surf | | | 2.8 | 5.4 | 8.7 | 13.5 |
| 0.4 Surf | | 1.0 | | 1.1 | 1.5 | 2.9 |
| 0.8 Surf | | | | 1.8 | 2.6 | 5.3 |
| 2.3 Surf | | | | | | 1.6 |
| 3.8 Surf | | | | | 1.3 | 2.6 |
| 4.1 Surf | | 0.1 | | | | 1.8 |
| **Total load** | 100.0 | 100.5 | 99.6 | 105.2 | 115.1 | 131.6 |

Table 3 indicates that the model is able to pick the original sources even when the measurements include uncertainty, but the strengths deviate from original values as the uncertainty increases (in particular, the strength of the bottom source at RM 1.4 decreases significantly). In addition, more sources are incorrectly identified by the inverse model as the measurement uncertainty increases.

The original sources chosen to generate the measurements in this example are located relatively close to each other and can be considered representative of a distributed source. Since the inverse model is able to identify all of these sources instead of selecting just one larger central source (in particular, when the measurements do not include uncertainty), it should in principle be able to identify distributed sources with real measurements as well, provided the measurement uncertainty is relatively small.

### 2.3.2 Using Passive Sampling Data

Ultimately, we are interested in using the inverse model with concentrations measured in the LDW using passive samplers. The 2016 sampling campaign represents an initial, large-scale survey conducted with "slow samplers" (spanning most of the extent of the LDW but at a fairly coarse resolution, see Appendix H), whereas the 2019 campaign represents a more focused, smaller scale survey with "fast samplers" (spanning an approximately 1-mile reach within the LDW). This is not unlike other studies in which investigators often return to a site to collect additional data, where measurement campaigns are independent and may be widely separated in time. Because the inverse model source assessment will be better constrained with more data, an investigator would ideally like to use the inverse model to infer sources by combining multiple measurement campaigns. For the LDW application, we are interested in combining 2019 measurements taken between RM 1.5 and 2.5 with 2016 measurements spread over the full 5 miles of the LDW. Again, at this site, combining data sets from different times may be complicated due to changing sources in response to local clean-up efforts during this period.

Certain assumptions need to be made in order to combine measurements from different sampling campaigns. The most important assumption is that the different sets of measurements are influenced by the same set of sources and that their relative strengths are also similar. In other words, no significant source reduction (e.g., via in-river or upland remediation) has taken place and no new sources have been introduced in the interim between different campaigns, and there is no significant difference in any of the processes that are not modeled such as sediment resuspension. Other assumptions are that any differences in the hydrodynamic conditions (tides and freshwater flow) between different campaigns can be correctly represented by the hydrodynamic model. Similarly, measured concentrations can be different (e.g., due to difference in hydrodynamics), but should be accurately measured.

In order to combine measurements from different sampling campaigns, unique tracer simulations need to be run for each potential source and for each sampling campaign (with corresponding hydrodynamic conditions and simulation period). The tracer concentrations from these runs then need to be averaged separately to generate fingerprints from each source location for each field campaign. Using these fingerprints and the measured concentrations, the inverse model can be used to assess source configurations and strengths. For example, if there were 2 sampling campaigns with 25 measurements each and 100 potential sources are considered, then the fingerprint matrix (variable **b** in Equation 2) has 100 columns with 50 entries each (25+25 corresponding to the locations in the two sampling surveys). The measured concentrations would in this case be combined similarly to give a column with 50 measurements (variable **C** in Equation 2). The inverse model can then be used to calculate source strengths for the 100 potential sources that best fit measurements across both campaigns.

In principle, we can integrate measurements with different deployment periods or made with different techniques and increase the robustness of the inverse model source assessment. However, the concentrations measured in 2019 are significantly higher than measurements made in 2016. Comparing concentrations measured at similar horizontal and vertical locations for three PCB congeners, the 2019 concentrations are on average higher by a factor of about 2 to 9 (Table 4). This suggests that the sources at the site and/or their strengths differed between the two campaigns, or that the measurement techniques are not consistent. In theory it is possible that the observed differences are due to inconsistencies in the tidal and freshwater forcings during the two periods, but modeling tests indicated that such hydrodynamic differences are unlikely to explain the observed difference in concentrations. For example, a comparison of EFDC simulated concentrations seen by four samplers on the west bank at RM 2.0 (at four different vertical locations) resulting from a single source on the bottom of the west bank at RM 1.7 indicated concentrations with 2016 hydrodynamic conditions to be higher than concentrations with 2019 conditions by approximately 25% on average.

We conclude that the prerequisite assumptions for combining the datasets are not valid. Consequently, the results presented below do not combine the two sets of measurements in assessing source strengths. We note that it is possible, in principle, to run the inverse model using just the 2019 model. This was attempted, but the results were unsatisfactory due to the fact that the measurements covered only a small portion of the domain, leaving concentrations in the remainder of the domain unconstrained. In view of these considerations, only the measurements taken in the 2016 campaign are used with the inverse model in the results presented below, as their larger spatial coverage provided a better constrained dataset than the more focused 2019 campaign.

**Table 4. Comparison of Concentrations Measured in 2019 to those Measured in 2016 at Similar Locations.**

| Sam-pling year | Horizontal location (RM) | Average depth of measure-ment (m) | Measured Concentrations (pg/L) | | | Averaged concentrations (pg/L) | | | 2019/2016 average concentration ratio | | |
|---|---|---|---|---|---|---|---|---|---|---|---|
| | | | PCB 28 | PCB 52 | PCB 101 | PCB 28 | PCB 52 | PCB 101 | PCB 28 | PCB 52 | PCB 101 |
| 2016 | 1.4 East | 5.9 | 23 | 22 | 16 | | | | 3.1 | 2.3 | 2.1 |
| 2019 | 1.4 West | 4.7 | 70 | 50 | 34 | | | | | | |
| 2016 | 2.3 West | 0.5 | 14 | 14 | 10 | | | | 3.4 | 2.3 | 2.4 |
| 2019 | 2.4 West | 0.6 | 48 | 33 | 23 | | | | | | |
| 2016 | 2.3 West | 1.9 | 20 | 21 | 17 | | | | | | |
| 2019 | 2.4 West | 1.5 | 86 | 50 | 21 | 173 | 123 | 66 | 8.7 | 6.0 | 3.8 |
| | 2.4 West | 1.9 | 259 | 196 | 110 | | | | | | |
| 2016 | 2.2 West | 3.6 | 65 | 56 | 36 | 101 | 76 | 34 | 1.8 | 1.7 | 2.0 |
| | 2.2 West | 4.4 | 138 | 96 | 33 | | | | | | |
| 2019 | 2.2 West | 3.6 | 207 | 167 | 92 | 181 | 132 | 68 | | | |
| | 2.3 West | 3.6 | 154 | 97 | 44 | | | | | | |

### 2.3.3 Results of Applying the Inverse Model to the 2016 Field Campaign

The inverse model source assessment was run using the passive sampling data from the 2016 survey with 126 potential sources (Figure 4), including sources in the surface and bottom layers at each EFDC model grid cell along the channel and at every other cell along the banks (roughly every 0.3 miles). Table 5 presents the inverse model results in terms of the identified sources and their strengths (dissolved mass loadings). For a given PCB congener, the average (over the deployment period) mass contributed by each identified source to the average mass in the domain (5-mile stretch of the LDW) is also reported in Table 5. This characterizes the fractional contribution of each identified source to the average dissolved concentration in the LDW over the deployment period. For example, for PCB 28, the source at RM 0.1 on the east bank (with a strength of 22 mg/d) contributes 64 mg of the 243 mg that was predicted to reside on average within the water column of the LDW (i.e., it contributes 26% of the mass contributed by all identified sources). This value can be calculated by integrating the tracer mass (concentration × volume) across all EFDC model cells within the LDW. Alternatively, the mass can be calculated by multiplying the source strength by the residence time of tracer originating from the source. Note that the fractional contribution of a source to the LDW average concentration differs is not equal to the fractional loading of that source to the total loading from all sources because PCB mass is lost to Elliot Bay and the residence time varies by source location.

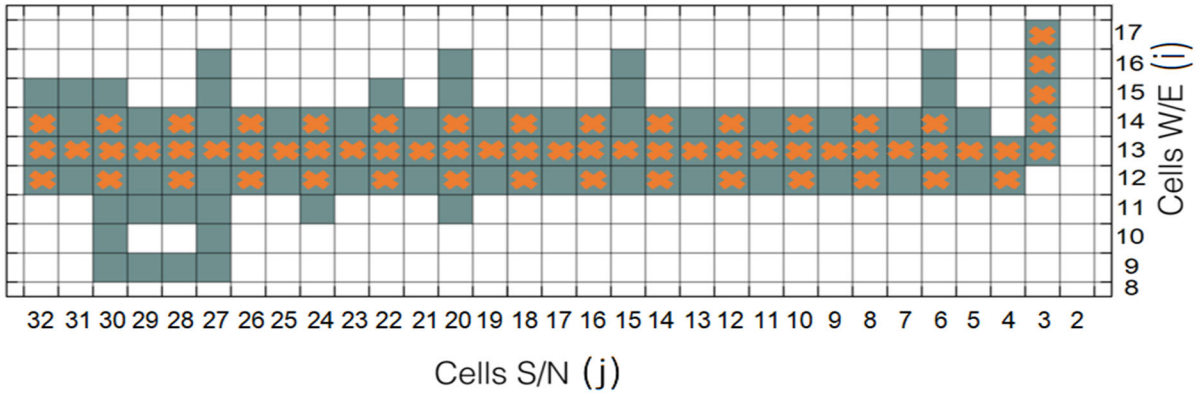


**Figure 4. Potential Source Locations (Marked with Crosses) Supplied to the Inverse Model for Source Assessment Using the 2016 Campaign Data.**

*Potential sources were simulated at the surface and bottom model grid layers at each of the marked locations.*

**Table 5. Source Strengths and Average Mass Contribution for Sources Selected by the Inverse Model Using the 2016 Campaign Data with 126 Potential Sources Simulated.**

| Source location (RM) | Congener | Bottom Sources | | | | | Surface sources | | |
|---|---|---|---|---|---|---|---|---|---|
| | | 0.1 East Bank | 0.4 East Bank | 0.8 West Bank | 1.7 West Bank | 3.8 East Bank | 0.4 East Bank | 3.8 East Bank | 4.1 East Bank |
| Source strength (mg/d) | PCB 28 | 22 | 4 | | 30 | 0.1 | 23 | 0.4 | |
| | PCB 52 | 27 | 3 | 9 | 19 | 0.5 | 3 | 1 | |
| | PCB 101 | 27 | 2 | 21 | 0.5 | 0.5 | | 1 | 0.2 |
| | | | | | | | | | |
| Average mass contribution (mg) | PCB 28 | 64 | 16 | | 147 | 0.2 | 16 | 0.5 | |
| | | 26% | 7% | | 61% | 0.1% | 6% | 0.2% | |
| | PCB 52 | 78 | 12 | 42 | 93 | 1 | 2 | 1 | |
| | | 34% | 5% | 18% | 41% | 0.5% | 0.9% | 0.6% | |
| | PCB 101 | 78 | 8 | 97 | 2 | 1 | | 1 | 0.4 |
| | | 41% | 4% | 51% | 1% | 0.6% | | 0.7% | |

The results in Table 5 suggest that for the three PCB congeners modeled, the major contribution of dissolved PCB mass comes from the downstream portion of the estuary (between RM 0 and 2) from sources along the bottom of the water column. The main sources identified by the inverse model are located on the west bank between RM 0.8 and 1.7 and on the east bank near the downstream boundary of the study region (RM 0.1). The latter identified source could also indicate sources beyond the mouth of the estuary (the inverse model was not supplied with potential sources in Elliot Bay).

The fitted concentrations are plotted against measurements in Figure 5. This figure demonstrates that the concentrations predicted by the inverse model agree moderately well with measurements on average, with predictions that are mostly within a factor of 2 of the measured concentration and all within a factor of 5. The RMS errors in absolute concentrations, natural log of concentrations and relative concentrations are 17.0 pg/L, 0.56 and 0.93, respectively, for PCB 28.

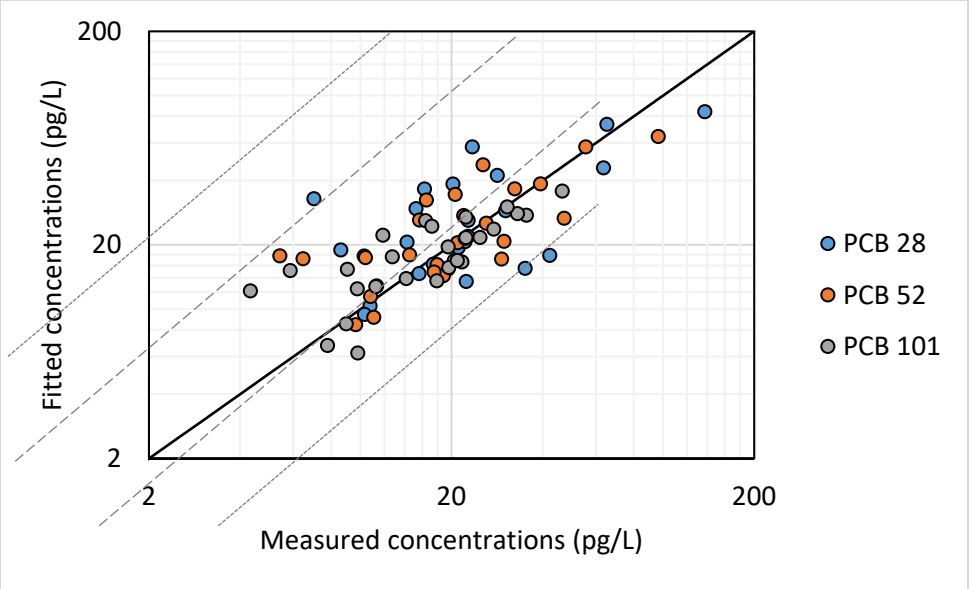


**Figure 5. Comparison of Fitted Concentrations and Measurements for Three Modeled PCB Congeners.**

*The solid line is the 1:1 line, while the dashed and dotted lines indicate factors of 2 and 5 difference, respectively.*

Figure 6 provides an additional comparison of fitted and measured concentrations, which also shows the longitudinal and vertical location of the measurements and the inferred contribution from each source identified by the inverse model. The longitudinal and vertical position (time-averaged) of the samplers are shown with black dots. The length of the black line segment extending upward from the black dot indicates the concentration measured by that sampler. The total congener concentration prediction at each sampler location is shown by stacking the contributions from individual sources (using line segments of different colors with their lengths indicating the concentration contributions from each source). At any given sampler location, the concentration contribution from the bottom source at RM 0.1 East Bank is shown using a red line segment starting at the black dot and extending upward. Next, the contribution from the bottom source at RM 0.8 West Bank is shown by a blue line segment, which starts where the red segment ends. Next, the green line segment, which starts where the blue segment ends, shows the contribution from the bottom source at RM 1.7 West Bank. The contributions from remaining sources identified by the inverse model are shown using the magenta line segment, which starts where the green line segment ends.

For congeners 28 and 52, the concentrations measured at RM 2.2 are high relative to measurements at other locations. Therefore, it makes sense that for these congeners, the inverse model assigns the biggest contribution of concentration as coming from a nearby source (bottom source at RM 1.7 on the west bank [green line segments]). On the other hand, for PCB 101, for which the measurements are more spatially uniform, the large contributors are at the bottom and close to the mouth of the estuary (RM 0.1 and 0.8). These inferred sources contribute concentration to most of the sampler locations (blue and green line segments).

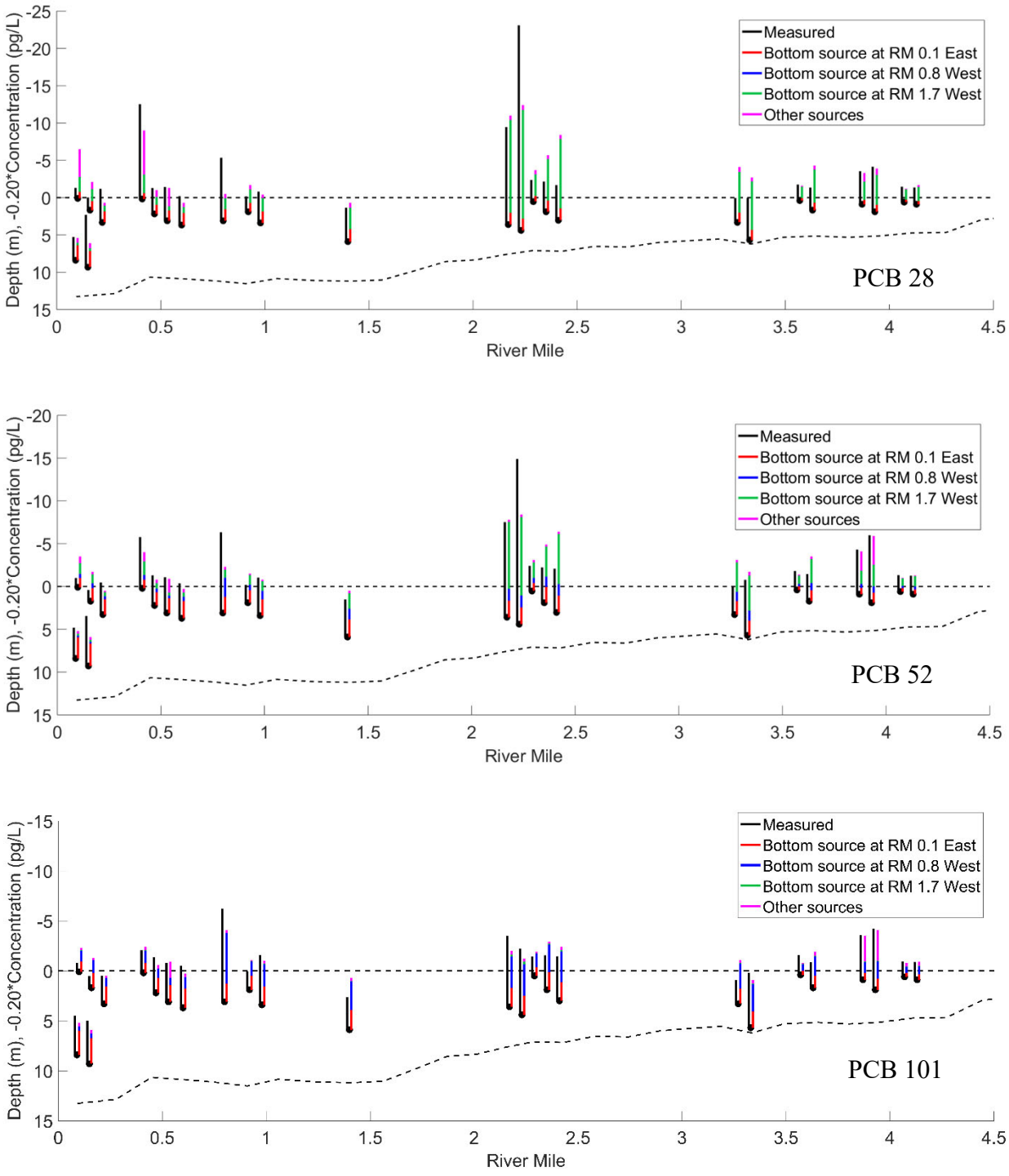


**Figure 6. Comparison of Measurements and Predicted Concentrations from Various Sources.**

Using the sources identified by the inverse model, one can use those results at inputs to the EFDC and generate the spatial distribution of PCB concentrations throughout the estuary (Figure 7). The concentrations shown are average concentrations over the 2016 deployment period.

Because most of the major inferred sources are along the bottom (Table 5), the concentrations are also highest close to the bottom and there is a vertical gradient of predicted concentrations. For all three congeners, the highest concentrations are near the bottom close to RM 1.7, even for PCB 101 where the dominant source loadings are predicted to be downstream of this location.

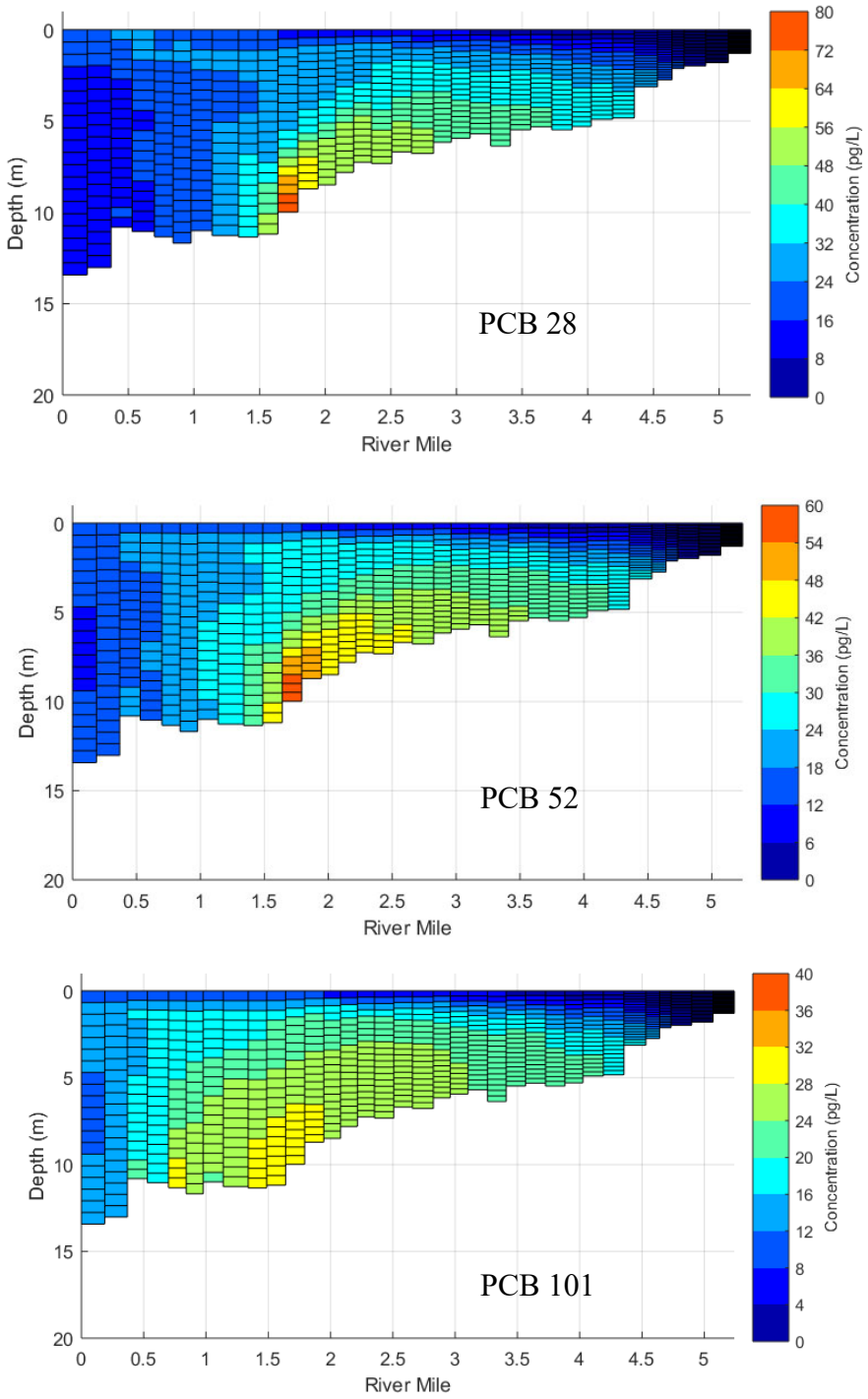


**Figure 7. Predicted Longitudinal Concentration Profiles Along the Center Channel of the LDW.**

### 2.3.4 Influence of Measurement Uncertainty on Predicted Source Strengths

The uncertainty in the strengths and locations of sources selected by the inverse model can in part be characterized by considering the uncertainty in measured concentrations. Using 1000 realizations, we generated the "measured" concentrations modified to reflect an uncertainty of 30% (see Apell and Gschwend, 2017). A random variable ($x$) drawn from a unit normal distribution with a mean of 0 was used to simulate uncertainty in the measurements as follows:

$$c' = c_{meas} + 0.3 c_{meas} x \quad (5)$$

where $c'$ is the modified concentration and $c_{meas}$ is the measured concentration.

The distribution of $x$ was truncated to exclude values below -2 and above +2 (i.e., excluding approximately the upper and lower 2% of the distribution) in order to avoid generating negative concentrations. For each source location, the average source strength and standard deviation across 1000 realizations are listed in Table 6 for three congeners. It should be noted that the calculated strengths are constrained to be non-negative, as discussed in Section 3, which causes the distributions of source strengths to not be normally distributed.

It is also noted that there are other sources of uncertainty to the inverse model results that are not captured in Table 6, such as the approach used to fitting the data and uncertainty in the numerical model transport predictions. The sensitivity of the inverse model to some of these factors is considered in the sections that follow.

**Table 6. Average Source Strengths and Their Standard Deviation Calculated Using the inverse Model with Measurements Modified to Include Uncertainty.**

*Only the locations for which the mean source strength was higher than 0.1 mg/d are listed.*

| Source location (RM) | | Source strengths (mg/d) | | | | | |
|---|---|---|---|---|---|---|---|
| | | PCB 28 | | PCB 52 | | PCB 101 | |
| | | Mean | Standard deviation | Mean | Standard deviation | Mean | Standard deviation |
| Bottom sources | 0.1 Center | | | | | 0.4 | 2.6 |
| | 0.1 East | 19.3 | 10.2 | 26.0 | 9.3 | 25.8 | 8.8 |
| | 0.4 East | 3.8 | 2.3 | 2.8 | 2.0 | 2.6 | 1.8 |
| | 0.8 West | 2.9 | 5.1 | 9.9 | 9.1 | 18.0 | 8.1 |
| | 0.8 East | | | 0.1 | 0.6 | 0.3 | 0.9 |
| | 1.7 West | 29.2 | 8.2 | 18.4 | 7.1 | 1.8 | 2.4 |
| | 2.0 West | | | | 0.2 | | |
| | 2.1 Center | | | 0.1 | 0.8 | | |
| | 3.3 Center | | | 0.1 | 0.5 | 0.6 | 1.0 |
| | 3.8 East | 0.2 | 0.2 | 0.6 | 0.4 | 0.5 | 0.3 |
| Surface sources | 0.4 East | 23.0 | 9.8 | 3.8 | 3.9 | | |
| | 3.8 East | 0.5 | 0.5 | 1.1 | 0.7 | 1.1 | 0.6 |
| | 4.1 East | 0.1 | 0.2 | 0.1 | 0.2 | 0.2 | 0.2 |

### 2.3.5 Influence of Fitting Scheme on Predicted Source Strengths

The influence of the three different fitting schemes discussed in Section 3.2 on the inverse model's predictions of source locations and strengths was also evaluated. For this test, the inverse model was run using the passive sampling data from the 2016 survey with 34 potential source locations (i.e., with a coarser configuration than the one for the base case assessment described earlier in this section). Here the potential sources were limited to the center channel, specifically the surface and bottom of every other longitudinal cell (roughly 0.3 miles apart, see Figure 8). The effects of varying selected sources and their strengths for each of the three fitting schemes is about a factor of 2 (Table 7 comparing a, b, and c). A comparison of fitted concentrations vs. model input "measurements" for PCB 28 for each scheme shows a small shift (Figure 9).

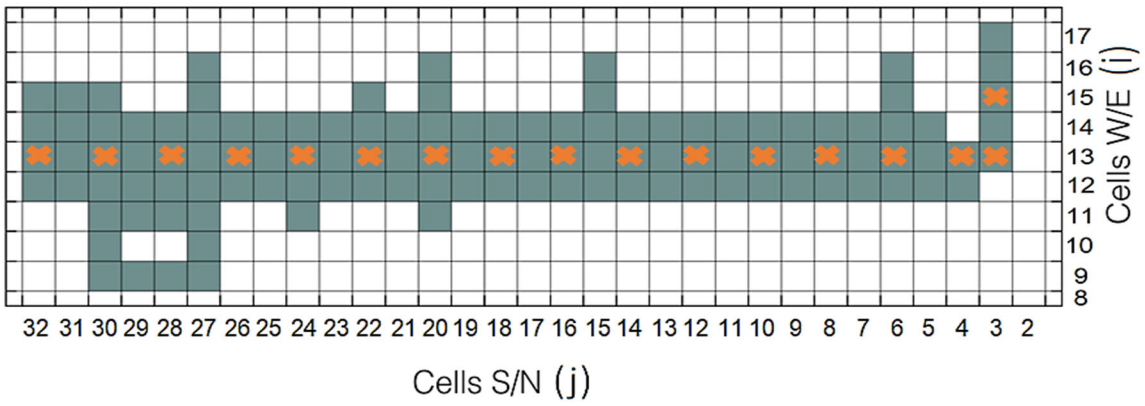


**Figure 8. Potential Source Locations (Marked with Crosses) Used for the Inverse Model Application to Test Sensitivity to Different Fitting Schemes.**

*Sources were chosen to be at the surface and the bottom at each of the marked locations.*

**Table 7a. Source Strengths (in mg/d) Calculated for PCB 28 for Three Different Fitting Schemes Using the Inverse Model with 2016 Measurements and the Potential Sources in Figure 8.**

| Source location (RM) | Scheme 1 (minimizing squared error in absolute concentrations) | Scheme 2 (minimizing squared error in natural log of concentrations) | Scheme 3 (minimizing squared error in relative concentrations) |
|---|---|---|---|
| 0.1 Bottom | 25 | 44 | 15 |
| 0.4 Bottom | | 7 | 23 |
| 1.7 Bottom | 33 | 11 | 5 |
| 4.8 Bottom | | | 4 |
| 0.4 Surface | 39 | 5 | |
| 3.8 Surface | | 9 | |
| 4.1 Surface | | | 1 |

**Table 7b. Source Strengths (in mg/d) Calculated for PCB 52 for Three Different Fitting Schemes Using the Inverse Model with 2016 Measurements and the Potential Sources in Figure 8.**

| Source location (RM) | Scheme 1 (minimizing squared error in absolute concentrations) | Scheme 2 (minimizing squared error in natural log of concentrations) | Scheme 3 (minimizing squared error in relative concentrations) |
|---|---|---|---|
| 0.1 Bottom | 42 | 45 | 15 |
| 0.4 Bottom | | 6 | 15 |
| 1.7 Bottom | 22 | 10 | 9 |
| 4.8 Bottom | | 4 | 1 |
| 3.8 Surface | 3 | 1 | |
| 4.1 Surface | | | 1 |

**Table 7c. Source Strengths (in mg/d) Calculated for PCB 101 for Three Different Fitting Schemes Using the Inverse Model with 2016 Measurements and the Potential Sources in Figure 8.**

| Source location (RM) | Scheme 1 (minimizing squared error in absolute concentrations) | Scheme 2 (minimizing squared error in natural log of concentrations) | Scheme 3 (minimizing squared error in relative concentrations) |
|---|---|---|---|
| 0.1 Bottom | 55 | 44 | 18 |
| 0.4 Bottom | | 6 | 11 |
| 1.7 Bottom | 2 | 1 | 6 |
| 3.8 Bottom | 2 | | |
| 4.8 Bottom | 1 | 4 | |
| 3.8 Surface | 1 | | |
| 4.1 Surface | | | 1 |

As seen in Figure 5, schemes 2 and 3 perform better for small measured concentrations whereas scheme 1 fits the large measurements better. By design, the three schemes minimize different error measures (Section 3.2). This is demonstrated in Table 8 for PCB 28.

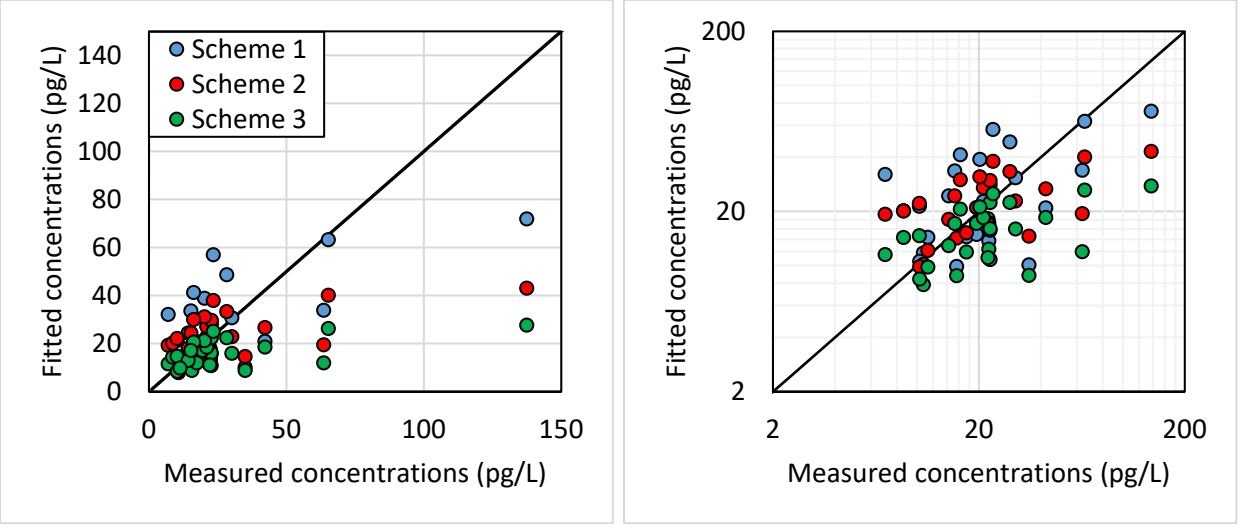


**Figure 9. Comparison of Fitted Concentrations and Measurements for PCB 28 Using the Three Fitting Schemes Considered.**

*(Left: linear scale; right: log scale.)*

The results in Table 7 demonstrate that the fitting scheme affects the sources that are identified and their relative strengths. However, looking at the comparisons in Figure 9 and Table 8, no one scheme clearly outperforms the other schemes in goodness-of-fit. As noted in Section 3.2, fitting scheme 1 (minimizing the sum of squared error in absolute concentrations) was used for most of the results reported herein because it yields better agreement at high measured concentrations, which are the most important ones from a risk perspective.

**Table 8. PCB 28 Error Measures for the Three Different Fitting Schemes**

*(n = number of measurements)*

| Error measure | Expression | Scheme 1 | Scheme 2 | Scheme 3 |
|---|---|---|---|---|
| RMS error in absolute concentration | $\sqrt{\frac{1}{n}\sum\left(c_{fit}-c_{meas}\right)^2}$ | 20.0 pg/L | 22.8 pg/L | 26.5 pg/L |
| RMS error in natural log of concentration | $\sqrt{\frac{1}{n}\sum\left[\ln c_{fit}-\ln c_{meas}\right]^2}$ | 0.65 | 0.55 | 0.67 |
| RMS error in relative concentration | $\sqrt{\frac{1}{n}\sum\left[\left(c_{fit}-c_{meas}\right)/c_{meas}\right]^2}$ | 0.99 | 0.62 | 0.43 |

### 2.3.6 Sensitivity of Inverse Model Results to EFDC Model Configuration and Parameterization

The numerical model predictions by EFDC may be sensitive to the model configuration and parameterization, which introduces uncertainty into the inverse model's identified source locations and strengths and may contribute to differences between predicted and measured concentration (Figure 7). In this section, we test the potential sensitivity of inverse model results to several EFDC settings, including representing mass loss processes, vertical and horizontal mixing, and model grid resolution.

Another reason for the difference between predictions and measurements could be the presence of sub-grid scale sources in the real world.

### 2.3.7 First Order Decay

The inverse model's ability to correctly identify source locations and strengths and to predict concentrations that are consistent with measurements may be limited by unmodeled transformation and transport processes (e.g., sediment dynamics and sorption processes, air-water exchange, etc.). For example, mass loss processes can lead to more distinct source signatures and yield a better fit between predicted and measured concentrations, as discussed in Section 4. To test whether including such processes could potentially improve the agreement of inverse model concentration predictions with data, a first order decay of the tracer mass was added to the EFDC tracer simulations used to generate the fingerprints used by the inverse model. Sources selected by the inverse model and their calculated strengths are expected to change with the decay rate for two main reasons. First, as the decay rate increases, larger source strengths will be needed to reach the average concentrations of the measured data. Second, more sources are likely to be identified with faster decay because the source fingerprints become increasingly local, i.e., for a fast decay, sources will mainly affect concentrations close to them. The potential improvement of representing such processes was judged by evaluating the goodness-of-fit of the predicted concentrations for first order decay rates of 1/day and 4/day (i.e., reflecting characteristic timescales of 1 day and 6 hours). The inverse model was run with the simplified potential source configuration described in Section 7.2 and shown in Figure 8 (i.e., with 34 potential sources along the center channel). Table 9 shows inverse model results with and without decay for three PCB congeners. Only source locations that are identified with any of the decay rates are listed in the table.

**Table 9a. Comparison of Selected Source Locations, Their Strengths and the Goodness-of-fit of the Inverse Model Concentration Predictions for Different Values of a First Order Decay Rate for PCB 28.**

| Decay rate | Source locations (river mile) and strengths (mg/d) | | | | | | | | | | | | | | RMS error (pg/L) |
|---|---|---|---|---|---|---|---|---|---|---|---|---|---|---|---|
| | Bottom sources | | | | | | | | | | | Surface sources | | | |
| | 0.1 | 0.4 | 0.8 | 1.0 | 1.7 | 2.0 | 3.2 | 3.8 | 4.1 | 4.4 | 4.8 | 0.4 | 0.8 | 3.8 | |
| **No decay** | 27 | | | | 33 | | | | | | | | 32 | | 20.1 |
| **1 day$^{-1}$** | 204 | 27 | | | 153 | | | 9 | | | 4 | | 59 | 22 | 16.5 |
| **4 day$^{-1}$** | 1089 | 30 | 91 | 105 | | 307 | 14 | 38 | 7 | 65 | 4 | 124 | 36 | | 15.7 |

**Table 9b. Comparison of Selected Source Locations, Their Strengths and the Goodness-of-fit of the Inverse Model Concentration Predictions for Different Values of a First Order Decay Rate for PCB 52.**

| Decay rate | Source locations (river mile) and strengths (mg/d) | | | | | | | | | | | | | | RMS error (pg/L) |
|---|---|---|---|---|---|---|---|---|---|---|---|---|---|---|---|
| | Bottom sources | | | | | | | | | | Surface sources | | | | |
| | 0.1 | 0.4 | 0.8 | 1.0 | 1.7 | 2.0 | 3.2 | 3.8 | 4.1 | 4.4 | 0.4 | 2.3 | 3.5 | 3.8 | |
| No decay | 42 | | | | 22 | | | | | | | | | 3 | 13.3 |
| 1 day$^{-1}$ | 227 | 19 | 8 | | 114 | | 3 | 22 | | | | | | 30 | 10.2 |
| 4 day$^{-1}$ | 1069 | 3 | 168 | 51 | 207 | 153 | 21 | 58 | 2 | 27 | 44 | 3 | 1 | 54 | 9.4 |

**Table 9c. Comparison of Selected Source Locations, Their Strengths and the Goodness-of-fit of the Inverse Model Concentration Predictions for Different Values of a First Order Decay Rate for PCB 101.**

| Decay rate | Source locations (river mile) and strengths (mg/d) | | | | | | | | | | | | | | RMS error (pg/L) |
|---|---|---|---|---|---|---|---|---|---|---|---|---|---|---|---|
| | Bottom sources | | | | | | | | | | Surface sources | | | | |
| | 0.1 | 0.4 | 0.8 | 1.7 | 2.6 | 3.2 | 3.8 | 4.1 | 4.4 | 4.8 | 0.4 | 2.3 | 3.5 | 3.8 | |
| No decay | 55 | | | 2 | | | 2 | | | 1 | | | | 1 | 7.8 |
| 1 day$^{-1}$ | 224 | 5 | 33 | 45 | | 8 | 18 | | | 2 | | | | 17 | 5.7 |
| 4 day$^{-1}$ | 1006 | | 202 | 270 | 33 | 17 | 43 | 3 | 1 | 2 | 4 | 4 | 9 | 49 | 5.4 |

As expected, the inverse model identifies more sources close to the measurement locations with faster decay, and the RMS error (in absolute concentrations) decreases. However, the error is still considerable even with a relatively fast decay rate of 4/day. The reduction in RMS error when the decay rate is increased from 1/day to 4/day is small, and the RMS error is not expected to decrease much with further increase in the decay rate.

### 2.3.8 Vertical Eddy Viscosity

Three different EFDC calibrations were considered based on model-data comparisons of measured salinity profiles and data-based estimates of salt wedge location as a function of flow. The three calibration settings differed in the choice of background vertical eddy viscosity. To assess the impact of this uncertainty in calibration settings on the inverse model's source assessment, we calculated source strengths using EFDC runs with each of the three calibration settings. As in preceding sensitivity tests, only potential sources along the center channel were considered for this exercise (34 potential sources at the horizontal locations shown in Figure 8). The source locations and strengths identified by the inverse model are shown in Table 10 for each case. Only source locations that are identified with any of the three calibrations are listed in the table.

**Table 10a. Source Strengths (in mg/d) Predicted for PCB 28 Using the Inverse Model with 2016 Measurements and Three Different EFDC Calibration Settings.**

| Source location (RM) | Calibration 1 (vertical eddy viscosity = 1E-3.5 $m^2/s$) | Calibration 2 (vertical eddy viscosity = 1E-5 $m^2/s$) | Calibration 3 (vertical eddy viscosity = 1E-7 $m^2/s$) |
|---|---|---|---|
| 0.1 Bottom | 37 | 25 | 25 |
| 1.7 Bottom | 39 | 33 | 32 |
| 0.4 Surface | 32 | 39 | |
| 0.8 Surface | | | 32 |
| 4.1 Surface | 1 | | |

**Table 10b. Source Strengths (in mg/d) Predicted for PCB 52 Using the Inverse Model with 2016 Measurements and Three Different EFDC Calibration Settings.**

| Source location (RM) | Calibration 1 (vertical eddy viscosity = 1E-3.5 $m^2/s$) | Calibration 2 (vertical eddy viscosity = 1E-5 $m^2/s$) | Calibration 3 (vertical eddy viscosity = 1E-7 $m^2/s$) |
|---|---|---|---|
| 0.1 Bottom | 50 | 42 | 41 |
| 1.7 Bottom | 26 | 22 | 22 |
| 4.8 Bottom | 4 | | |
| 3.8 Surface | | 3 | |
| 4.1 Surface | 1 | | |

**Table 10c. Source Strengths (in mg/d) Predicted for PCB 101 Using the Inverse Model with 2016 Measurements and Three Different EFDC Calibration Settings.**

| Source location (RM) | Calibration 1 (vertical eddy viscosity = 1E-3.5 $m^2/s$) | Calibration 2 (vertical eddy viscosity = 1E-5 $m^2/s$) | Calibration 3 (vertical eddy viscosity = 1E-7 $m^2/s$) |
|---|---|---|---|
| 0.1 Bottom | 61 | 55 | 54 |
| 1.7 Bottom | 1 | 2 | 2 |
| 3.5 Bottom | 5 | | |
| 3.8 Bottom | | 2 | 3 |
| 4.8 Bottom | 5 | 1 | 2 |
| 3.8 Surface | | 1 | |

Table 10 indicates that, for a given congener, the model chooses 2-5 sources (out of 34 potential sources) and similar sources are chosen for each calibration, i.e., the choice of this calibration setting does not strongly affect the predicted source location. However, the source strengths are somewhat different for the three calibrations. Note that for all other inverse model results presented herein, EFDC simulations were based on the calibration 2 settings of vertical eddy viscosity.

### 2.3.9 Horizontal Diffusivity

The horizontal diffusivity of tracers is another EFDC setting for which the sensitivity of inverse model predictions was tested. All inverse model results presented thus far are based on EFDC runs with horizontal diffusivity set to 40 $m^2/s$. To test the sensitivity of inverse model results to this parameter, a set of EFDC tracer simulations were run with a much lower horizontal diffusivity of 0.4 $m^2/s$. A reduced diffusivity may improve model predictions by reducing the horizontal impact of a given source and making its impact more localized. For this sensitivity test, potential sources were located at every other cell longitudinally with sources on the east and west banks as well as along the center channel (90 potential sources at the horizontal locations shown in Figure 10). Table 11 shows a comparison of inverse model results for the two values of horizontal diffusivity.

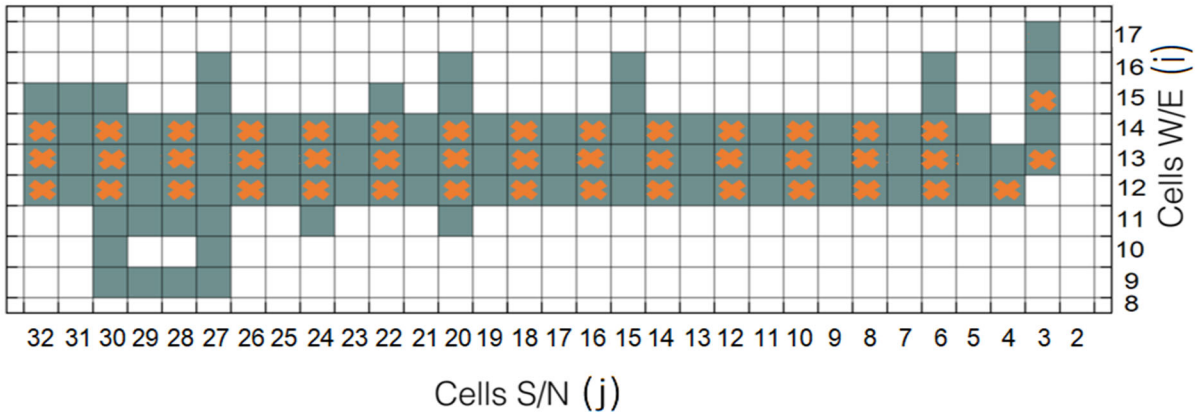


**Figure 10. Potential Source Locations (Marked with Crosses) Used in Tests of Inverse Model Sensitivity to the Horizontal Diffusivity in EFDC.**

*Potential sources were simulated at the surface and the bottom at each of the marked locations.*

**Table 11a. Comparison of Selected Source Locations, their Strengths and the Goodness-of-Fit of the Inverse Model Concentration Predictions for PCB 28 for Different Values of Horizontal Diffusivity in EFDC.**

| Horizontal diffusivity ($m^2/s$) | Source locations (river mile) and strengths (mg/d) | | | | | | | | RMS error (pg/L) |
|---|---|---|---|---|---|---|---|---|---|
| | Bottom sources | | | | | | Surface sources | | |
| | 0.1 East | 0.4 East | 0.8 West | 1.7 West | 2.0 West | 3.8 East | 0.4 East | 3.8 East | |
| 40 | 22 | 4 | | 30 | | 0.1 | 23 | 0.4 | 17.0 |
| 0.4 | 66 | 6 | 21 | | 44 | | 34 | 0.1 | 16.5 |

**Table 11b. Comparison of Selected Source Locations, their Strengths and the Goodness-of-Fit of the Inverse Model Concentration Predictions for PCB 52 with Different Values of Horizontal Diffusivity in EFDC.**

| Horizontal diffusivity ($m^2/s$) | Source locations (river mile) and strengths (mg/d) | | | | | | | | RMS error (pg/L) |
|---|---|---|---|---|---|---|---|---|---|
| | Bottom sources | | | | | | Surface sources | | |
| | 0.1 East | 0.4 East | 0.8 West | 1.7 West | 2.0 West | 3.8 East | 0.4 East | 3.8 East | |
| 40 | 27 | 3 | 9 | 19 | | 0.5 | 3 | 1 | 11.0 |
| 0.4 | 62 | 6 | 33 | | 30 | 0.6 | 5 | 0.9 | 10.1 |

**Table 11c. Comparison of Selected Source Locations, their Strengths and the Goodness-of-Fit of the Inverse Model Concentration Predictions forPCB 101 with Different Values of Horizontal Diffusivity in EFDC.**

| Horizontal diffusivity ($m^2/s$) | Source locations (river mile) and strengths (mg/d) | | | | | | | | | RMS error (pg/L) |
|---|---|---|---|---|---|---|---|---|---|---|
| | Bottom sources | | | | | | | Surface sources | | |
| | 0.1 Center | 0.1 East | 0.4 East | 0.8 West | 1.7 West | 2.0 West | 3.8 East | 3.8 East | 4.1 East | |
| 40 | | 27 | 2 | 21 | 0.5 | | 0.5 | 1 | 0.2 | 5.6 |
| 0.4 | 16 | 49 | 7 | 39 | | 7 | 0.6 | 1 | | 4.6 |

Table 11 indicates that although the source distribution shifts somewhat in response to reducing the horizontal diffusivity by a factor of 100, the goodness-of-fit does not improve much meaning that other factors must dominate the discrepancies between model and data.

To test whether the goodness-of-fit for the low horizontal diffusivity case is sensitive to the longitudinal density of potential sources, the inverse model was also run with a denser distribution of potential sources between RM 1.0 and RM 3.0 (138 potential sources at the horizontal locations shown in Figure 11) using the smaller horizontal diffusivity (0.4 $m^2/s$). The denser distribution of potential sources yielded inverse model results that are in better agreement with measured concentrations (Table 12), suggesting that using a denser coverage of potential candidate sources may be a valuable refinement when the horizontal diffusivity is small enough to keep nearby sources distinct.

The improvement of the inverse model's goodness-of-fit to the measured data with a denser spatial coverage also raises the possibility that the inverse model's performance may be limited by EFDC grid resolution, to the extent that the real sources are of a sub-grid scale. Representing a highly localized source with a much coarser EFCC grid cell means that unrealistic initial mixing will occur when the source's loading is effectively distributed uniformly over the grid cell in which it is introduced (regardless of the horizontal diffusivity setting). The potential impact of sub-grid scale effects is considered in the next section.

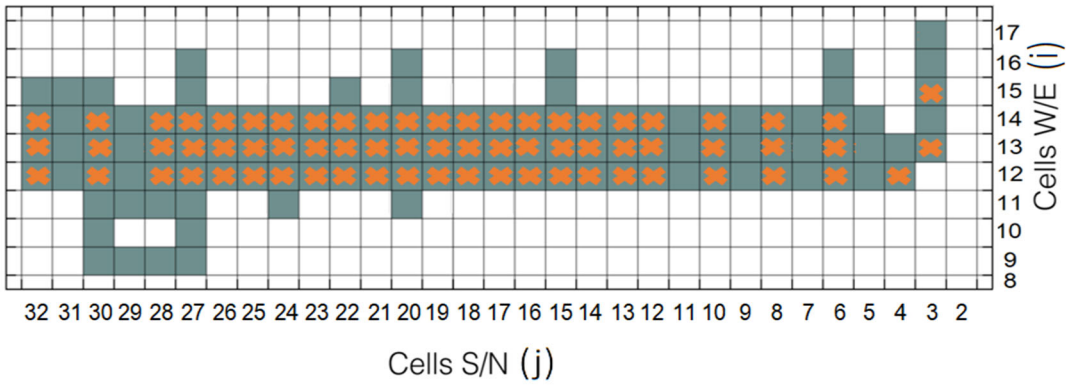


**Figure 11. Potential Source Locations (Marked with Crosses) with Dense Distribution between RM 1.0 and 3.0.**

*Potential sources were simulated at the surface and the bottom at each of the marked locations with horizontal diffusivity of 0.4 m2/s.*

**Table 12. Source Strengths for Sources Selected by the Inverse Model Out of 138 Potential Sources with Horizontal Diffusivity of 0.4 $m^2/s$.**

| Congener | Source locations (river mile) and strengths (mg/d) | | | | | | | | RMS error |
|---|---|---|---|---|---|---|---|---|---|
| | Bottom Sources | | | | | | Surface sources | | |
| | 0.1 Center | 0.1 East | 0.4 East | 0.8 West | 2.1 West | 3.8 East | 0.4 East | 3.8 East | |
| PCB 28 | | 69 | 7 | 26 | 19 | 0.4 | 42 | 0.8 | 11.4 |
| PCB 52 | | 64 | 7 | 37 | 13 | 0.9 | 10 | 1.3 | 6.7 |
| PCB 101 | 30 | 44 | 6 | 38 | 3 | 0.6 | | 1.2 | 4.3 |

### 2.3.10 Sub-grid Scale Sources

To test the potential impact of sub-grid scale sources on inverse model results, we used a simpler setup in which the concentration field can be specified analytically: a vertically well-mixed rectangular channel with uniform flow and homogenous diffusion. In such a setting, the concentration field resulting from a continuous line source (at longitudinal location $x = x_d$) can be calculated analytically as:

$$c(x,y) = \frac{q'}{2\{\pi u E_y (x - x_d)\}^{1/2}} \exp\left[-\frac{y^2 u}{4E_y(x - x_d)} - \frac{k(x - x_d)}{u}\right] \quad (6)$$

where $q'$ is the mass injection rate per unit depth of the source, $u$ is the longitudinal flow velocity, $E_y$ is the lateral diffusion coefficient, $y$ is the lateral distance away from the source, and $k$ is the first order decay rate for the contaminant.

For this test, concentration "measurements" for the inverse model are generated by considering two line sources with strengths of 8 and 20, located at $x = 3000$ m and $x = 6000$ m, respectively, in a 9840 m long, 180 m wide rectangular channel. The two sources are assumed to be discharging a conservative contaminant (decay rate of zero). Eight evenly spaced measurement locations are chosen between $x = 840$ m and 9240 m. The velocity in the channel ($u$) and the lateral diffusion coefficient ($E_y$) are chosen to be 0.1 m/s and 0.02 m$^2$/s, respectively. Figure 12 shows the resulting concentration distribution at $y = 0$ along with the "measured" concentrations.

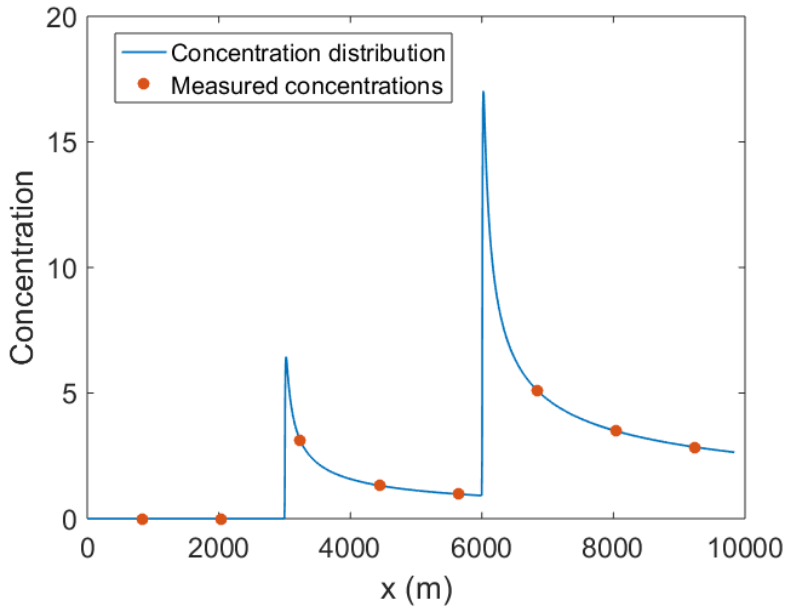


**Figure 12. Analytical Concentration Distribution at $y = 0$ Resulting from Two Line Sources Located at 3000 m and 6000 m with Strengths of 8 and 20, Respectively.**

*Also shown are the 8 measured concentrations used in this test, which are evenly spaced at locations between 840 m and 9240 m.*

To assess the impact of applying the inverse model to a grid of finite resolution, two different grid sizes (over which the inverse model fingerprints would be averaged) are considered: a coarser grid with $\Delta x = 240$ m and $\Delta y = 60$ m, and a finer grid with $\Delta x = 80$ m and $\Delta y = 36$ m (the grid sizes and measurement locations are chosen such that the measurement locations are at grid cell centers). 19 potential equally-spaced source locations between $x = 500$ m and $x = 9500$ m are specified, and the inverse model fingerprints are the concentrations resulting from these sources after spatially averaging the analytical solution concentrations over the grid cells.

Table 13 shows inverse model results for the two grid sizes. The "real" measured concentrations from sub-grid scale sources (as specified by the analytical solution) cannot be exactly explained using spatially averaged concentrations (averaged over grid cells) as evidenced by the non-zero error between measured and predicted concentration. As expected, the agreement with real concentrations gets better as the grid size is reduced.

**Table 13. Inverse Model Results When Potential Sources with Spatial Averaging Are Used. The "Real Sources" Are Located at 3000 m and 6000 m.**

| Grid size | Source locations (m) and strengths | | | | RMS error |
|---|---|---|---|---|---|
| | 3000 | 6500 | 7500 | 8500 | |
| **Coarse grid ($\Delta x = 240$ m, $\Delta y = 60$ m)** | 13.9 | 20.3 | | | 0.45 |
| **Fine grid ($\Delta x = 80$ m, $\Delta y = 36$ m)** | 10.4 | 15.0 | 0.9 | 0.4 | 0.18 |

The test was repeated using potential sources that released tracer undergoing a first order decay, to check whether better agreement with real concentrations can be achieved. Decay rates of 1/(24 hours), 1/(6 hours) and 1/(1 hour) were used (Table 14). Figure 13 shows the concentration distributions resulting from the sources selected by the inverse model. Using a fast decay rate can result in good agreement between measured and predicted concentrations at the measurement locations (small or zero RMS error) but the predicted concentration distributions are very different from the "real" concentration distribution generated by the sub-grid scale sources. With faster decay, the inverse model selects more sources to fit concentrations at the measurement locations, but the improvement in goodness-of-fit is artificial in that the inverse model and the selected sources do not help in locating the real sources.

**Table 14. Inverse Model Results When Potential Sources with Spatial Averaging and Decay Used.**

| Grid size | Decay rate | Source locations (m) and strengths | | | | | | | | | | RMS error |
|---|---|---|---|---|---|---|---|---|---|---|---|---|
| | | 2500 | 3000 | 4000 | 5000 | 5500 | 6500 | 7500 | 8000 | 8500 | 9000 | |
| **Coarse grid** | $(24\ h)^{-1}$ | 18.6 | | | | | 25.6 | | | | 1.5 | 0.26 |
| | $(6\ h)^{-1}$ | 28.2 | | | | 2.0 | 32.8 | 9.4 | | | 8.2 | 0.02 |
| | $(1\ h)^{-1}$ | | 35.8 | 25.2 | | 8.2 | 77.6 | | 39.6 | 30.7 | | 0 |
| | | | | | | | | | | | | |
| **Fine grid** | $(24\ h)^{-1}$ | | 11.2 | | | | 16.5 | 3.0 | | 2.6 | | 0.08 |
| | $(6\ h)^{-1}$ | | 12.3 | 1.3 | 2.4 | | 18.7 | 8.1 | | 8.2 | | 0 |
| | $(1\ h)^{-1}$ | | 17.7 | 12.6 | | 9.2 | 29.7 | 35.2 | | | 20.8 | 0 |

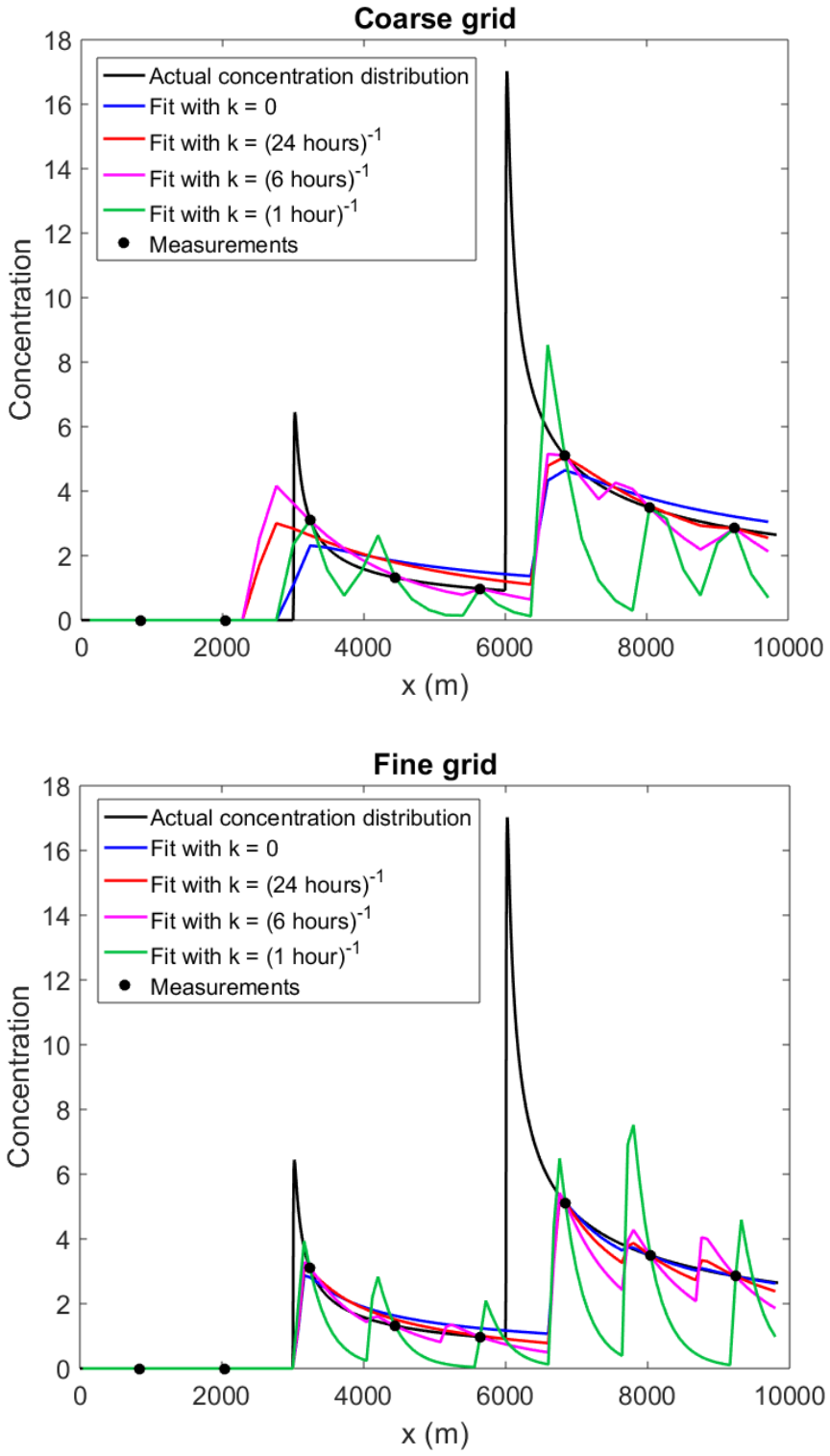


**Figure 13. Comparison of Actual Concentration Distribution with Concentration Distributions Resulting from Sources Selected by the Inverse Model for the Coarse (Top) and Fine Grid (Bottom).**

It can be seen from this exercise that the ability of the inverse model to locate sources depends strongly on the grid resolution. The model cannot identify sources if the concentrations are not well resolved. Better resolution can be obtained by using a finer grid or by using Lagrangian particle tracking.

The exercise also demonstrates that introducing additional processes such as decay can improve the goodness-of-fit of the inverse model without necessarily improving the accuracy of the source location; the processes must be physically realistic in order to yield useful results.

## 2.4 CONCLUDING COMMENTS

### 2.4.1 Summary and Implications

The inverse model provides a way to infer potential sources of contamination using concentration measurements. This is demonstrated conceptually with a simple setup of a vertically well-mixed rectangular tidal channel and applied to the more complex LDW domain using the 2016 passive sampler measurements. An important result from the conceptual model, and reinforced with the LDW numerical model, is that the accuracy of the inverse model source identification depends strongly on the precision of the measurements. In the LDW, the inverse model results suggest that concentrations measured in 2016 are consistent with bottom sources of dissolved concentration in the downstream region (RM 0-2) for PCB 28, 52 and 101. Multiple hydrodynamic model calibration settings (with different vertical and horizontal mixing settings) were considered and this finding was not highly sensitive to the choice of calibration. Other tests demonstrate that the inferred source distribution may be sensitive to factors such as the density of candidate source locations considered, modeled fate and transport processes, and the numerical model grid's resolution.

The dissolved concentrations predicted by the inverse model agree moderately well with the measurements on average, with predictions that are mostly within a factor of two of the measured concentration and all within a factor of 5 (Figure 5). Potential contributors to such differences includes transformation and transport processes that are not modeled in the EFDC simulations (e.g., sediment dynamics and sorption processes, air-water exchange, etc.) or the presence of sub-grid scale sources in the real world which cannot be resolved by the EFDC grid. The sensitivity of inverse model results to uniform first order decay (e.g., depth-averaged water-to-air exchanges, Apell and Gschwend, 2017) and changes to the horizontal diffusivity are evaluated, but the goodness-of-fit was not strongly affected. For example, regardless of the horizontal diffusivities input to the model, each source is effectively distributed uniformly over the grid cell in which it is introduced, resulting in unrealistic initial mixing. Such spurious mixing is particularly detrimental to the model's ability to distinguish local sources. Other approximations, such as the use of a straight arithmetic average (instead of the exponential filter) to calculate tracer concentrations for samplers, and the use of average concentrations for the vertical layer in which the sampler resides (instead of an interpolated value), could also lead to some divergence between measurements and predictions. However, these differences are shown to be small.

Using the sources identified by the inverse model, dissolved water column contaminant concentrations within the study area can be predicted (as shown in Figure 9). These predictions can then be used as input to the FWM which determines exposure to marine life. This is done by identifying horizontal cells that belong to each of the larger cells of the FWM.

For example, in the application described in Section 1 of this document, the volume-weighted concentrations from EFDC simulations (which represent variation in time and space) for each cell of the FWM were approximated by a log-normal distribution and the corresponding values of mean and standard deviation for the distribution are calculated and used to assign dissolved phase concentrations in the FWM. We note that pelagic organisms swim over large portions of the LDW and hence sample spatial variability in concentrations. The accuracy of the EFDC-predicted concentrations may be limited by unresolved processes as described above, but the large-scale predicted concentration distribution is constrained by mass conservation in the LDW, thus rendering the model forgiving for related the food web calculations.

Identification of source locations by inverse modeling is evaluated as a potentially helpful approach to inform further site investigations and remediation efforts. However, the sources identified by the inverse model in the LDW application are all point sources and do not include any adjacent sources, which could indicate a distributed source (i.e., one that reflects the combined inputs from nearby locations). Perhaps, sources in the real world seem are, in fact, likely to be distributed (at least, the ones on the bottom to the extent they represent a sediment source). The absence of identified adjacent sources makes it difficult to determine the spatial extent of the sources identified. Obviously, the ability of the inverse model to identify a distributed source is in part limited by the resolution of the EFDC grid and the density of potential sources with which the inverse model is supplied. If the size of a distributed source is large compared to the grid cell size and the inverse model is provided with a sufficiently dense grid of potential source locations, the inverse model approach would in principle be able to identify it as shown in Section 5 above.

With the sources identified by the inverse model, potential effects of source removal or reduction can in principle be assessed at a high level. To demonstrate the potential effects of source removal, concentration heat maps are plotted in Figure 14 after the removal of one source for each of the three congeners (PCB 28, 52 and 101; see Figure 7 for the concentrations without source removal). The source here chosen to be removed is the one with the largest contribution to the average mass of that PCB congener (Table 5) – a source at RM 1.7 west bottom for PCB 28 and 52, and a source at RM 0.8 west bottom for PCB 101.

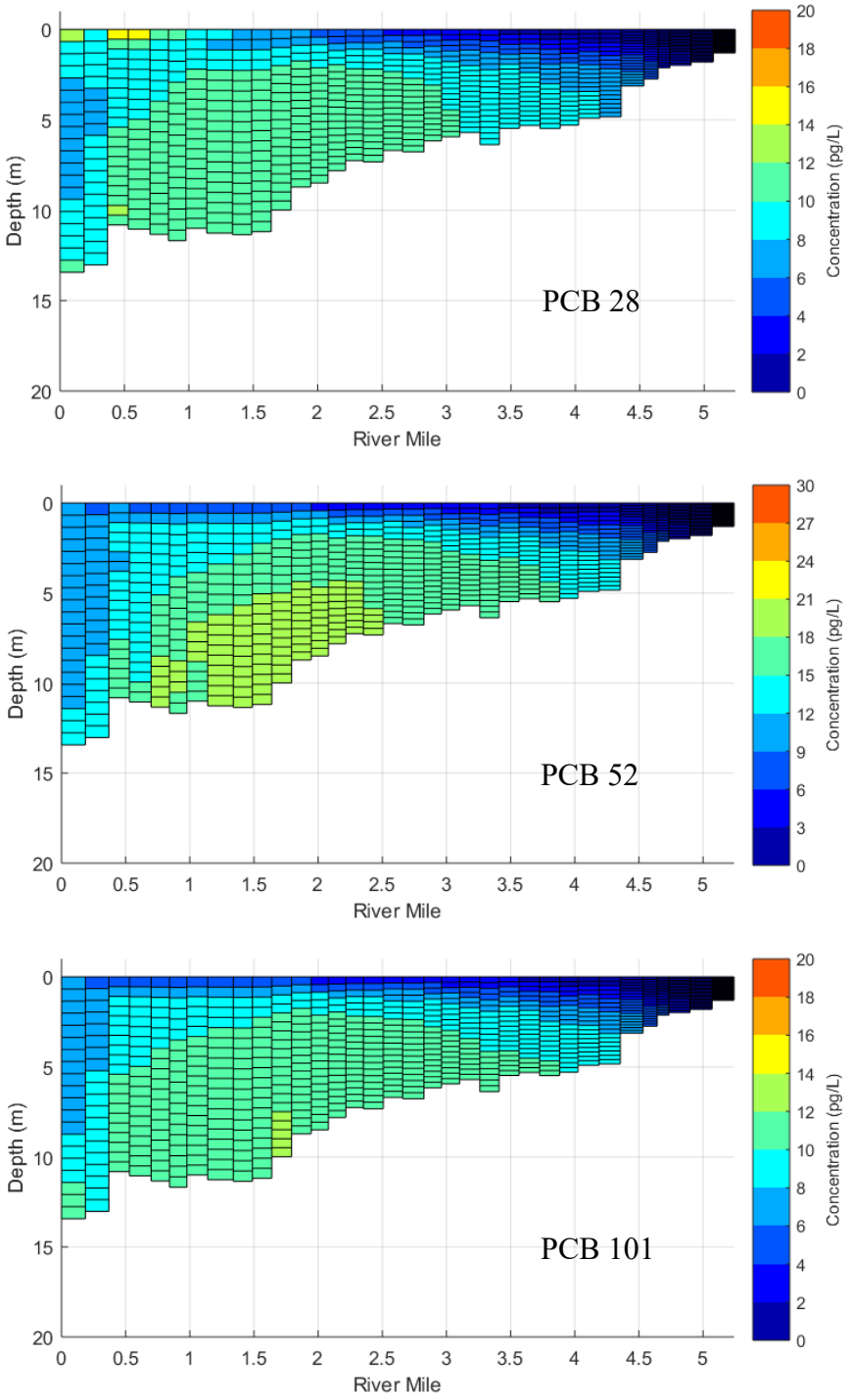


**Figure 14. Predicted Longitudinal Concentration Profiles Along the Center Channel of the LDW after Hypothetical Removal of One Identified Source.**

*For PCB 28 and 52, the source removed is the bottom source at RM 1.7 on the west bank. For PCB 101, the bottom source at RM 0.8 on the west bank is removed.*

Comparing heat maps in Figure 14 to those in Figure 7 suggests the removal of said sources could lead to a significant reduction in dissolved phase concentrations (e.g., about a factor of 2 for PCB 101, see Figure 15). However, the importance of such a change, especially relative to some cost associated with removal of such a source, may only be gaged by coupling these results with a FWM.

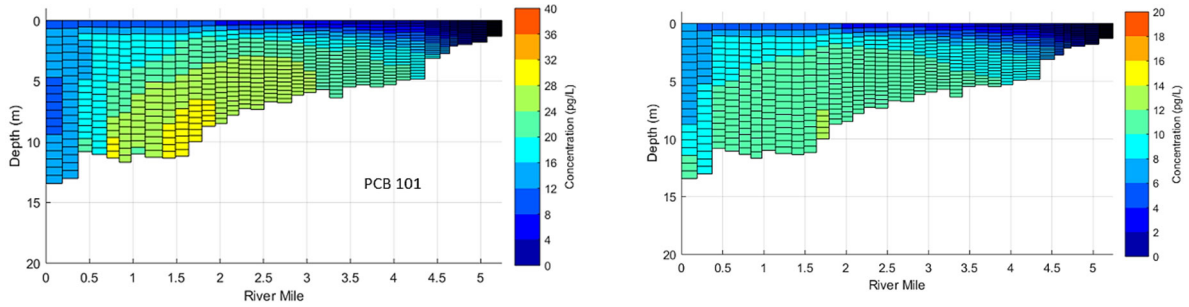


**Figure 15. Comparison of EFDC-inferred Water Concentrations of PCB101 for Before (Left Panel) and After (Right Panel) Source Removal at RM 0.8.**

*Note the overall scale for the left panel is a factor of 2 greater.*

However, it should be noted that the source removal exercise makes several simplifying assumptions which limits its robustness in regard to evaluating remedial benefit. Most notably, it considers the hypothetical removal of the dissolved phase concentration contributions from a source without assuming anything about the type of source, its size and how it relates to bulk PCB contamination in the system. For example, in the real world, remediation of a sediment bed source usually involves dredging and/or capping, but the source area can be re-contaminated and continue to act as a source if its PCB levels reflect the influence of other sources (e.g., via intermittent loading from an outfall or upstream source). But for this exercise, it is assumed that a removed source results in complete removal of the dissolved concentrations contributed by it. As such, remedial benefit inferred from this exercise is likely to be an upper bound. Also, the spatial extent and nature of the source is not known, which would be required further evaluation of remediation options for the source (e.g., by dredging/capping for sediment sources) and to be able to characterize their impacts on the food web and contributions to risk. The latter is required to assess remedial benefits beyond the reduction in dissolved water column concentration.

Nevertheless, even if the nature of a source cannot be inferred from the inverse modeling, having some estimate of its size and extent can help guide future sampling to investigate the source and potential remedial strategies. An identified point source can be considered as occurring over the area between the identified source and adjacent unidentified sources. For example, in results presented above, the model identifies a source at RM 1.7 on the west bank for PCB 28, but does not identify the adjacent sources longitudinally (at RM 1.4 and 2.0 on the west bank) or laterally (at RM 1.7 along the center channel), suggesting a source area on the order of 480 m × 60 m or less (an average grid cell is 240 m long and 60 m wide).

### 2.4.2 Key Conclusions

- The accuracy of source assessment would likely be more robust through use of a more comprehensive fate and transport model that modeled total chemical (rather than just dissolved) and included processes such as sediment transport and contaminant sorption and desorption.
- The ability of the inverse model to distinguish among closely spaced potential sources depends in part on near source resolution. This ability would in principle improve through either increased grid refinement, or the use of Lagrangian particle tracking to handle transport near sources.
- Inverse model results depend strongly on the precision of measured concentration; less accurate measurements adversely impacts source identification.
- Related to above, if "fast" passive samplers are deemed to be accurate and precise, they open up the possibility of sequential sampling over shorter temporal timescales—i.e., combine an initial set of measurements with the inverse model to generate an approximate source distribution, then return to the site to make an iteration.
- While the above considerations limit the accuracy of the model to identify precise source locations and magnitudes, the model-predicted distributions are constrained by mass-conservation to give results that are on-average consistent with the data on a LDW-wide basis, which may be adequate for specifying the water column exposure of pelagic organisms in food web calculations.
- Although the inverse model findings can in principle be used to estimate an upper bound remedial benefit of source removal to reduce dissolved phase concentrations, such an exercise makes several simplifying assumptions which limits its robustness and it cannot be reliably extended to estimate a risk reduction without additional information because the nature and extent of the inferred dissolved concentration source and its relationship to bulk contaminant concentration is unknown.

Finally, this inverse modeling methodology certainly fits in the "toolkit" of current contaminated sediment investigations.

## 2.5 REFERENCES

Akaike, H., 1974. A new look at the statistical model identification. IEEE Transactions on Automatic Control 19, 716–723. https://doi.org/10.1109/TAC.1974.1100705

Apell, J.N., Gschwend, P.M., 2017. The atmosphere as a source/sink of polychlorinated biphenyls to/from the Lower Duwamish Waterway Superfund site. Environ. Pollution 227: 263-270. http://dx.doi.org/10.1016/j.envpol.2017.04.070

Burnham, K.P., Anderson, D.R., 2004. Multimodel Inference: Understanding AIC and BIC in Model Selection. Sociological Methods & Research 33, 261–304. https://doi.org/10.1177/0049124104268644

Foy, B. de, Wiedinmyer, C., Schauer, J.J., 2012. Estimation of mercury emissions from forest fires, lakes, regional and local sources using measurements in Milwaukee and an inverse

method. Atmospheric Chemistry and Physics 12, 8993–9011. https://doi.org/10.5194/acp-12-8993-2012

Henze, D.K., Seinfeld, J.H., Shindell, D.T., 2009. Inverse modeling and mapping US air quality influences of inorganic PM2.5 precursor emissions using the adjoint of GEOS-Chem. Atmospheric Chemistry and Physics 9, 5877–5903. https://doi.org/10.5194/acp-9-5877-2009

McCormick, N.J., 1992. Inverse Radiative Transfer Problems: A Review. Nuclear Science and Engineering 112, 185–198. https://doi.org/10.13182/NSE112-185

Ozisik, M.N., 2018. Inverse Heat Transfer: Fundamentals and Applications. Routledge. https://doi.org/10.1201/9780203749784

Stohl, A., Seibert, P., Arduini, J., Eckhardt, S., Fraser, P., Greally, B.R., Lunder, C., Maione, M., Mühle, J., O'Doherty, S., Prinn, R.G., Reimann, S., Saito, T., Schmidbauer, N., Simmonds, P.G., Vollmer, M.K., Weiss, R.F., Yokouchi, Y., 2009. An analytical inversion method for determining regional and global emissions of greenhouse gases: Sensitivity studies and application to halocarbons. Atmospheric Chemistry and Physics 9, 1597–1620. https://doi.org/10.5194/acp-9-1597-2009

Sugiura, N., 1978. Further analysts of the data by akaike' s information criterion and the finite corrections. Communications in Statistics - Theory and Methods 7, 13–26. https://doi.org/10.1080/03610927808827599

Tarantola, A., 2005. Inverse Problem Theory and Methods for Model Parameter Estimation. SIAM.

Wiggins, R.A., 1972. The general linear inverse problem: Implication of surface waves and free oscillations for Earth structure. Reviews of Geophysics 10, 251–285. https://doi.org/10.1029/RG010i001p00251

Yeh, W.W.-G., 1986. Review of Parameter Identification Procedures in Groundwater Hydrology: The Inverse Problem. Water Resources Research 22, 95–108. https://doi.org/10.1029/WR022i002p00095

# SECTION 3 FOOD WEB MODELING TO ASSESS PCB CONCENTRATIONS IN BIOTA BASED ON PASSIVE SAMPLING OF A SITE'S SEDIMENT BED AND WATER COLUMN AND ASSUMING FUTURE REMEDIATED CONDITIONS

## 3.1 BACKGROUND

If the cleanups of sediment-contaminated sites are driven by reducing risks to aquatic life and other organisms (birds and humans), then we need to be able relate the changing presence of contaminants to exposures experienced by those organisms. Recently, a great step forward has been taken in this regard by the development of FWMs (FWMs, Arnot and Gobas, 2004; Gobas and Arnot, 2010). These models connect the concentrations of contaminants in a site's surface water, sediments, and pore waters to the body burdens of all the organisms comprising the food web. As a result, risks to organisms, including humans, can be estimated if environmental exposures are known.

But until recently, combining tools to characterize exposures of organisms with understanding of the combinations of uptake and depuration processes dictating those biota's concentrations has been lacking. As an example, as part of the LDW Remedial Investigation (Windward 2010), the Gobas FWM was employed. In this case, the PCBs in the system were modeled by Nairn (2009) using a site-calibrated version of the EFDC. Nairn allowed diffusive fluxes from the bed to the overlying bottom water, where the Duwamish sediments were characterized using surface-area-weighted-averages of measured PCB concentrations in the bed over four regions. Unfortunately, the model treated all the PCBs as a single entity with singular properties (e.g., a really constant $K_d$ value of 140,000 L/kg used to calculate porewater concentrations everywhere). Finally, the model was calibrated by adjusting the mass transfer coefficient quantifying the rates of PCBs exiting the bed sediments to match the few reported water column ∑PCB concentrations (King County, 2006). In so doing, average water column and porewater concentrations could be found and used in the Gobas FWM (LDW Remedial Investigation, Appendix D, 2010). The resultant FWM, also unfortunately run with the ∑PCBs treated as a singular compound, was also calibrated to fit observed tissue concentrations (which it could do to within about a factor of only 1.2 after calibration.)

Given this “state of the art," we sought to combine the "tools" of (a) passive sampling to measure porewater and surface water concentrations of PCBs in the LDW, (b) mass balance modeling to synthesize those site- and media-specific data to establish the spatially varying exposure field, and (c) utilize that measurement/modeling understanding to estimate the corresponding biota concentrations with previously established coefficients in the Gobas and Arnot and Gobas FWMs AND the spatially varying conditions from site-to-site via the statistical sampling of such subareas by biota according to their lifestyles. In so doing, we expect to demonstrate how such tools can be used to assess risks, and changing risks, for organisms interacting with particular contaminated ecosystems like the PCBs in the LDW estuary.

## 3.2 METHODS

### 3.2.1 Modeling

The FWMis based on the biological modeling expressions of Arnot and Gobas (2004) and assess the importance of spatial contamination heterogeneity as done by von Stackelberg et al. (2017) with several important flexibilities added:

1. The user can run the model for sets of specific nonionic contaminants (e.g. 20 specific PCB congeners) to find each compound's accumulation in each species modeled;

2. Species modeled that may be included are (a) widely roaming and even migrating species like bass, (b) limited range carnivorous and/or herbivorous species; (c) benthic invertebrates like mussels and oligochaetes, (d) fixed macroalgal/plant species; (e) zooplankton, and (f) phytoplankton.

3. The user may employ direct porewater measures from passive sampling OR estimates of porewater concentrations from sediment concentrations and estimates of sorption coefficients (e.g., $K_d = f_{oc} K_{oc}$);

4. The user may input $K_{ow}$ values to estimate $K_{oc}$, $K_{lip\text{-}water}$, and $K_{nonlip\text{-}water}$ coefficients with default relationships from Arnot and Gobas (2004) or may input partition coefficient values directly from the literature of the user's experience (e.g. adjusted for site temperatures);

5. The user can solve for bioaccumulation from the ecosystem from a time course calculation or simply via a steady state deterministic approach.

6. The time course output can provide propagated "uncertainty" that has arisen from uncertain inputs such as a species lipid content or from the variable positioning and feeding of widely roaming species sampling a heterogeneously contaminated site;
   Additionally, several practical improvements have been made:

7. The code has been transformed from Fortran to Python to facilitate future modeling improvements;

8. Excel spreadsheets are used to upload relevant site, contaminant, and biota data; explanatory comments are included on each tab to assist users to recognize "necessary" entries as opposed to others that will be used if no information is input (e.g., if no porewater concentrations are entered, then sediment concentrations, sediment organic contents, and $K_{ow}$ information will be used in a default calculation);

9. The latest version of the code can be downloaded for free from
   https://github.com/totorotoby/
   FishRand and a User's Manual describing installation on either Mac's or PC's (Windows) and all aspects of operating the model. Sample input sheets are also provided to insure the user can run the model with a correctly prepared input file.

### 3.2.2 Model Testing

As a primary goal of our related ESTCP project (ER-201431 Integrated Passive Sampler-Food Web Modeling Framework for Monitoring Remedy Effectiveness), we have been exercising and improving the FWM using a site with contemporaneous measures of water and sediment and biota concentrations of specific PCB congeners. This effort has allowed us to demonstrate the model's ability to operate and to identify key information for users.

With respect to the LDW, we have successfully performed the following modeling efforts:

1. Using the latitudes and longitudes of site locations from a field campaign in which porewater, bottom water, and water column concentrations were measured using PE passive samplers, the new model successfully produces a site map with Thiessen polygons drawn and areas calculated for the site and that particular sampling effort (Figure 1).

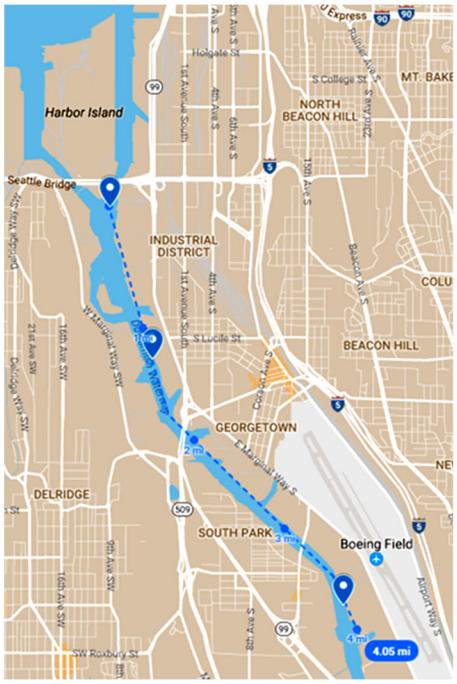


**Comparison of map created by (python) FishRand using 2014 sampling station lat' x long's to road map (shown left panel)**

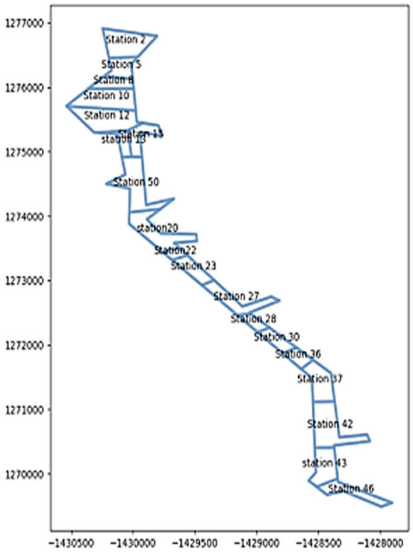


**Thiessen polygon areas calculated by (python) FishRand for map in middle panel.**

```
Polygon Areas:
|Station 2 |  133917.7
|Station 5 |  59647.17
|Station 8 |  53190.45
|Station 10|144010.49
|Station 12|158622.98
|station 13|  36897.12
|Station 15|  65754.79
|Station 50|154337.82
|station20 |136665.59
|Station22 |  20401.63
|Station 23|  60656.94
|Station 27|  93672.79
|Station 28|  32083.66
|Station 30|  49707.48
|Station 36|  38996.44
|Station 37|101213.51
|Station 42|161080.01
|station 43|  97677.9
|Station 46|  72123.39
```

**Figure 1. (left) Street Map Showing the Layout of the Approximately 4-mile-long LDW (in blue); (middle) Map Produced by the New FWM Showing Sampling Locations and Thiessen Polygons Around Each of These; and (Right) Areas of Each Thiessen Polygon if Surface Area-weighted Concentration Averages Are of Interest.**

2. We have examined the impact of various time-step choices on model outputs (Figure 2). Further, such outputs revealed the times needed for bioaccumulation to reach steady state levels for various organisms, both for uptake (shown in Figure 2) and for depuration (not shown) after a remedial effort.

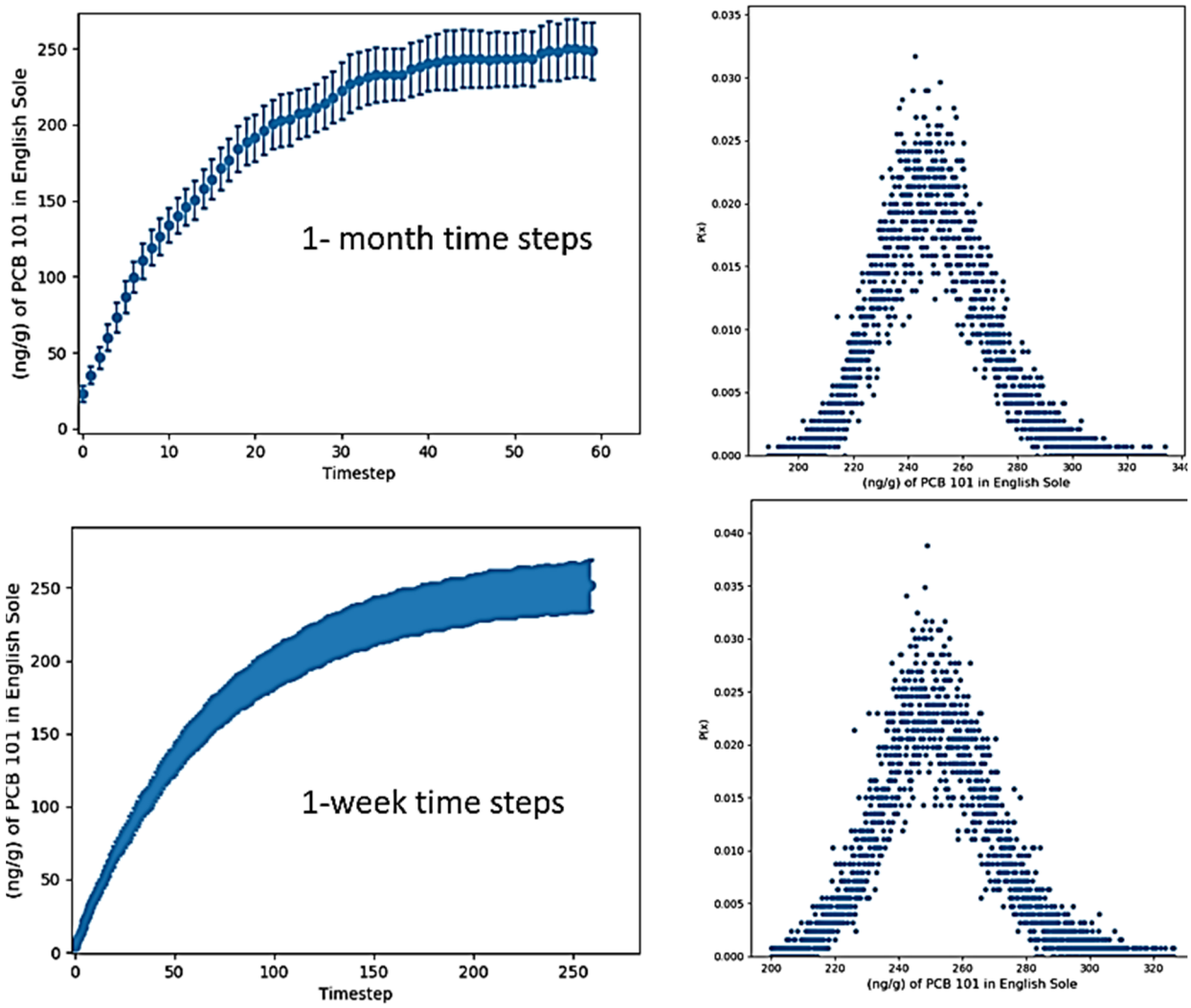


**Figure 2. Testing Sensitivity of Model Output for PCB101 Bioaccumulation of English Sole to the Choice of Modeling Time Steps: (Upper Left) Monthly vs (Lower Left) Weekly, Showing Comparable Plateau Concentrations (near 250 ng/g) and Similar Means and Standard Deviations (Right Panels).**

Likewise, the FWM proved to be sensitive to biological factors such as the set of food preferences consumed by each species. For example, comparing the PCB congener bioaccumulation in (softshell) clams between the case where they are assumed to only consume plankton with the case where the intake a substantial fraction (40% of their diet) of resuspended bottom sediment, one sees the PCB concentrations in the clams are about a factor of 4 greater if they include this much sediment intake in their diet, using the concentrations of PCBs in the LDW sediments (Figure 3). Note that the standard deviations (std in the table) associated with each modeling calculation imply this dietary impact is significant.

Lower Food Web Mean Concentrations and Standard Deviations Weighted by Regional Area (ng/g ww) — clams only filter feeders on plankton (50% phytos, 50% zoops)

| All Regions | PCB 28 mean | PCB 28 std | PCB 52 mean | PCB 52 std | PCB 101 mean | PCB 101 std | PCB 153 mean | PCB 153 std | PCB 180 mean | PCB 180 std |
|---|---|---|---|---|---|---|---|---|---|---|
| Phytoplankton | 0.19 | 0.08 | 0.32 | 0.12 | 0.67 | 0.22 | 0.91 | 0.30 | 0.52 | 0.18 |
| Zooplankton | 0.24 | 0.11 | 0.37 | 0.15 | 1.11 | 0.42 | 2.28 | 0.86 | 2.17 | 0.82 |
| Benthic Invertebrate | 14.34 | 3.91 | 11.75 | 2.28 | 22.04 | 5.49 | 47.63 | 14.74 | 31.06 | 8.31 |
| Clam | 0.77 | 0.43 | 1.18 | 0.47 | 2.39 | 0.63 | 4.08 | 1.18 | 3.15 | 1.01 |

Lower Food Web Mean Concentrations and Standard Deviations Weighted by Regiona. Area (ng/g ww) — clams filter feeders on 40% seds, 50% phytos, 10% zoops

| All Regions | PCB 28 mean | PCB 28 std | PCB 52 mean | PCB 52 std | PCB 101 mean | PCB 101 std | PCB 153 mean | PCB 153 std | PCB 180 mean | PCB 180 std |
|---|---|---|---|---|---|---|---|---|---|---|
| Phytoplankton | 0.19 | 0.08 | 0.32 | 0.12 | 0.67 | 0.22 | 0.91 | 0.30 | 0.52 | 0.18 |
| Zooplankton | 0.24 | 0.11 | 0.37 | 0.15 | 1.11 | 0.42 | 2.28 | 0.86 | 2.17 | 0.82 |
| Benthic Invertebrate | 14.34 | 3.91 | 11.75 | 2.29 | 22.03 | 5.50 | 47.63 | 14.75 | 31.06 | 8.32 |
| Clam | 5.46 | 1.42 | 4.65 | 0.88 | 8.85 | 2.14 | 18.28 | 5.41 | 12.00 | 3.08 |

**Figure 3. Comparison Showing Food Web-model-predicted Impacts of Changing Feeding Preferences for a Prominent Species, Softshell Clams, Often Eaten by Humans.**

## 3.3 RESULTS AND DISCUSSION

### 3.3.1 Food Web Expectations for LDW Organisms

Using our most spatially complete data set obtained via passive samplers deployed at 19 stations in the LDW (2014), we employed the EFDC model to estimate the resultant surface water concentrations (PCB101 in Figure 4). Not surprisingly, the porewater concentrations were higher than the surface water levels by about a factor of 5.

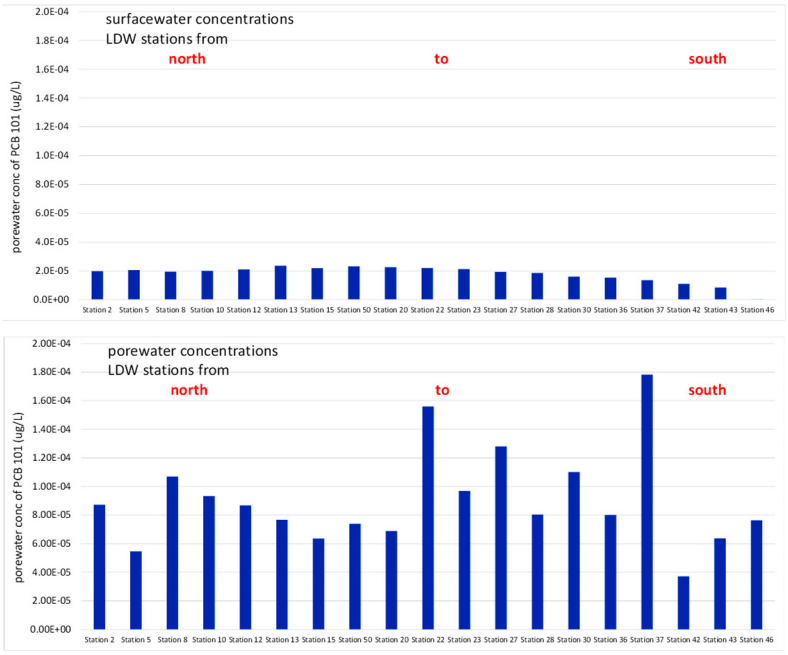


**Figure 4. (Upper) EFDC-based Estimates of Surface Water Concentrations of PCB101 (ug/L) Using Estimated Bed-water Fluxes and LDW Flushing. (lower) Passive Sampling Data for Porewater Concentrations of PCB101 (ug/L); NOTE: 1.00E-4 ug/L = 100 pg/L.**

With these (and sediment concentration) exposure fields, the FishRand FWM was then employed to estimate biota concentrations of several PCB congeners (Figure 5 for #28, #52, #101< #153, an #180 PCBs, a trichloro, a tetrachloro, and pentachloro, a hexachloro, and a heptachloro, respectively). Given the model used much lower surface water concentrations (about a factor of 5) than porewater concentrations, it is not surprising that the model predicts plankton concentrations that are much lower than those of benthic fauna (e.g., about 1 ng PCB101/gww for plankton, but about 10 to 20 ng PCB101/gww for benthic invertebrates and (softshell) clams). Further, based on the food web model, higher trophic level species like shiner surfperch and English sole are expected to accumulate PCB101 to levels near 100 ng/gww.

| **Lower Food Web Mean Concentrations and Standard Deviations Weighted by Regional Area (ng/g ww)** | **PCB 28** | | **PCB 52** | | **PCB 101** | | **PCB 153** | | **PCB 180** | |
|---|---|---|---|---|---|---|---|---|---|---|
| **All Regions** | **mean** | **std** | **mean** | **std** | **mean** | **std** | **mean** | **std** | **mean** | **std** |
| Phytoplankton | 0.19 | 0.08 | 0.32 | 0.12 | 0.67 | 0.22 | 0.91 | 0.30 | 0.52 | 0.18 |
| Zooplankton | 0.24 | 0.11 | 0.37 | 0.15 | 1.11 | 0.42 | 2.28 | 0.86 | 2.17 | 0.82 |
| Benthic Invertebrate | 14 | 4 | 12 | 2 | 22 | 5 | 48 | 15 | 31 | 8 |
| Clam | 5 | 1 | 5 | 1 | 9 | 2 | 18 | 5 | 12 | 3 |
| Juvenile Fish | 8 | 2 | 9 | 2 | 31 | 8 | 77 | 24 | 37 | 10 |
| Slender Crab | 13 | 4 | 14 | 3 | 43 | 11 | 107 | 33 | 53 | 14 |
| Dungeness Crab | 13 | 4 | 16 | 4 | 60 | 17 | 144 | 48 | 47 | 13 |
| **Upper Food Web Concentrations (ng/g ww) (Mean, Standard Deviation)** | | | | | | | | | | |
| | **PCB 28** | | **PCB 52** | | **PCB 101** | | **PCB 153** | | **PCB 180** | |
| | **mean** | **std** | **mean** | **std** | **mean** | **std** | **mean** | **std** | **mean** | **std** |
| Pacific Staghorn Sculpin | 14 | 1 | 15 | 1 | 55 | 5 | 136 | 14 | 56 | 5 |
| Shiner Surfperch | 26 | 3 | 28 | 2 | 87 | 8 | 194 | 17 | 73 | 6 |
| English Sole | 48 | 4 | 49 | 3 | 136 | 9 | 264 | 18 | 83 | 7 |

**Figure 5. FishRand Output File Showing Estimated Concentrations of Five PCB Congeners in Several Species Living in the LDW in 2014.**

### 3.3.2 Correspondence between Model Estimates and Measures

Next, we sought to examine the reasonableness of such food web model estimates. Previous investigators had collected shellfish and finfish samples and analyzed those for PCBs. For example, in 2004 (softshell) clams were obtained at several stations between river mile 0.2 and 4 from eight stations. The PCB contents measured in these were similar to the model output (Table 1).

**Table 1. Measures of Five PCB Congener Concentrations in Clams Collected in 2004 Versus Values Estimated Using the Food Web Model.**

| Clam concentrations (ng/gww) | PCB28 | PCB52 | PCB101 | PCB153 | PCB180 |
|---|---|---|---|---|---|
| **Measures in 2004 clam samples** | 2 ± 3 | 19 ± 38 | 11 ± 15 | 11 ± 11 | 5 ± 7 |
| **Food web model estimates** | 5 ± 1 | 5 ± 1 | 9 ± 2 | 18 ± 5 | 12 ± 3 |

Likewise, when we contrasted FishRand modeling estimates of PCBs in two common LDW fish species, shiner surfperch and starry flounder, we found reported measured total PCB contents were statistically indistinguishable from the modeled expectations. This is particularly true when one includes both the variations in measured results and the expected impacts of using uncertain inputs in the food web model (Figure 6). Hence, these comparisons support the conclusion that the food web modeling using FishRand in the LDW is providing reasonably accurate estimates.

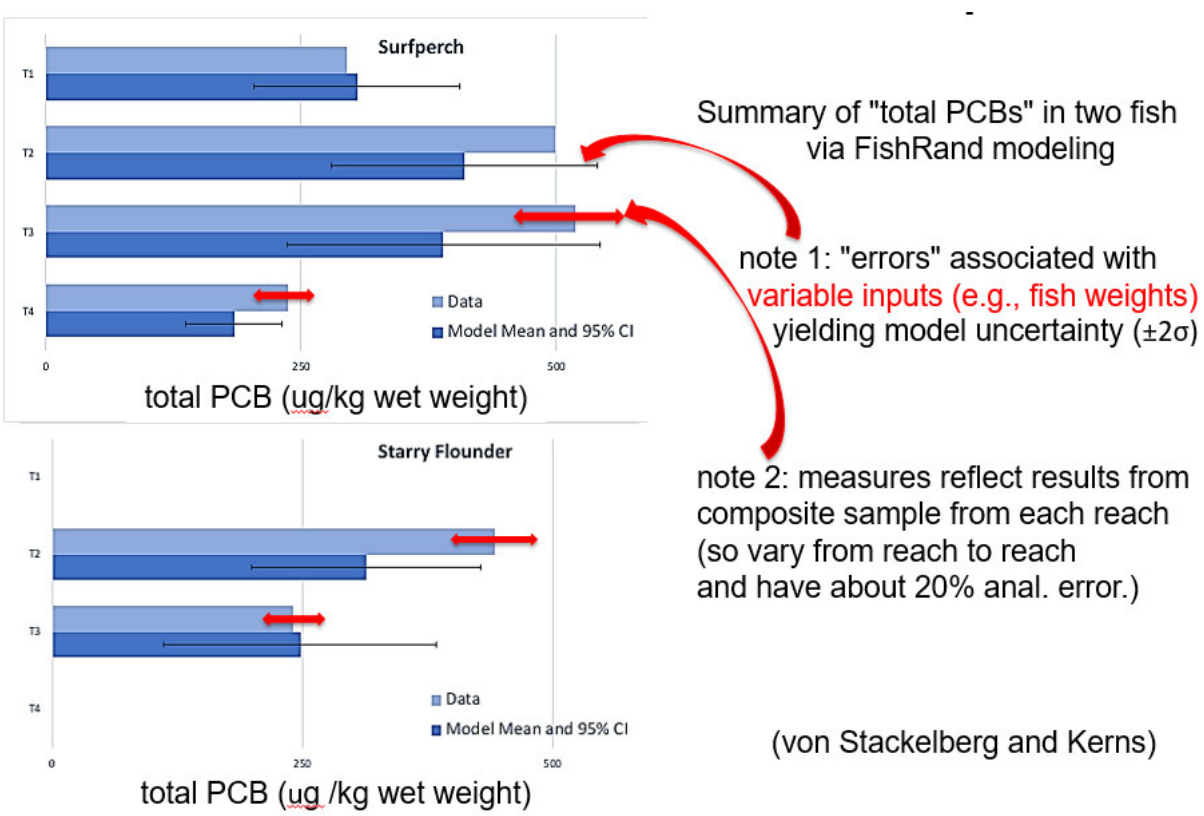


**Figure 6. Comparisons of Measured Total PCB Concentrations in Two LDW Fish Species, Surfperch (Upper) and Flounder (Lower), with FishRand FWM Expectations.**

*The bars are show with measurement uncertainty near ±20% and propagated errors in the modeling derived from uncertainties in key biological parameters like fish weights and lipid contents (±2σ errors plotted).*

### 3.3.3 Impact of Remediation

One of the primary motivations for combining the food web modeling tool with the passive sampling/mass balance modeling tools, it to explore effectiveness of proposed remedial approaches. Here we examine the case in which a site is cleaned up (e.g., capping) so as to remove a source/bed flux from a particular subregion of a site like the LDW. In this context, we can use the EFDC tool which has been set up with both site mixing/flushing information AND quantitation and spatial knowledge of PCB inputs (e.g., as described in sections 1 and 2 of this report, bed-to-water column fluxes or estimates of source strengths from the inverse modeling tool) to generate the distribution of surface water concentrations for rest of site. Having this "baseline" condition, we use this information to drive the initial FishRand model.

Subsequently, one may consider the impact of removing any particular PCB source without necessarily knowing how this will be done. But this change causes the EFDC model to recalculate the distribution of PCBs in the surface water, thereby making a key change to the FishRand inputs. Rerunning the model with everything else held the same (e.g., porewater concentrations at the rest of the site, feeding preferences...) allows the investigator to evaluate the expected impacts with respect to lowering shellfish and finfish tissue concentrations.

As an example, we have considered a hypothetical case in which a primary source of PCBs 28 and 52 (i.e., near RM 2) is remediated or a primary source of PCB 101 (i.e., near RM 0.8) is fully remediated. With such changes, the EFDC is rerun with these inputs set to zero and a new distribution of these PCB congeners in the waters of the LDW is produced. Uploading this new concentration information to the FishRand input file, the food web model is rerun and the results compared with the case before remediation.

Focusing on Dungeness crabs, the combination of EFDC modeling tool and the FishRand modeling indicate one should expect a decreased PCB52 and PCB 101 concentrations between 10 to 20% (Figure 7). This, of course, allows the regulator to evaluate the change in risk for people eating such crab, and thereby judge the worthiness of the cleanup investment.

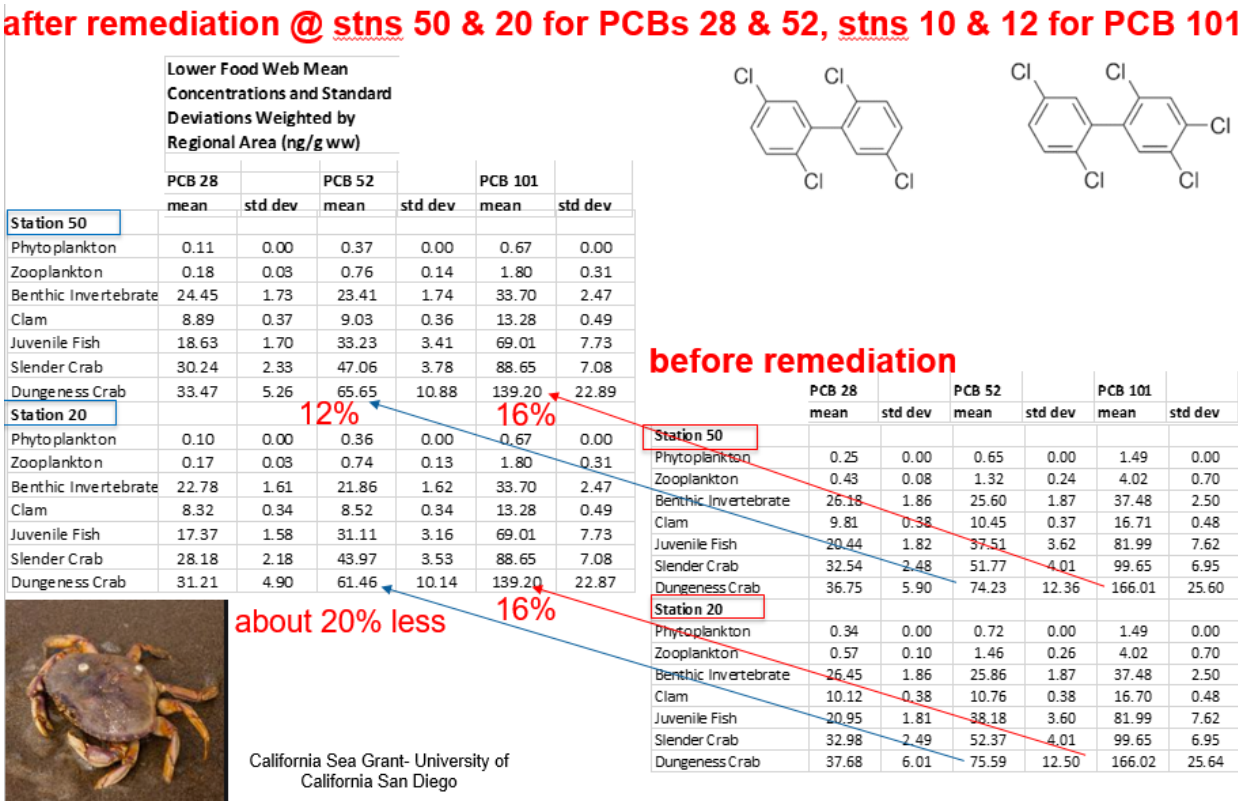


**Figure 7. Comparison of Food Web Model Outputs Before Remediating (Lower Right Table) and After Remediation (Upper Left Table).**

## 3.4 SUMMARY

While passive samplers may yield very useful insights regarding the spatially heterogeneous presence of contaminants of interest like PCBs, their use without a means to synthesize those observations via fate/source modeling (i.e., via tools like EFDC or Inverse Models) is limited. This is particularly true with respect to assessing the contaminant exposures at sites of interest. Moreover, judging the extent of expect changes with time (e.g., monitored natural recovery) or in response to employing particular clean up strategies (e.g., capping, dredging, or employing activated carbon) requires all three "tools": measures, contaminant fate modeling, and food web modeling.

An important aspect of food web modeling involves the need to capture the certainty with which one knows the result. This is particularly important as the inputs to such models are necessarily uncertain. All chemical measurements are uncertain. Key properties like food preferences and organism sizes within a single population are variable. And, of course, all environmental settings are heterogeneous in space and time. Hence, we must seek to understand the impacts of such factors on the bottom line: risks to ecosystems and human populations. The FishRand tool is a good beginning in this regard!

## 3.5 REFERENCES

Arnot JA and Gobas FAPC. 2004. A food web bioaccumulation model for organic chemicals in aquatic ecosystems. Environ. Toxicol. Chem. 23(10):2343–2355.

Gobas, F.A.P.C. and Arnot, J.A. Food web bioaccumulation model for polychlorinated biphenyls in San Francisco Bay, California, USA. Environ. Toxicol. Chem. 29, 1385-1395, 2010.

Nairn, B. EFDC calibration process for predicting PCB water concentrations in Lower Duwamish Waterway. Memorandum to J Stern and D Williston, King County Department of Natural Resources and Parks, Seattle WA. Nov. 2009.

von Stackelberg, K., M.A. Williams, J. Clough, and M.S. Johnson. 2017. Spatially explicit bioaccumulation modeling in aquatic environments: Results from 2 demonstration sites. Integrated Environmental Assessment and Management, 13(6):1023-1037.

Windward Environmental. Data Report: Survey and Sampling of Lower Duwamish Waterway Seeps. submitted to the US EPA Region 10 and Washington State Department of Ecology, Northwest regional Office. Nov. 2004.

# APPENDIX A PE SAMPLER LOCATIONS, DEPLOYMENT TIMES AND SITE DEPTHS, IN THE LDW IN THE SUMMER OF 2014.

Designations for corresponding EFDC cells ae shown. And locations of sites with water samplers deployed are identified. (Prendergast and Apell et al. in prep.)

| Site ID | River Mile[a] | Latitude (north) | Longitude (west) | Deploy Date | Recovery Date | Total Time | Mean Depth | EFDC Cell[b] | | WC?[c] |
|---|---|---|---|---|---|---|---|---|---|---|
| | [mi] | | | [M/D/Y] | [M/D/Y] | [days] | [m] | I | J | |
| **2** | 0.15 | 47.567736 | -122.348271 | 8/18/14 | 10/7/14 | 50 | 13.6 | 14 | 32 | Yes |
| **5** | 0.5 | 47.563601 | -122.346097 | 7/21/14 | 10/7/14 | 78 | 4.3 | 15 | 30 | Yes |
| **8** | 0.5 | 47.562117 | -122.345941 | 7/21/14 | 10/7/14 | 78 | 4.8 | 14 | 29 | No |
| **10** | 0.65 | 47.560803 | -122.345389 | 8/18/14 | 10/7/14 | 50 | 6.5 | 14 | 28 | No |
| **12** | 0.9 | 47.556418 | -122.344404 | 8/18/14 | 10/8/14 | 51 | 8.8 | 12 | 27 | No |
| **13** | 1.1 | 47.555011 | -122.343490 | 8/18/14 | 10/8/14 | 51 | 10.9 | 12 | 26 | No |
| **15** | 1.1 | 47.555391 | -122.341913 | 8/18/14 | 10/8/14 | 51 | 7.8 | 14 | 26 | No |
| **50** | 1.45 | 47.549743 | -122.340297 | 8/19/14 | 10/8/14 | 50 | 11.7 | 12 | 24 | No |
| **20** | 2.05 | 47.541360 | -122.334050 | 7/22/14 | 10/7/14 | 77 | 6.7 | 12 | 20 | No |
| **22** | 2.2 | 47.539557 | -122.331925 | 7/22/14 | 10/8/14 | 78 | 5.5 | 12 | 19 | Yes |
| **23** | 2.35 | 47.539305 | -122.331537 | 7/22/14 | 10/8/14 | 78 | 4.6 | 12 | 18 | No |
| **27** | 2.8 | 47.534722 | -122.322205 | 8/18/14 | 10/8/14 | 51 | 5.7 | 14 | 15 | No |
| **28** | 2.95 | 47.532553 | -122.320760 | 8/18/14 | 10/6/14 | 49 | 4.8 | 12 | 14 | No |
| **30** | 3.2 | 47.530526 | -122.317143 | 8/19/14 | 10/8/14 | 50 | 4 | 12 | 12 | No |
| **36** | 3.4 | 47.528367 | -122.312798 | 8/19/14 | 10/6/14 | 48 | 7.4 | 13 | 11 | No |
| **37** | 3.55 | 47.528039 | -122.311344 | 8/19/14 | 10/8/14 | 50 | 6.5 | 13 | 10 | No |
| **42** | 4.2 | 47.518797 | -122.307044 | 7/23/14 | 10/8/14 | 77 | 4.4 | 12 | 6 | No |
| **43** | 4.35 | 47.515920 | -122.305808 | 7/23/14 | 10/8/14 | 77 | 3.1 | 12 | 5 | Yes |
| **46** | 4.8 | 47.512196 | -122.298690 | 8/19/14 | 10/6/14 | 48 | 2.9 | 15 | 3 | Yes |

[a]Miles upriver from downstream border of study area. [b]Model cell coordinates containing sampler. *I* increases from east to west, *J* increases from south to north. See Figure S1. [c]Water column sampler attached 1 m above sediment-water interface.

# APPENDIX B FRACTIONS OF PRC LOSSES MEASURED FROM SEDIMENT-SIDE (0-5 CM BELOW INTERFACE) PE PASSIVE SAMPLERS DEPLOYED IN THE SUMMER OF 2014.

(Prendergast and Apell et al. in prep.)

| | Fraction Loss | | | | | | |
|---|---|---|---|---|---|---|---|
| | 13C PCB 28 | 13C PCB 54 | 13C PCB 47 | 13C PCB 97 | 13C PCB 111 | 13C PCB 153 | 13C PCB 178 |
| **Site 2 (50 d)** | 0.940 | 0.987 | 0.836 | 0.595 | 0.385 | 0.187 | 0.145 |
| **Site 5 (78 d)** | 0.777 | 0.938 | 0.652 | 0.522 | 0.313 | 0.221 | 0.180 |
| **Site 8 (78 d)** | 0.546 | 0.787 | 0.481 | 0.419 | 0.229 | 0.154 | 0.154 |
| **Site 10 (50 d)** | 0.494 | 0.761 | 0.473 | 0.278 | 0.207 | 0.098 | 0.079 |
| **Site 12 (51 d)** | 0.515 | 0.739 | 0.408 | 0.351 | 0.223 | 0.134 | 0.124 |
| **Site 13 (51 d)** | 0.930 | 0.993 | 0.795 | 0.612 | 0.391 | 0.227 | 0.185 |
| **Site 15 (51 d)** | 0.940 | 0.996 | 0.772 | 0.600 | 0.381 | 0.184 | 0.140 |
| **Site 20 (77 d)** | 0.493 | 0.718 | 0.355 | 0.271 | 0.179 | 0.154 | 0.155 |
| **Site 22 (78 d)** | 0.703 | 0.874 | 0.603 | 0.488 | 0.334 | 0.242 | 0.205 |
| **Site 23 (78 d)** | 0.869 | 0.958 | 0.783 | 0.612 | 0.423 | 0.358 | 0.309 |
| **Site 27 (51 d)** | 0.694 | 0.888 | 0.580 | 0.416 | 0.254 | 0.190 | 0.150 |
| **Site 28 (49 d)** | 0.609 | 0.809 | 0.478 | 0.302 | 0.175 | 0.094 | 0.083 |
| **Site 30 (50 d)** | 0.742 | 0.893 | 0.615 | 0.449 | 0.308 | 0.144 | 0.148 |
| **Site 36 (48 d)** | 0.424 | 0.576 | 0.285 | 0.248 | 0.175 | 0.144 | 0.135 |
| **Site 37 (50 d)** | 0.832 | 0.940 | 0.696 | 0.466 | 0.256 | 0.144 | 0.080 |
| **Site 42 (77 d)** | 0.499 | 0.751 | 0.374 | 0.302 | 0.137 | 0.056 | 0.040 |
| **Site 43 (77 d)** | 0.863 | 0.983 | 0.713 | 0.478 | 0.269 | 0.255 | 0.208 |
| **Site 46 (48 d)** | 0.791 | 0.913 | 0.612 | 0.484 | 0.290 | 0.137 | 0.152 |
| **Site 50 (50 d)** | 0.951 | 0.997 | 0.787 | 0.535 | 0.302 | 0.118 | 0.054 |
| **Average (%/day)** | 1.3% | 1.5% | 1.04% | 0.77% | 0.48% | 0.29% | 0.24% |
| **Std Dev** | 0.44% | 0.38% | 0.38% | 0.27% | 0.17% | 0.094% | 0.086% |
| **Rel Dev (%)** | 34.7% | 25.3% | 36.7% | 34.6% | 36.1% | 32.8% | 35.7% |

# APPENDIX C FRACTIONS OF PRC LOSSES MEASURED FROM WATER-SIDE (0-5 CM ABOVE INTERFACE) PE PASSIVE SAMPLERS DEPLOYED IN THE SUMMER OF 2014.

(Prendergast and Apell et al. in prep.)

| | Fraction Loss | | | | | | |
|---|---|---|---|---|---|---|---|
| | 13C PCB 28 | 13C PCB 54 | 13C PCB 47 | 13C PCB 97 | 13C PCB 111 | 13C PCB 153 | 13C PCB 178 |
| **Site 2** | 0.979 | 0.998 | 0.888 | 0.632 | 0.321 | 0.289 | 0.224 |
| **Site 5** | 0.948 | 0.996 | 0.872 | 0.690 | 0.448 | 0.278 | 0.279 |
| **Site 8** | 0.930 | 0.995 | 0.856 | 0.649 | 0.368 | 0.231 | 0.136 |
| **Site 10** | 0.896 | 0.984 | 0.763 | 0.464 | 0.271 | 0.205 | 0.131 |
| **Site 12** | 0.926 | 0.994 | 0.767 | 0.531 | 0.340 | 0.196 | 0.156 |
| **Site 13** | 0.916 | 0.993 | 0.925 | 0.444 | 0.261 | 0.189 | 0.150 |
| **Site 15** | 0.932 | 0.996 | 0.761 | 0.500 | 0.328 | 0.108 | 0.139 |
| **Site 20** | 0.936 | 0.993 | 0.845 | 0.655 | 0.392 | 0.194 | 0.147 |
| **Site 22** | 0.949 | 0.995 | 0.855 | 0.645 | 0.415 | 0.314 | 0.277 |
| **Site 23** | 0.966 | 0.992 | 0.928 | 0.719 | 0.478 | 0.352 | 0.321 |
| **Site 27** | 0.902 | 0.992 | 0.731 | 0.439 | 0.253 | 0.149 | 0.118 |
| **Site 28** | 0.927 | 0.996 | 0.775 | 0.530 | 0.305 | 0.165 | 0.126 |
| **Site 30** | 0.948 | 0.995 | 0.832 | 0.622 | 0.421 | 0.275 | 0.167 |
| **Site 36** | 0.903 | 0.981 | 0.759 | 0.537 | 0.302 | 0.182 | 0.165 |
| **Site 37** | 0.953 | 0.997 | 0.790 | 0.535 | 0.302 | 0.190 | 0.163 |
| **Site 42** | 0.871 | 0.973 | 0.732 | 0.554 | 0.340 | 0.168 | 0.132 |
| **Site 43** | 0.873 | 0.887 | 0.833 | 0.651 | 0.434 | 0.287 | 0.218 |
| **Site 46** | 0.982 | 0.997 | 0.932 | 0.752 | 0.476 | 0.315 | 0.260 |
| **Site 50** | 0.936 | 0.993 | 0.762 | 0.469 | 0.249 | 0.143 | 0.131 |
| **Average (%/day)** | 1.6% | 1.7% | 1.4% | 0.99% | 0.60% | 0.38% | 0.31% |
| **Std Dev** | 0.34% | 0.37% | 0.29% | 0.20% | 0.13% | 0.12% | 0.93% |
| **Rel Dev (%)** | 21% | 21% | 20% | 20% | 22% | 31% | 30% |

# APPENDIX D FRACTIONS OF PRC LOSSES MEASURED FROM PE PASSIVE SAMPLERS DEPLOYED 1 METER ABOVE THE SEDIMENT-WATER INTERFACE IN THE SUMMER OF 2014.

(Prendergast and Apell et al. in prep.)

| | Fraction Loss | | | | | | |
|---|---|---|---|---|---|---|---|
| | 13C PCB 28 | 13C PCB 54 | 13C PCB 47 | 13C PCB 97 | 13C PCB 111 | 13C PCB 153 | 13C PCB 178 |
| **Site 2** | 0.954 | 0.995 | 0.848 | 0.582 | 0.363 | 0.159 | 0.122 |
| **Site 5** | 0.935 | 0.996 | 0.785 | 0.594 | 0.356 | 0.185 | 0.142 |
| **Site 22** | 0.935 | 0.996 | 0.802 | 0.599 | 0.414 | 0.282 | 0.247 |
| **Site 43** | 0.960 | 0.998 | 0.889 | 0.691 | 0.413 | 0.202 | 0.132 |
| **Site 46** | 0.980 | 0.998 | 0.934 | 0.768 | 0.496 | 0.315 | 0.221 |
| **Average (%/day)** | 1.5% | 1.6% | 1.4% | 1.0% | 0.66% | 0.37% | 0.28% |
| **Std Dev** | 0.42% | 0.41% | 0.43% | 0.35% | 0.23% | 0.17% | 0.12% |
| **Rel Dev (%)** | 28% | 26% | 31% | 34% | 36% | 46% | 43% |

# APPENDIX E SEDIMENT-SIDE (0-5 CM BELOW SEDIMENT-WATER INTERFACE) FREELY DISSOLVED CONCENTRATIONS (PG/L) INFERRED FROM PRC-CORRECTED PE SAMPLERS DEPLOYED IN THE SUMMER OF 2014.

Brackets indicates ±2σ uncertainty found via error propagation. NC means not calculated because congener was not detected in the PE. (Prendergast and Apell et al. in prep.)

| | PCB 8 | | PCB 18 | | PCB 28 | | PCB 52 | |
|---|---|---|---|---|---|---|---|---|
| Site 2 | 44 | [24 - 79] | 97 | [54 - 170] | 91 | [49 - 170] | 72 | [39 - 140] |
| Site 5 | 99 | [54 - 180] | 210 | [110 - 380] | 280 | [140 - 530] | 100 | [50 - 200] |
| Site 8 | 56 | [29 - 110] | 180 | [90 - 360] | 270 | [120 - 580] | 130 | [59 - 310] |
| Site 10 | 60 | [31 - 120] | 180 | [91 - 370] | 240 | [100 - 530] | 120 | [50 - 270] |
| Site 12 | 38 | [19 - 76] | 99 | [48 - 200] | 140 | [64 - 330] | 110 | [49 - 260] |
| Site 13 | NC | NC | 44 | [24 - 78] | 100 | [55 - 180] | 69 | [37 - 130] |
| Site 15 | NC | NC | 23 | [13 - 41] | 61 | [33 - 110] | 55 | [30 - 100] |
| Site 20 | 20 | [10 - 42] | 82 | [38 - 180] | 95 | [41 - 220] | 110 | [45 - 260] |
| Site 22 | 52 | [28 - 96] | 220 | [120 - 410] | 330 | [170 - 670] | 260 | [120 - 530] |
| Site 23 | 9 | [5 - 17] | 47 | [26 - 86] | 93 | [50 - 170] | 110 | [59 - 210] |
| Site 27 | NC | NC | 59 | [31 - 110] | 94 | [46 - 190] | 150 | [71 - 320] |
| Site 28 | 20 | [11 - 37] | 78 | [40 - 150] | 100 | [47 - 220] | 140 | [62 - 310] |
| Site 30 | 7 | [4 - 12] | 43 | [23 - 80] | 65 | [33 - 130] | 120 | [60 - 250] |
| Site 36 | NC | NC | 96 | [42 - 220] | 86 | [35 - 210] | 160 | [64 - 400] |
| Site 37 | 22 | [12 - 40] | 210 | [120 - 380] | 330 | [170 - 620] | 300 | [150 - 590] |
| Site 42 | 7 | [4 - 14] | 43 | [21 - 86] | 46 | [20 - 100] | 62 | [26 - 150] |
| Site 43 | 9 | [5 - 16] | 54 | [30 - 98] | 75 | [40 - 140] | 120 | [63 - 230] |
| Site 46 | NC | NC | 40 | [22 - 73] | 53 | [27 - 100] | 110 | [57 - 230] |
| Site 50 | 6 | [3 - 10] | 31 | [17 - 57] | 65 | [35 - 120] | 60 | [32 - 110] |

| | PCB 44 | | PCB 66 | | PCB 77 | | PCB 101 | |
|---|---|---|---|---|---|---|---|---|
| Site 2 | 44 | [24 - 81] | 23 | [12 - 45] | 1 | [0 - 2] | 43 | [21 - 92] |
| Site 5 | 61 | [31 - 120] | 25 | [11 - 54] | 2 | [1 - 3] | 28 | [12 - 63] |
| Site 8 | 84 | [38 - 180] | 42 | [17 - 100] | 3 | [1 - 7] | 59 | [23 - 150] |
| Site 10 | 70 | [31 - 160] | 32 | [12 - 83] | 2 | [1 - 7] | 56 | [21 - 150] |
| Site 12 | 70 | [30 - 160] | 33 | [13 - 85] | NC | NC | 49 | [18 - 130] |
| Site 13 | 39 | [21 - 73] | 25 | [13 - 50] | 2 | [1 - 3] | 37 | [18 - 78] |
| Site 15 | 32 | [17 - 60] | 22 | [11 - 44] | 1 | [0 - 3] | 30 | [14 - 63] |
| Site 20 | 55 | [23 - 130] | 22 | [8 - 57] | NC | NC | 39 | [14 - 100] |
| Site 22 | 160 | [79 - 330] | 79 | [35 - 180] | 4 | [2 - 9] | 84 | [36 - 200] |
| Site 23 | 50 | [27 - 94] | 26 | [13 - 52] | 1 | [0 - 3] | 52 | [25 - 110] |
| Site 27 | 54 | [26 - 110] | 25 | [11 - 59] | 2 | [1 - 4] | 67 | [28 - 160] |
| Site 28 | 56 | [25 - 120] | 26 | [10 - 65] | 1 | [0 - 3] | 65 | [24 - 170] |
| Site 30 | 43 | [21 - 86] | 20 | [9 - 45] | 1 | [0 - 3] | 58 | [24 - 140] |
| Site 36 | 56 | [22 - 140] | 20 | [7 - 53] | 0.9 | [0 - 3] | 45 | [16 - 130] |
| Site 37 | 130 | [65 - 240] | 34 | [15 - 75] | 2 | [1 - 4] | 90 | [38 - 210] |
| Site 42 | 22 | [9 - 52] | 10 | [4 - 27] | NC | NC | 24 | [9 - 68] |
| Site 43 | 38 | [20 - 72] | 16 | [8 - 33] | NC | NC | 31 | [14 - 69] |
| Site 46 | 34 | [17 - 67] | 16 | [7 - 36] | NC | NC | 38 | [16 - 91] |
| Site 50 | 32 | [17 - 60] | 19 | [9 - 39] | 1 | [1 - 3] | 34 | [15 - 74] |

## APPENDIX E (cont'd)

| | PCB 118 | | PCB 105 | | PCB 126 | | PCB 153 | |
|---|---|---|---|---|---|---|---|---|
| **Site 2** | 20 | [7 - 53] | 7 | [3 - 17] | NC | NC | 37 | [11 - 120] |
| **Site 5** | 12 | [4 - 33] | 5 | [2 - 12] | NC | NC | 13 | [4 - 39] |
| **Site 8** | 22 | [8 - 64] | 10 | [3 - 26] | NC | NC | 24 | [8 - 73] |
| **Site 10** | 20 | [7 - 58] | 8 | [3 - 22] | NC | NC | 26 | [8 - 82] |
| **Site 12** | 17 | [6 - 51] | 7 | [3 - 20] | NC | NC | 20 | [7 - 61] |
| **Site 13** | 17 | [6 - 43] | 6 | [3 - 15] | NC | NC | 26 | [8 - 84] |
| **Site 15** | 14 | [5 - 38] | 5 | [2 - 14] | NC | NC | 25 | [7 - 83] |
| **Site 20** | 13 | [4 - 36] | 5 | [2 - 13] | NC | NC | 14 | [5 - 44] |
| **Site 22** | 29 | [11 - 79] | 11 | [4 - 29] | NC | NC | 35 | [12 - 100] |
| **Site 23** | 18 | [8 - 45] | 7 | [3 - 15] | NC | NC | 25 | [9 - 72] |
| **Site 27** | 26 | [9 - 74] | 8 | [3 - 22] | NC | NC | 31 | [10 - 99] |
| **Site 28** | 26 | [9 - 76] | 8 | [3 - 25] | NC | NC | 31 | [10 - 100] |
| **Site 30** | 23 | [8 - 66] | 7 | [3 - 19] | NC | NC | 34 | [11 - 110] |
| **Site 36** | 14 | [5 - 42] | 5 | [2 - 15] | NC | NC | 12 | [4 - 36] |
| **Site 37** | 48 | [17 - 140] | 14 | [5 - 39] | NC | NC | 53 | [15 - 180] |
| **Site 42** | 10 | [3 - 32] | 4 | [1 - 12] | NC | NC | 12 | [4 - 39] |
| **Site 43** | 14 | [5 - 38] | 4 | [2 - 11] | NC | NC | 16 | [5 - 52] |
| **Site 46** | 18 | [6 - 52] | 5 | [2 - 14] | NC | NC | 17 | [5 - 56] |
| **Site 50** | 20 | [7 - 58] | 6 | [2 - 17] | NC | NC | 35 | [9 - 130] |

| | PCB 138 | | PCB 128 | | PCB 187 | | PCB 180 | |
|---|---|---|---|---|---|---|---|---|
| **Site 2** | 26 | [9 - 76] | 4 | [2 - 11] | 15 | [3 - 70] | 28 | [4 - 180] |
| **Site 5** | 9 | [3 - 27] | 2 | [1 - 6] | 3 | [1 - 13] | 5 | [1 - 24] |
| **Site 8** | 19 | [6 - 54] | 4 | [1 - 12] | 6 | [2 - 19] | 7 | [2 - 24] |
| **Site 10** | 20 | [7 - 61] | 4 | [1 - 13] | 6 | [2 - 19] | 6 | [2 - 23] |
| **Site 12** | 17 | [6 - 51] | 4 | [1 - 11] | 3 | [1 - 10] | 4 | [1 - 16] |
| **Site 13** | 18 | [6 - 52] | 3 | [1 - 9] | 11 | [2 - 49] | 20 | [3 - 130] |
| **Site 15** | 18 | [6 - 54] | 3 | [1 - 9] | 9 | [2 - 44] | 16 | [3 - 110] |
| **Site 20** | 11 | [4 - 33] | 3 | [1 - 8] | 3 | [1 - 10] | 3 | [1 - 11] |
| **Site 22** | 25 | [9 - 71] | 5 | [2 - 13] | 10 | [3 - 37] | 12 | [3 - 53] |
| **Site 23** | 17 | [6 - 45] | 3 | [1 - 8] | 8 | [2 - 32] | 10 | [2 - 55] |
| **Site 27** | 22 | [7 - 66] | 5 | [2 - 13] | 9 | [2 - 33] | 11 | [2 - 50] |
| **Site 28** | 22 | [7 - 69] | 5 | [2 - 15] | 8 | [2 - 29] | 9 | [2 - 37] |
| **Site 30** | 23 | [8 - 68] | 5 | [2 - 13] | 10 | [3 - 39] | 13 | [3 - 61] |
| **Site 36** | 10 | [3 - 30] | 2 | [1 - 7] | 2 | [1 - 8] | 2 | [1 - 7] |
| **Site 37** | 37 | [12 - 120] | 7 | [3 - 21] | 15 | [3 - 68] | 25 | [4 - 140] |
| **Site 42** | 9 | [3 - 27] | 2 | [1 - 6] | 4 | [1 - 13] | 4 | [1 - 15] |
| **Site 43** | 11 | [4 - 33] | 2 | [1 - 7] | 5 | [1 - 21] | 7 | [1 - 37] |
| **Site 46** | 15 | [5 - 44] | 4 | [1 - 10] | 5 | [1 - 21] | 6 | [1 - 30] |
| **Site 50** | 20 | [6 - 65] | 4 | [1 - 11] | 17 | [3 - 88] | 34 | [5 - 240] |

## APPENDIX E (contd.)

| | PCB 170 | | PCB 195 | | PCB 206 | | PCB 209 | |
|---|---|---|---|---|---|---|---|---|
| **Site 2** | 13 | [2 - 70] | NC | NC | NC | NC | NC | NC |
| **Site 5** | 3 | [1 - 13] | NC | NC | NC | NC | NC | NC |
| **Site 8** | 4 | [1 - 13] | NC | NC | NC | NC | NC | NC |
| **Site 10** | 3 | [1 - 12] | NC | NC | NC | NC | NC | NC |
| **Site 12** | 3 | [1 - 10] | NC | NC | NC | NC | NC | NC |
| **Site 13** | 8 | [2 - 45] | NC | NC | NC | NC | NC | NC |
| **Site 15** | 7 | [1 - 40] | NC | NC | NC | NC | NC | NC |
| **Site 20** | 2 | [1 - 6] | NC | NC | NC | NC | NC | NC |
| **Site 22** | 6 | [1 - 23] | NC | NC | NC | NC | NC | NC |
| **Site 23** | 4 | [1 - 20] | NC | NC | NC | NC | NC | NC |
| **Site 27** | 5 | [1 - 21] | NC | NC | NC | NC | NC | NC |
| **Site 28** | 5 | [1 - 19] | NC | NC | NC | NC | NC | NC |
| **Site 30** | 6 | [1 - 25] | NC | NC | NC | NC | NC | NC |
| **Site 36** | 1 | [0 - 4] | NC | NC | NC | NC | NC | NC |
| **Site 37** | 12 | [2 - 58] | NC | NC | NC | NC | NC | NC |
| **Site 42** | 2 | [1 - 8] | NC | NC | NC | NC | NC | NC |
| **Site 43** | 3 | [1 - 16] | NC | NC | NC | NC | NC | NC |
| **Site 46** | 2 | [1 - 11] | NC | NC | NC | NC | NC | NC |
| **Site 50** | 13 | [2 - 81] | NC | NC | NC | NC | NC | NC |

# APPENDIX F BOTTOM WATER (0-5 CM ABOVE SEDIMENT-WATER INTERFACE) FREELY DISSOLVED CONCENTRATIONS (PG/L) OF 16 PCBS INFERRED FROM PRC-CORRECTED PE SAMPLERS DEPLOYED IN THE SUMMER OF 2014.

Brackets indicates ±2σ uncertainty found via error propagation. NC means not calculated because congener was not detected in the PE. (Prendergast and Apell et al. in prep.)

| | PCB 8 | | PCB 18 | | PCB 28 | | PCB 52 | |
|---|---|---|---|---|---|---|---|---|
| Site 2 | 32 | [20-63] | 75 | [43-140] | 82 | [44-130] | 59 | [31-84] |
| Site 5 | 19 | [11-36] | 53 | [31-98] | 120 | [62-190] | 76 | [38-110] |
| Site 8 | 6 | [4-12] | 41 | [24-75] | 110 | [58-170] | 83 | [45-120] |
| Site 10 | 12 | [8-24] | 46 | [28-84] | 110 | [65-170] | 94 | [53-130] |
| Site 12 | 9 | [5-17] | 37 | [21-66] | 98 | [53-150] | 99 | [53-130] |
| Site 13 | 6 | [4-12] | 31 | [18-55] | 63 | [36-98] | 65 | [38-94] |
| Site 15 | 8 | [5-15] | 33 | [19-59] | 70 | [40-110] | 72 | [41-100] |
| Site 20 | 7 | [4-14] | 55 | [31-100] | 110 | [58-170] | 150 | [83-220] |
| Site 22 | 6 | [3-11] | 52 | [30-93] | 130 | [69-210] | 180 | [86-240] |
| Site 23 | 6 | [4-12] | 39 | [22-71] | 88 | [45-140] | 130 | [61-180] |
| Site 27 | 7 | [4-14] | 37 | [22-67] | 99 | [58-150] | 200 | [120-280] |
| Site 28 | 11 | [7-21] | 51 | [30-93] | 110 | [64-160] | 190 | [110-270] |
| Site 30 | 7 | [4-14] | 35 | [20-64] | 76 | [40-120] | 140 | [73-200] |
| Site 36 | 7 | [4-13] | 54 | [32-97] | 120 | [66-180] | 220 | [120-310] |
| Site 37 | 3 | [2-6] | 44 | [25-79] | 100 | [55-150] | 210 | [110-280] |
| Site 42 | 9 | [6-17] | 49 | [29-89] | 89 | [49-130] | 190 | [100-260] |
| Site 43 | 6 | [4-12] | 50 | [35-110] | 100 | [67-200] | 220 | [110-310] |
| Site 46 | NC | NC | 31 | [18-55] | 53 | [28-85] | 130 | [66-190] |
| Site 50 | 7 | [4-14] | 44 | [26-80] | 92 | [53-140] | 85 | [50-120] |

| | PCB 44 | | PCB 66 | | PCB 77 | | PCB 101 | |
|---|---|---|---|---|---|---|---|---|
| Site 2 | 32 | [17-47] | 19 | [10-24] | 1 | [0-2] | 45 | [25-60] |
| Site 5 | 38 | [19-55] | 28 | [13-34] | 2 | [1-3] | 56 | [28-68] |
| Site 8 | 40 | [22-60] | 45 | [24-57] | 3 | [2-4] | 86 | [48-120] |
| Site 10 | 48 | [27-69] | 40 | [22-54] | 3 | [2-4] | 83 | [50-130] |
| Site 12 | 51 | [28-73] | 41 | [21-52] | 2 | [1-3] | 78 | [44-110] |
| Site 13 | 33 | [19-49] | 27 | [16-37] | 2 | [1-2] | 51 | [32-76] |
| Site 15 | 34 | [19-50] | 30 | [17-40] | 2 | [1-3] | 57 | [34-84] |
| Site 20 | 61 | [33-92] | 44 | [24-57] | 2 | [1-3] | 120 | [68-160] |
| Site 22 | 76 | [38-110] | 67 | [31-77] | 4 | [2-4] | 130 | [62-160] |
| Site 23 | 45 | [23-67] | 38 | [17-45] | 2 | [0-2] | 100 | [49-120] |
| Site 27 | 58 | [34-84] | 46 | [27-63] | 2 | [1-3] | 140 | [89-220] |
| Site 28 | 63 | [36-93] | 51 | [28-67] | 2 | [1-3] | 130 | [78-190] |
| Site 30 | 41 | [21-61] | 33 | [17-40] | 2 | [0-2] | 89 | [47-110] |
| Site 36 | 72 | [40-100] | 55 | [29-71] | 3 | [1-4] | 150 | [87-220] |
| Site 37 | 64 | [34-90] | 54 | [28-66] | 2 | [1-3] | 130 | [71-170] |
| Site 42 | 59 | [32-84] | 42 | [22-53] | 2 | [1-3] | 120 | [68-180] |
| Site 43 | 57 | [34-98] | 49 | [23-58] | 2 | [1-3] | 160 | [70-180] |
| Site 46 | 33 | [17-50] | 27 | [14-35] | 1 | [0-2] | 77 | [40-97] |
| Site 50 | 44 | [26-64] | 38 | [22-51] | 3 | [2-4] | 79 | [48-120] |

## APPENDIX F (cont'd)

| | PCB 118 | | PCB 105 | | PCB 126 | | PCB 153 | |
|---|---|---|---|---|---|---|---|---|
| **Site 2** | 19 | [12-30] | 7 | [4-11] | NC | NC | 24 | [18-48] |
| **Site 5** | 24 | [13-35] | 9 | [5-13] | NC | NC | 25 | [17-47] |
| **Site 8** | 45 | [27-69] | 17 | [10-25] | NC | NC | 51 | [35-94] |
| **Site 10** | 37 | [27-72] | 14 | [9-25] | NC | NC | 39 | [35-97] |
| **Site 12** | 35 | [23-63] | 14 | [9-24] | NC | NC | 39 | [33-94] |
| **Site 13** | 24 | [16-40] | 10 | [6-16] | NC | NC | 25 | [19-50] |
| **Site 15** | 27 | [18-47] | 11 | [7-18] | NC | NC | 31 | [25-69] |
| **Site 20** | 53 | [31-81] | 17 | [10-24] | NC | NC | 66 | [45-120] |
| **Site 22** | 49 | [28-76] | 17 | [9-25] | NC | NC | 48 | [36-100] |
| **Site 23** | 40 | [21-55] | 13 | [7-17] | NC | NC | 37 | [24-66] |
| **Site 27** | 62 | [45-120] | 20 | [13-35] | NC | NC | 60 | [53-140] |
| **Site 28** | 54 | [36-94] | 18 | [11-30] | NC | NC | 55 | [43-120] |
| **Site 30** | 37 | [22-59] | 13 | [7-19] | NC | NC | 36 | [26-73] |
| **Site 36** | 60 | [41-110] | 20 | [13-35] | NC | NC | 53 | [46-130] |
| **Site 37** | 54 | [35-93] | 18 | [11-28] | NC | NC | 42 | [35-96] |
| **Site 42** | 51 | [34-95] | 16 | [10-28] | NC | NC | 47 | [40-120] |
| **Site 43** | 66 | [33-89] | 22 | [10-26] | NC | NC | 60 | [34-97] |
| **Site 46** | 35 | [19-47] | 11 | [6-14] | NC | NC | 29 | [18-49] |
| **Site 50** | 33 | [22-59] | 13 | [9-22] | NC | NC | 32 | [27-71] |

| | PCB 138 | | PCB 128 | | PCB 187 | | PCB 180 | |
|---|---|---|---|---|---|---|---|---|
| **Site 2** | 17 | [12-32] | 4 | [2-6] | 5 | [5-14] | 5 | [7-19] |
| **Site 5** | 21 | [13-36] | 5 | [3-7] | 3 | [2-7] | 5 | [6-18] |
| **Site 8** | 40 | [26-70] | 9 | [6-15] | 13 | [12-32] | 14 | [15-42] |
| **Site 10** | 32 | [26-73] | 8 | [6-16] | 8 | [10-29] | 8 | [14-40] |
| **Site 12** | 34 | [27-73] | 8 | [5-15] | 8 | [10-30] | 7 | [12-36] |
| **Site 13** | 19 | [14-36] | 5 | [3-8] | 6 | [6-16] | 7 | [8-22] |
| **Site 15** | 24 | [18-49] | 5 | [3-9] | 6 | [7-19] | 6 | [8-23] |
| **Site 20** | 48 | [31-82] | 10 | [6-16] | 16 | [14-39] | 16 | [17-47] |
| **Site 22** | 37 | [24-69] | 8 | [5-13] | 10 | [11-32] | 9 | [13-40] |
| **Site 23** | 29 | [17-46] | 6 | [4-9] | 7 | [6-18] | 6 | [8-22] |
| **Site 27** | 45 | [37-99] | 10 | [8-20] | 12 | [14-39] | 11 | [16-46] |
| **Site 28** | 42 | [31-83] | 9 | [6-17] | 11 | [12-33] | 11 | [14-41] |
| **Site 30** | 31 | [21-56] | 7 | [4-12] | 7 | [7-19] | 7 | [9-27] |
| **Site 36** | 43 | [34-93] | 9 | [7-18] | 10 | [13-37] | 9 | [16-46] |
| **Site 37** | 34 | [26-70] | 8 | [6-15] | 7 | [8-24] | 6 | [10-28] |
| **Site 42** | 38 | [29-82] | 9 | [6-18] | 9 | [11-32] | 8 | [14-42] |
| **Site 43** | 51 | [26-72] | 12 | [6-16] | 10 | [8-24] | 8 | [10-30] |
| **Site 46** | 23 | [14-36] | 5 | [3-8] | 5 | [4-12] | 5 | [5-14] |
| **Site 50** | 27 | [21-54] | 6 | [4-11] | 6 | [7-19] | 6 | [9-24] |

## APPENDIX F (cont'd)

| | PCB 170 | | PCB 195 | | PCB 206 | | PCB 209 | |
|---|---|---|---|---|---|---|---|---|
| **Site 2** | 3 | [4-10] | NC | NC | NC | NC | NC | NC |
| **Site 5** | 6 | [6-19] | NC | NC | NC | NC | NC | NC |
| **Site 8** | 8 | [8-23] | NC | NC | NC | NC | NC | NC |
| **Site 10** | 5 | [7-20] | NC | NC | NC | NC | NC | NC |
| **Site 12** | NC | NC | NC | NC | NC | NC | NC | NC |
| **Site 13** | 4 | [4-10] | NC | NC | NC | NC | NC | NC |
| **Site 15** | 4 | [5-14] | NC | NC | NC | NC | NC | NC |
| **Site 20** | 9 | [9-24] | NC | NC | NC | NC | NC | NC |
| **Site 22** | 5 | [6-18] | NC | NC | NC | NC | NC | NC |
| **Site 23** | 3 | [4-10] | NC | NC | NC | NC | NC | NC |
| **Site 27** | 6 | [8-23] | NC | NC | NC | NC | NC | NC |
| **Site 28** | 5 | [7-18] | NC | NC | NC | NC | NC | NC |
| **Site 30** | 4 | [4-13] | NC | NC | NC | NC | NC | NC |
| **Site 36** | 7 | [10-28] | NC | NC | NC | NC | NC | NC |
| **Site 37** | 4 | [5-15] | NC | NC | NC | NC | NC | NC |
| **Site 42** | 4 | [6-19] | NC | NC | NC | NC | NC | NC |
| **Site 43** | 5 | [4-14] | NC | NC | NC | NC | NC | NC |
| **Site 46** | 3 | [2-6] | NC | NC | NC | NC | NC | NC |
| **Site 50** | 4 | [5-13] | NC | NC | NC | NC | NC | NC |

# APPENDIX G WATER COLUMN (1 M ABOVE SEDIMENT-WATER INTERFACE) FREELY DISSOLVED CONCENTRATIONS (PG/L) OF INDIVIDUAL PCB CONGENERS FOUND USING PE PASSIVE SAMPLERS.

Brackets indicates ±2σ uncertainty. NC means not calculated due to non-detections in the PE samplers. (Prendergast and Apell et al. in prep.)

| | PCB 8 | | PCB 18 | | PCB 28 | | PCB 52 | |
|---|---|---|---|---|---|---|---|---|
| Site 2 | 4 | [2-7] | 17 | [9-30] | 33 | [20-56] | 36 | [23-59] |
| Site 5 | 8 | [4-14] | 33 | [19-59] | 86 | [52-150] | 78 | [49-130] |
| Site 22 | 12 | [7-21] | 90 | [51-160] | 190 | [110-320] | 210 | [130-360] |
| Site 43 | 6 | [3-11] | 61 | [34-110] | 120 | [74-220] | 210 | [130-350] |
| Site 46 | 8 | [4-14] | 35 | [20-61] | 64 | [36-110] | 130 | [77-230] |
| | PCB 44 | | PCB 66 | | PCB 77 | | PCB 101 | |
| Site 2 | 19 | [12-32] | 13 | [9-21] | 0.6 | [0.4-1] | 32 | [21-49] |
| Site 5 | 42 | [26-70] | 33 | [22-51] | 2 | [1-4] | 62 | [41-98] |
| Site 22 | 87 | [53-150] | 67 | [43-110] | 4 | [3-6] | 130 | [80-200] |
| Site 43 | 64 | [39-110] | 43 | [28-66] | 2 | [1-3] | 130 | [83-190] |
| Site 46 | 34 | [20-60] | 24 | [15-39] | 1 | [0-2] | 71 | [46-110] |
| | PCB 118 | | PCB 105 | | PCB 126 | | PCB 153 | |
| Site 2 | 15 | [9-24] | 5 | [3-8] | NC | NC | 19 | [12-31] |
| Site 5 | 28 | [17-46] | 10 | [7-17] | NC | NC | 33 | [20-54] |
| Site 22 | 49 | [29-81] | 18 | [11-29] | NC | NC | 44 | [26-75] |
| Site 43 | 61 | [39-96] | 18 | [12-28] | NC | NC | 60 | [38-97] |
| Site 46 | 31 | [20-48] | 10 | [6-15] | NC | NC | 27 | [17-44] |
| | PCB 138 | | PCB 128 | | PCB 187 | | PCB 180 | |
| Site 2 | 14 | [9-23] | 3 | [2-5] | 4 | [3-7] | 4 | [3-7] |
| Site 5 | 27 | [16-44] | 5 | [3-9] | 7 | [4-12] | 7 | [4-12] |
| Site 22 | 37 | [22-62] | 8 | [5-14] | 9 | [5-15] | 8 | [4-14] |
| Site 43 | 46 | [29-73] | 10 | [7-17] | 13 | [8-22] | 15 | [9-25] |
| Site 46 | 21 | [14-34] | 5 | [3-7] | 5 | [3-8] | 5 | [3-8] |
| | PCB 170 | | PCB 195 | | PCB 206 | | PCB 209 | |
| Site 2 | 3 | [2-4] | NC | NC | NC | NC | NC | NC |
| Site 5 | 5 | [3-9] | 1 | [0-2] | NC | NC | NC | NC |
| Site 22 | 4 | [3-8] | NC | NC | NC | NC | NC | NC |
| Site 43 | 7 | [4-12] | NC | NC | NC | NC | NC | NC |
| Site 46 | 3 | [2-5] | NC | NC | NC | NC | NC | NC |

# APPENDIX H SAMPLER LOCATIONS AND OTHER SITE DETAILS FOR FIELD SAMPLING IN SUMMER, 2016.

(Prendergast).

| Sampler ID | River Mile [a] | EFDC Cell [b] | | Configuration[c] | Mean Depth [m] | Depth Range [m] | Average Salinity [PSU] | Deploy Date M/D/Y | Recovery Date M/D/Y | Latitude North | Longitude West |
|---|---|---|---|---|---|---|---|---|---|---|---|
| | | I | J | | | | | | | | |
| 1 | -1.4 | 10 | 41 | Floating, Top | 2.5 | [2.5 - 2.5] | 29.2 | 06/08/16 | 07/25/16 | 47.58611 | 122.36381 |
| 2 | -0.28 | 13 | 34 | Fixed, Top | 4.2 | [2.3 - 6.2] | 29.2 | 06/08/16 | 07/25/16 | 47.57236 | 122.35400 |
| 3 | 0.16 | 15 | 32 | Floating, Top | 0.1 | [0.1 - 0.1] | 9.35 | 06/08/16 | 07/25/16 | 47.56781 | 122.34594 |
| 4 | 0.16 | 15 | 32 | Floating, Top | 1.7 | [1.7 - 1.7] | 21.2 | 06/08/16 | 07/25/16 | 47.56781 | 122.34594 |
| 5 | 0.16 | 15 | 32 | Floating, Top | 3.3 | [3.3 - 3.3] | 26.0 | 06/08/16 | 07/25/16 | 47.56781 | 122.34594 |
| 6 | 0.12 | 15 | 32 | Fixed, Bottom | 8.4 | [5.5 - 10.4] | 29.2 | 06/08/16 | 07/25/16 | 47.56844 | 122.34706 |
| 7 | 0.12 | 15 | 32 | Fixed, Bottom | 9.3 | [6.5 - 11.3] | 29.2 | 06/08/16 | 07/25/16 | 47.56844 | 122.34706 |
| 8 | 0.47 | 15 | 30 | Floating, Top | 0.2 | [0.2 - 0.2] | 8.12 | 06/07/16 | 07/25/16 | 47.56318 | 122.34535 |
| 9 | 0.47 | 15 | 30 | Fixed, Bottom | 2.2 | [0.0 - 4.2] | 25.0 | 06/07/16 | 07/25/16 | 47.56314 | 122.34536 |
| 10 | 0.47 | 15 | 30 | Fixed, Bottom | 3.1 | [0.3 - 5.1] | 26.7 | 06/07/16 | 07/25/16 | 47.56314 | 122.34536 |
| 11 | 0.60 | 14 | 29 | Fixed, Bottom | 3.7 | [0.8 - 5.7] | 27.9 | 06/08/16 | 07/25/16 | 47.56122 | 122.34533 |
| 12 | 0.80 | 11 | 28 | Fixed, Bottom | 3.1 | [0.2 - 5.1] | 27.0 | 06/07/16 | 07/25/16 | 47.55803 | 122.34600 |
| 13 | 0.95 | 12 | 27 | Fixed, Top | 1.9 | [0.0 - 3.9] | 25.7 | 06/07/16 | 07/25/16 | 47.55610 | 122.34460 |
| 14 | 0.95 | 12 | 27 | Fixed, Top | 3.4 | [0.6 - 5.4] | 26.6 | 06/07/16 | 07/25/16 | 47.55610 | 122.34460 |
| 15 | 1.4 | 14 | 25 | Fixed, Bottom | 5.9 | [3.0 - 7.8] | 28.6 | 06/07/16 | 07/26/16 | 47.55104 | 122.33981 |
| 16 | 2.3 | 12 | 18 | Floating, Top | 0.5 | [0.5 - 0.5] | 11.1 | 06/07/16 | 07/26/16 | 47.53892 | 122.33038 |
| 17 | 2.3 | 12 | 18 | Floating, Top | 1.9 | [0.7 - 2.0] | 23.1 | 06/07/16 | 07/26/16 | 47.53892 | 122.33038 |
| 18 | 2.3 | 12 | 18 | Floating, Top | 3.0 | [0.7 - 3.3] | 26.6 | 06/07/16 | 07/26/16 | 47.53892 | 122.33038 |
| 19 | 2.2 | 12 | 19 | Fixed, Bottom | 3.6 | [0.8 - 5.6] | 27.9 | 06/07/16 | 07/26/16 | 47.53955 | 122.33188 |
| 20 | 2.2 | 12 | 19 | Fixed, Bottom | 4.4 | [1.5 - 6.4] | 28.2 | 06/07/16 | 07/26/16 | 47.53955 | 122.33188 |
| 21 | 3.3 | 13 | 11 | Fixed, Top | 3.3 | [3.3 - 3.3] | 25.8 | 06/06/16 | 07/26/16 | 47.52944 | 122.31400 |
| 22 | 3.3 | 13 | 11 | Fixed, Top | 5.7 | [3.5 - 6.0] | 27.2 | 06/06/16 | 07/26/16 | 47.52944 | 122.31400 |
| 23 | 3.6 | 13 | 10 | Floating, Top | 0.4 | [0.4 - 0.4] | 5.88 | 06/06/16 | 07/26/16 | 47.52692 | 122.31075 |
| 24 | 3.6 | 13 | 10 | Floating, Top | 1.7 | [1.7 - 1.7] | 19.0 | 06/06/16 | 07/26/16 | 47.52692 | 122.31075 |
| 25 | 4.1 | 14 | 6 | Fixed, Top | 0.6 | [0.0 - 2.2] | 22.5 | 06/06/16 | 07/27/16 | 47.52000 | 122.30634 |
| 26 | 4.1 | 14 | 6 | Fixed, Top | 0.9 | [0.0 - 2.6] | 22.5 | 06/06/16 | 07/27/16 | 47.52000 | 122.30634 |
| 27 | 3.9 | 14 | 8 | Fixed, Bottom | 0.9 | [0.0 - 2.5] | 19.9 | 06/06/16 | 07/27/16 | 47.52288 | 122.30757 |
| 28 | 3.9 | 14 | 8 | Fixed, Bottom | 1.9 | [0.0 - 3.8] | 19.9 | 06/06/16 | 07/27/16 | 47.52288 | 122.30757 |
| 29 | 6.4 | 24 | 3 | Floating, Top | 0.6 | [0.6 - 0.6] | 29.2 | 06/05/16 | 07/24/16 | 47.50042 | 122.28731 |
| 30 | 16.2 | 55 | 3 | Fixed, Top | 1.8 | [1.2 - 3.4] | 0.00 | 06/05/16 | 07/24/16 | 47.42300 | 122.26511 |

[a] Miles upriver from downstream border of study area.
[b] Model cell coordinates containing sampler. I increases from east to west, J increases from south to north (upriver to downriver). See Figure S1.
[c] Configuration of sampler rope line, which determines the vertical position of the sampler relative to the water column.

# APPENDIX I FRACTIONS OF PRCS LOST DURING THE SUMMER 2016 DEPLOYMENT OF PE PASSIVE SAMPLERS IN THE LDW WATER COLUMN

(Prendergast).

| Sampler ID | Deployment Time [Days] | Fraction Lost | | | | | | |
|---|---|---|---|---|---|---|---|---|
| | | $^{13}$C PCB 28 | $^{13}$C PCB 54 | $^{13}$C PCB 47 | $^{13}$C PCB 97 | $^{13}$C PCB 111 | $^{13}$C PCB 153 | $^{13}$C PCB 178 |
| 1 | 47 | 1.00 | 1.00 | 0.97 | 0.79 | 0.36 | 0.13 | 0.21 |
| 2 | 47 | 0.84 | 0.99 | 0.58 | 0.38 | 0.11 | 0.06 | 0.04 |
| 3 | 47 | 1.00 | 1.00 | 1.00 | 0.82 | 0.45 | 0.15 | 0.22 |
| 4 | 47 | 1.00 | 1.00 | 0.96 | 0.71 | 0.37 | 0.12 | 0.19 |
| 5 | 47 | 0.88 | 1.00 | 0.66 | 0.37 | 0.14 | 0.08 | 0.06 |
| 6 | 47 | 0.68 | 0.96 | 0.37 | 0.26 | 0.09 | 0.04 | 0.01 |
| 7 | 47 | 0.76 | 0.99 | 0.61 | 0.29 | 0.13 | 0.08 | 0.03 |
| 8 | 48 | 0.97 | 1.00 | 0.94 | 0.73 | 0.38 | 0.20 | 0.14 |
| 9 | 48 | 0.80 | 0.98 | 0.43 | 0.31 | 0.12 | 0.05 | 0.01 |
| 10 | 48 | 0.87 | 0.99 | 0.67 | 0.44 | 0.20 | 0.08 | 0.01 |
| 11 | 47 | 0.82 | 0.99 | 0.68 | 0.38 | 0.19 | 0.09 | 0.01 |
| 12 | 48 | 0.72 | 0.97 | 0.51 | 0.25 | 0.12 | 0.05 | 0.02 |
| 13 | 48 | 0.96 | 1.00 | 0.90 | 0.65 | 0.32 | 0.10 | 0.06 |
| 14 | 48 | 0.91 | 0.99 | 0.67 | 0.42 | 0.11 | 0.02 | 0.00 |
| 15 | 49 | 0.86 | 1.00 | 0.67 | 0.38 | 0.20 | 0.04 | 0.05 |
| 16 | 49 | 0.94 | 1.00 | 0.74 | 0.51 | 0.22 | 0.10 | 0.05 |
| 17 | 49 | 0.93 | 1.00 | 0.73 | 0.53 | 0.24 | 0.09 | 0.04 |
| 18 | 49 | 0.93 | 1.00 | 0.74 | 0.55 | 0.25 | 0.08 | 0.04 |
| 19 | 49 | 0.74 | 0.98 | 0.48 | 0.34 | 0.14 | 0.03 | 0.00 |
| 20 | 49 | 0.45 | 0.97 | 0.35 | 0.09 | 0.11 | 0.02 | 0.04 |
| 21 | 50 | 0.92 | 1.00 | 0.71 | 0.50 | 0.22 | 0.09 | 0.04 |
| 22 | 50 | 0.89 | 1.00 | 0.68 | 0.50 | 0.11 | 0.00 | 0.00 |
| 23 | 50 | 0.98 | 1.00 | 0.93 | 0.73 | 0.34 | 0.10 | 0.00 |
| 24 | 50 | 0.94 | 1.00 | 0.80 | 0.60 | 0.23 | 0.02 | 0.00 |
| 25 | 51 | 0.99 | 1.00 | 0.95 | 0.76 | 0.42 | 0.19 | 0.11 |
| 26 | 51 | 0.97 | 1.00 | 0.94 | 0.76 | 0.42 | 0.24 | 0.14 |
| 27 | 51 | 0.97 | 1.00 | 0.82 | 0.64 | 0.28 | 0.13 | 0.00 |
| 28 | 51 | 0.69 | 0.97 | 0.59 | 0.37 | 0.17 | 0.02 | 0.00 |
| 29 | 49 | 1.00 | 1.00 | 0.99 | 0.94 | 0.63 | 0.35 | 0.19 |
| 30 | 49 | 0.98 | 1.00 | 0.97 | 0.85 | 0.46 | 0.21 | 0.07 |
| Average Lost | | 0.88 | 0.99 | 0.73 | 0.53 | 0.25 | 0.10 | 0.06 |
| Standard Deviation | | 0.12 | 0.01 | 0.19 | 0.21 | 0.13 | 0.08 | 0.07 |
| Relative Dev (%) | | 14% | 1% | 26% | 40% | 53% | 78% | 111% |

# APPENDIX J FREELY-DISSOLVED PRC-CORRECTED CONCENTRATIONS OF PCB CONGENERS MEASURED USING PE PASSIVE SAMPLERS IN THE WATER COLUMN OF THE LDW IN THE SUMMER OF 2016.

$K_{PEW}$ values are site-specific based on average salinity estimated by EFDC (Appendix H) and an average measured temperature of 18.4 °C (Prendergast).

| Sampler ID | Freely-Dissolved Concentration [pg/L] | | | | | | | | | |
|---|---|---|---|---|---|---|---|---|---|---|
| | PCB 008 | PCB 018 | PCB 028 | PCB 044 | PCB 052 | PCB 066 | PCB 077 | PCB 101 | PCB 105 | PCB 118 |
| 1 | 1 | 3 | 4 | 3 | 5 | 2 | 1 | 4 | 1 | 2 |
| 2 | 2 | 8 | 11 | 16 | 36 | 8 | 1 | 35 | 7 | 20 |
| 3 | 4 | 6 | 7 | 4 | 5 | 2 | 1 | 4 | 1 | 2 |
| 4 | 3 | 7 | 9 | 5 | 6 | 3 | 1 | 6 | 1 | 3 |
| 5 | 9 | 21 | 22 | 10 | 19 | 7 | 1 | 14 | 2 | 6 |
| 6 | 3 | 7 | 16 | 10 | 18 | 9 | 1 | 20 | 4 | 10 |
| 7 | 11 | 30 | 35 | 21 | 29 | 11 | 1 | 22 | 4 | 10 |
| 8 | 25 | 67 | 64 | 21 | 30 | 8 | 1 | 11 | 2 | 5 |
| 9 | 3 | 9 | 17 | 11 | 18 | 8 | 1 | 18 | 3 | 9 |
| 10 | 4 | 13 | 23 | 13 | 21 | 9 | 1 | 19 | 4 | 11 |
| 11 | 3 | 12 | 19 | 12 | 20 | 9 | 1 | 21 | 4 | 11 |
| 12 | 6 | 21 | 42 | 29 | 47 | 20 | 1 | 46 | 8 | 24 |
| 13 | 4 | 9 | 10 | 5 | 10 | 4 | 1 | 9 | 2 | 5 |
| 14 | 4 | 11 | 21 | 12 | 22 | 10 | 1 | 25 | 5 | 13 |
| 15 | 6 | 14 | 23 | 13 | 22 | 8 | ND | 16 | 3 | 8 |
| 16 | 5 | 12 | 14 | 7 | 15 | 5 | 0 | 10 | 2 | 5 |
| 17 | 5 | 14 | 20 | 11 | 21 | 8 | 1 | 17 | 3 | 9 |
| 18 | 4 | 14 | 23 | 14 | 25 | 11 | 1 | 22 | 4 | 12 |
| 19 | 10 | 36 | 65 | 39 | 56 | 29 | 2 | 35 | 7 | 18 |
| 20 | 19 | 90 | 140 | 79 | 96 | 34 | 2 | 33 | 5 | 15 |
| 21 | 5 | 13 | 16 | 9 | 17 | 6 | 0 | 12 | 2 | 6 |
| 22 | 5 | 16 | 28 | 17 | 32 | 13 | 1 | 28 | 5 | 14 |
| 23 | 5 | 10 | 11 | 5 | 11 | 4 | 0 | 10 | 2 | 6 |
| 24 | 5 | 12 | 15 | 8 | 16 | 5 | 0 | 13 | 2 | 7 |
| 25 | 4 | 9 | 10 | 5 | 10 | 3 | 0 | 8 | 1 | 4 |
| 26 | 4 | 10 | 11 | 6 | 11 | 4 | 0 | 9 | 1 | 5 |
| 27 | 5 | 14 | 22 | 13 | 26 | 9 | 1 | 22 | 3 | 11 |
| 28 | 6 | 19 | 30 | 19 | 39 | 13 | 1 | 31 | 4 | 17 |
| 29 | 4 | 5 | 4 | 2 | 4 | 1 | ND | 3 | 1 | 2 |
| 30 | ND | 0 | 1 | 0 | 1 | 0 | ND | 1 | 0 | 1 |

ND=Non-detect.

## APPENDIX J (cont'd)

| Sampler ID | Freely-Dissolved Concentration [pg/L] | | | | | | | | | |
|---|---|---|---|---|---|---|---|---|---|---|
| | PCB 126 | PCB 128 | PCB 138 | PCB 153 | PCB 170 | PCB 180 | PCB 187 | PCB 195 | PCB 206 | PCB 209 |
| 1 | ND | 0 | 2 | 3 | 0 | 1 | 1 | ND | ND | ND |
| 2 | ND | 4 | 13 | 21 | 3 | 12 | 12 | ND | ND | ND |
| 3 | ND | 1 | 2 | 3 | 0 | 1 | 1 | ND | ND | ND |
| 4 | ND | 1 | 3 | 5 | 1 | 2 | 1 | ND | ND | ND |
| 5 | ND | 1 | 7 | 10 | 2 | 3 | 3 | ND | ND | ND |
| 6 | ND | 3 | 10 | 15 | 2 | 5 | 4 | ND | ND | ND |
| 7 | ND | 2 | 10 | 15 | 2 | 5 | 4 | ND | ND | ND |
| 8 | ND | 1 | 4 | 6 | 1 | 2 | 2 | ND | 0 | 0 |
| 9 | ND | 2 | 9 | 12 | 2 | 4 | 3 | ND | ND | ND |
| 10 | ND | 2 | 10 | 14 | 2 | 5 | 4 | ND | ND | ND |
| 11 | ND | 2 | 10 | 14 | 2 | 5 | 4 | ND | ND | ND |
| 12 | ND | 4 | 20 | 28 | 4 | 9 | 7 | ND | ND | ND |
| 13 | ND | 1 | 4 | 6 | 1 | 2 | 2 | ND | ND | ND |
| 14 | ND | 3 | 11 | 15 | 2 | 5 | 4 | ND | ND | ND |
| 15 | ND | 1 | 7 | 10 | 1 | 3 | 3 | ND | ND | ND |
| 16 | ND | 1 | 5 | 6 | 1 | 2 | 2 | ND | ND | ND |
| 17 | ND | 2 | 7 | 11 | 1 | 3 | 3 | ND | ND | ND |
| 18 | ND | 3 | 10 | 15 | 2 | 4 | 4 | ND | ND | ND |
| 19 | ND | 4 | 14 | 22 | 3 | 8 | 6 | ND | ND | ND |
| 20 | ND | 2 | 11 | 17 | 2 | 5 | 4 | ND | ND | ND |
| 21 | ND | 1 | 5 | 7 | 1 | 2 | 2 | ND | ND | ND |
| 22 | ND | 3 | 12 | 18 | 2 | 6 | 5 | ND | ND | ND |
| 23 | ND | 1 | 5 | 6 | 1 | 2 | 2 | ND | ND | ND |
| 24 | ND | 2 | 6 | 8 | 1 | 2 | 2 | ND | ND | ND |
| 25 | ND | 1 | 3 | 5 | 1 | 2 | 1 | ND | 0 | ND |
| 26 | ND | ND | 4 | 6 | 1 | 2 | 2 | ND | ND | ND |
| 27 | ND | 3 | 10 | 15 | 2 | 4 | 4 | ND | ND | ND |
| 28 | ND | 3 | 13 | 16 | 2 | 6 | 5 | ND | ND | ND |
| 29 | ND | 0 | 1 | 2 | 0 | 1 | 1 | ND | ND | ND |
| 30 | ND | 0 | 0 | 0 | 0 | 0 | 0 | ND | ND | ND |

ND=Non-detect.

# APPENDIX K FREELY-DISSOLVED PCB CONGENERS MEASURED USING "FAST" PE PASSIVE SAMPLERS IN THE WATER COLUMN OF HE LDW IN 2019

Freely-dissolved, PRC-corrected concentrations (pg/L) of three PCB congeners measured using PE passive samplers deployed for only 2 days in the water column at 4 depths (usually 2 feet and five feet below the water surface 2 feet and 5 feet above the sediment bed) at locations near the west bank (W) or east bank (E) aboout every 0.1 mile between river mile 1.4 and river mile 2.5 of the LDW in the summer of 2019.

| | | PCB Congener Concentration (pg/L) | | |
|---|---|---|---|---|
| Station RM | position | PCB 28 | PCB 52 | PCB 101 |
| 1.4W | 2' below surface | 58 | 54 | 34 |
| | 5' below surface | 125 | 95 | 53 |
| | 5' above bottom | 132 | 107 | 65 |
| | 2' above bottom | 77 | 56 | 38 |
| 1.5E | 2' below surface | 135 | 88 | 29 |
| | 4' below surface | 172 | 112 | 37 |
| | 5' above bottom | 117 | 73 | 26 |
| | 2' above bottom | | | |
| 1.7E | 2' below surface | 229 | 166 | 73 |
| | 4' below surface | 169 | 130 | |
| | 5' above bottom | | | |
| | 2' above bottom | 256 | 161 | 121 |
| 1.6W | 2' below surface | 83 | 62 | 32 |
| | 5' below surface | 41 | 36 | 25 |
| | 5' above bottom | 59 | 41 | 26 |
| | 2' above bottom | 90 | 67 | 39 |
| 1.7W | 2' below surface | 83 | 65 | 36 |
| | 5' below surface | 137 | 84 | 41 |
| | 5' above bottom | 342 | 287 | 167 |
| | 2' above bottom | 344 | 225 | 128 |
| 1.8E | 2' below surface | 109 | 67 | 40 |
| | 5' below surface | 84 | 62 | 28 |
| | 5' above bottom | 76 | 50 | 36 |
| | 2' above bottom | | | |
| 1.9W | 2' below surface | 98 | 65 | 36 |
| | 5' below surface | 92 | 52 | 24 |
| | 5' above bottom | 86 | 64 | 33 |
| | 2' above bottom | | | |
| 1.9E | 2' below surface | 187 | 143 | 73 |
| | 5' below surface | 230 | 143 | 73 |
| | 5' above bottom | 95 | 71 | 38 |
| | 2' above bottom | 204 | 120 | 45 |
| 2.0W | 2' below surface | | | |
| | 5' below surface | 81 | 60 | 43 |
| | 5' above bottom | 132 | 97 | 54 |
| | 2' above bottom | | | |
| 2.0E | 2' below surface | 100 | 68 | 29 |
| | 5' below surface | 142 | 109 | 45 |
| | 5' above bottom | 296 | 200 | 78 |
| | 2' above bottom | 140 | 103 | 53 |

| | | PCB Congener Concentration (pg/L) | | |
|---|---|---|---|---|
| Station RM | position | PCB 28 | PCB 52 | PCB 101 |
| 2.1W | 2' below surface | 247 | 169 | 68 |
| | 5' below surface | 115 | 84 | 46 |
| | 5' above bottom | 142 | 112 | 51 |
| | 2' above bottom | 99 | 70 | 43 |
| 2.1E | 2' below surface | | | |
| | 5' below surface | 84 | 55 | 32 |
| | 5' above bottom | 115 | 73 | 27 |
| | 2' above bottom | 154 | 108 | 68 |
| 2.2W | 2' below surface | | | |
| | 5' below surface | 320 | 237 | 132 |
| | 5' above bottom | 264 | 208 | 104 |
| | 2' above bottom | 182 | 146 | 80 |
| 2.3W | 2' below surface | 106 | 69 | 30 |
| | 5' below surface | 190 | 132 | 58 |
| | 5' above bottom | 108 | 69 | 39 |
| | 2' above bottom | 160 | 101 | 46 |
| 2.2E | 2' below surface | 67 | 55 | 27 |
| | 5' below surface | 66 | 46 | 25 |
| | 5' above bottom | 79 | 60 | 30 |
| | 2' above bottom | 85 | 61 | 33 |
| 2.3E | 2' below surface | 87 | 57 | 26 |
| | 5' below surface | 96 | 68 | 38 |
| | 5' above bottom | 137 | 87 | 46 |
| | 2' above bottom | 112 | 74 | 43 |
| 2.4W | 2' below surface | 81 | 60 | 43 |
| | 5' below surface | 131 | 83 | 35 |
| | 5' above bottom | 216 | 162 | 90 |
| | 2' above bottom | | | |
| 2.4E | 2' below surface | 121 | 96 | 50 |
| | 5' below surface | 106 | 86 | 44 |
| | 5' above bottom | | | |
| | 2' above bottom | 200 | 152 | 87 |
| 2.5W | 2' below surface | 86 | 54 | 27 |
| | 5' below surface | 140 | 83 | 37 |
| | 5' above bottom | 146 | 95 | 35 |
| | 2' above bottom | 283 | 210 | 123 |